EFFECTS OF THE TROPOSPHERE DELAY MAPPING FUNCTIONS AND THE ELEVATION CUT OFF ANGLES ON THE TIME SERIES OF STATION AND RADIO SOURCE COORDINATES AS WELL AS EARTH ORIENTATION PARAMETERS AS ESTIMATED FROM THE OBSERVATIONS OF THE VLBI TECHNIQUE

VLBI TEKNİĞİ ÖLÇÜLERİNDEN KESTİRİLEN İSTASYON VE RADYO KAYNAĞI KOORDİNATLARI İLE BİRLİKTE YER YÖNELİM PARAMETRELERİ ZAMAN SERİLERİNE TROPOSFER SİNYAL GECİKMESİ İZDÜŞÜM FONKSİYONLARI VE YÜKSELİM KESME AÇILARININ ETKİLERİ

BURAK KOF

ASSIST. PROF. DR. KAMİL TEKE
Supervisor

Submitted to
Graduate School of Science and Engineering of Hacettepe University
as a Partial Fulfilment to th Requirements
for the Award of the Degree of Master of Science
in Geomatics Engineering.

2020

ÖZET

VLBI TEKNİĞİ ÖLÇÜLERİNDEN KESTİRİLEN İSTASYON VE RADYO KAYNAĞI KOORDİNATLARI İLE BİRLİKTE YER YÖNELİM PARAMETRELERİ ZAMAN SERİLERİNE TROPOSFER SİNYAL GECİKMESİ İZDÜŞÜM FONKSİYONLARI VE YÜKSELİM KESME AÇILARININ ETKİLERİ

Burak KOF

Yüksek Lisans, Geomatik Mühendisliği Bölümü
Tez Danışmanı: Dr. Öğr. Üyesi Kamil TEKE
Temmuz 2020, 115 sayfa

Çok Uzun Baz Enterferometrisi (VLBI), kuasarlardan (ekstra-galaktik sinyal kaynakları) gelen S ve X bandındaki radyo dalga sinyallerini, yer sabit antenleri (günümüzde geniş bant yani 2 ila 8 GHz arası gözlemler çeşitli gelişmiş VLBI anten ekipmanları ile algılanmaktadır) ve sayıllaştırılmış ve modellenmiş sinyallere zaman etiketi eklemek için de atomik saatleri kullanarak gözlemleyen bir uzay jeodezisi tekniğidir. VLBI tekniği sinyalin VLBI antenlerine ulaşma süreleri arasındaki süre farkını ölçer. Tarama, gecikme gözlemlerini çözümleyebilmek amacıyla iki veya daha fazla antenin aynı radyo kaynağına yeterli yayınımı elde edebilmek için yaklaşık birkaç dakikalık entegrasyon süreci boyunca bakması durumudur. Kuasarlar, çoğunlukla galaksimizden 5 ila 7 milyar ışık yılı mesafelerde yer alan radyo kaynaklarıdır. Jeodezik VLBI oturumları Uluslararası VLBI Jeodezi ve Astronomi Servisi (IVS, Schuh and Behrend, 2011) tarafından yürütülmektedir. IVS yoğun oturumları 2 ila 4 VLBI istasyonunun katılımıyla evrensel zamanı izlemek için düzenlenirken, 24 saat uzunluğundaki IVS oturumları ise daha fazla istasyonun katılımıyla çeşitli jeodezik ve astronomik parametreleri izlemek için düzenlenir. Troposfer, radyo dalgası uzay jeodezi tekniklerinin indirgenmiş gözlemlerinde yer alan en belirgin hata kaynağıdır. Bu nedenle bu tez ile VMF1 (Vienna izdüşüm fonksiyonu, Böhm, Werl and Schuh, 2006), VMF3 (Landskron and Böhm, 2018), GMF3 (Küresel izdüşüm fonksiyonu, Böhm et al., 2006) troposfer gecikme izdüşüm fonksiyonlarının yanı sıra 5, 7, 10, 15 derece yükselim kesme açılarını kullanmanın kestirilen jeodezik parametreler üzerindeki etkilerini değerlendirmeyi amaçladık. Bu tez kapsamında 2000 ila 2018 yıllarını kapsayan 24 saat uzunluğundaki VLBI oturumları Viyana VLBI ve Uydu Yazılımı (VieVS, Böhm et al., 2018) kullanılarak analiz edilmiştir. Troposfer başucu toplam gecikmesi (ZTD) 20 dakikalık aralıklarla, kaynak ve istasyon koordinatlarının yanı sıra yer yönelim parametreleri de (EOP) izdüşüm fonksiyonları: VMF1, VMF3, GMF3 ve 5, 7, 10 ve 15 derecelerindeki yükselim kesme açıları kullanılarak günlük olarak kestirilmiştir. Yukarıda bahsi geçen jeodezik parametrelerin zaman serileri her izdüşüm fonksiyonu ve yükselim kesme açısı için üretildikten sonra objektif ve tarafsız bir ölçüt olan ağırlıklı karekök ortalama (WRMS) tekrarlanabilirlikleri her kestirilen parametre seti için, WRMS farkları ise kestirilen parametre setleri arasında hesaplanmıştır. GMF3 izdüşüm fonksiyonu ZTD sonuçları VMF1 ve VMF3 ile yüksek korelasyon göstermektedir. GMF, VMF'nin küresel harmonik mevsimsel yaklaşımı olması sebebiyle bu beklenen bir durumdur. VMF1-VMF3 arasındaki ZTD uyumunun, WRMS farklılıkları açısından GMF3-VMF1 ve GMF3-VMF3 uyumlarından 2 ila 3 kat daha iyi olduğu görülmüştür. ZTD ve istasyon koordinatları karşılaştırıldığında, 15 veya 20 derece yükselim kesme açılarından büyük değerler için, izdüşüm fonksiyonları arasında kayda değer farklar görülmemiştir. Bu durum diğer izdüşüm fonksiyonlarına kıyasla VMF3 kullanmanın yararının yükselim kesme açısını 5-10 derece civarına düşürdükten sonra üstün bir şekilde başladığını göstermektedir. İstasyon günlük konumları ortalama sapmalarının (ağırlıklı ortalama, WM) izdüşüm fonksiyonu değişikliğine karşı duyarlı olmadığı gözlemlenmiştir. İzdüşüm fonksiyonları arasındaki istasyon konumu WRMS tekrarlanabilirlikleri yükselim kesme açısı arttığında azalmaktadır. EOP tekrarlanabilirlikleri, direkt olarak seçilen yükselim açısına bağlı olan gözlemin sayısına ve geometrisine karşı çok daha duyarlıdır. Kuzey yarım küreye kıyasla, güney yarım küre ve kutuplardaki toplam gözlem sayısı daha azdır ve geometrisi homojen değildir. Bu güney gök yarım küresi ve kutuplardaki radyo kaynağı günlük koordinatlarının WRMS tekrarlanabilirliklerini (arttırmıştır) kötüleştirmiştir.

Anahtar Kelimeler: VLBI, troposfer gecikmeleri, troposfer izdüşüm fonksiyonları, VMF1, VMF3, GMF3, yükselim kesme açısı, tekrarlanabilirlikler.

ABSTRACT

EFFECTS OF THE TROPOSPHERE DELAY MAPPING FUNCTIONS AND THE ELEVATION CUT OFF ANGLES ON THE TIME SERIES OF STATION AND RADIO SOURCE COORDINATES AS WELL AS EARTH ORIENTATION PARAMETERS AS ESTIMATED FROM THE OBSERVATIONS OF THE VLBI TECHNIQUE

Burak KOF

Master of Science, Department of Geomatics Engineering
Supervisor: Dr. Kamil TEKE
July 2020, 115 pages

Very Long Baseline Interferometry (VLBI) is a space geodetic technique that observes the radio wave signals at S and X radio frequencies using the Earth fixed antennas (nowadays broadband i.e. from 2 to 8 GHz observables are sensed using several sophisticated VLBI antenna equipments), coming from the quasars (extra-galactic radio sources), along with the atomic clocks to time tag the digitized and sampled signals. VLBI technique measures the arrival time differences of the signals between the multiple VLBI antennas. A scan is an event that two or more antennas target to the same radio source for an integration time of about a few minutes to gather enough radiation for resolving delay observables. Quasars are the radio sources which are mostly 5 to 7 billions of light-years far away blazars from our galaxy. Geodetic VLBI sessions are maintained by the International VLBI Service for Geodesy and Astrometry (IVS, Schuh and Behrend, 2011). IVS Intensive sessions are held with the participation of 2 to 4 VLBI stations to monitor universal time, whereas the IVS 24 hour-long sessions are held with the participation of more stations for monitoring several unique geodetic and astrometric parameters. The troposphere is the most significant error source remaining in the reduced observations of the radio wave space geodetic techniques. Hence, this thesis aims to assess the effects of using various troposphere delay mapping functions, i.e. VMF1 (Vienna mapping function, Böhm, Werl and Schuh, 2006), VMF3 (Landskron and Böhm, 2018), GMF3 (Global mapping function, Böhm et al., 2006), as well as elevation cut-off angles, i.e. 5, 7, 10, 15 degrees, on the estimated geodetic parameters. In the scope of this thesis, 24 hour-long (daily) VLBI sessions covering the years from 2000 to 2018 are analyzed using Vienna VLBI and Satellite Software (VieVS, Böhm et al., 2018). Troposphere zenith total delays (ZTD) at 20-minute intervals, source, and station coordinates, as well as Earth orientation parameters, are estimated daily using the mapping functions: VMF1, VMF3, and GMF3 and the elevation cut-off angles as 5, 7, 10, and 15 degrees. After, the time series of the above-mentioned geodetic parameters are produced for each mapping function and elevation cut-off angle, as an objective and unbiased metric, the weighted root-mean-square (WRMS) repeatabilities and WRMS differences were calculated for and between each set of the estimated parameters, respectively. GMF3 mapping function ZTD results exhibit high correlations with VMF1 and VMF3 mapping functions. This is expected since GMF is a global spherical harmonic seasonal approximation of VMF. ZTD agreement between VMF1-VMF3 is found to be 2 to 3 times better than GMF3-VMF1 and GMF3-VMF3 agreements in terms of the WRMS differences. Not a significant difference between mapping functions above e.g. 15 or 20 degrees elevation cut-off angle were found when the ZTD and station coordinates are compared. This result indicates that relative to the other mapping functions the benefit of using VMF3 is started dominantly after reducing the elevation cut-off angle to about 5-10 degrees. The mean biases (weighted mean, WM) of the stations' daily positions are seen as not sensitive to the change of mapping functions. The station position WRMS repeatabilities between the mapping functions decrease when the elevation cut-off angle increases. The repeatabilities of EOP are much more sensitive to the number and the geometry of the observations which depends directly on the selected elevation cut-off angle. The total number of observations and their geometry becomes less and inhomogeneous in the southern hemisphere and the poles relative to the northern hemisphere. This worsens (increases) the WRMS repeatabilities of the source daily coordinates at the southern celestial hemisphere and the poles.

Key Words: VLBI, troposphere delays, troposphere mapping function, VMF1, VMF3, GMF3, elevation cut-off angle, repeatabilities.

ACKNOWLEDGE

I am grateful to my esteemed advisor Kamil Teke who has always accompanied me throughout my master degree education in all sorts of subjects, from scientific issues related to my thesis to issues related to my daily life, with his sophisticated attitude. I owe him a debt of gratitude for the endless persistence and endeavour which has been shown without any retardation to overcome obstacles I encountered during the development and research of my thesis.

I extend heartfelt thanks to my wife and family, who have supported me in all conditions and haven't avoid any sacrifice, from the first day of my graduate education to the day I will present my thesis.

Burak KOF
July 2020, Ankara

CONTENTS

LIST OF TABLES

LIST OF FIGURES

SYMBOLS AND ABBREVATIONS

Symbols

c	Velocity of light
τ	VLBI delay
$\vec{b}$	Earth-fixed baseline vector
$\vec{k}$	Unit source vector defined in a space-fixed, barycentric and equatorial celestial system
$\underline{s}_0$	Direction to the space-fixed source
t	Observation epoch
$\Delta\tau_{retarded\ baseline}$	Delay correction of the motion of the second antenna in GCRS formed by during the propagation time of the wavefront between the first and second antenna
$\Delta\tau_{clock}$	Delay correction due to the synchronization and frequency discrepancies of atomic clocks at station 1 and station 2
$M_{\oplus}$	Rest Mass of Earth
E , d	CIP Coordinates of GCRS
$\Delta\tau_{iono}$	Ionosphere delay correction
s	CIO Locator
s'	TIO Locator
$\vec{K}$	The unit vector in the absence of gravitational and bending effects from the barycenter to the source
$\Delta\tau_{trop}$	Troposphere delay correction
G	Gravitational constant
δ	Declination
α	Right ascension
$\vec{X}_{\oplus}$	Barycentric coordinates of the geocenter
$\vec{V}_{\oplus}$	Barycentric velocity vector the geocenter

$\hat{K}$	The unit vector which Neglects the gravitational bending effects
U	Geo-centered gravity potential created by neglecting the effects of Earth mass
$\vec{R}_{\oplus\odot}$	Vector from the Sun to the geocenter
$M_{\oplus}$	Rest mass of the Earth
M_J	Rest mass of the J^{th} gravitating body
oc	Subtracting the computed value from the observed value for the relevant observation
ε	Elevation cut-off angle
ΔL_{trop}	Slant path delay
$N_{h,w}$	Hydrostatic and wet refractivities
n	Refractive index
$\Delta\tau_{clk}^{POLY}(t)$	Clock delay error at the t exhibited by quadratic polynomial
$\Delta\tau_{clk}^{CPWLOF}(t)$	Clock delay error at the t exhibited by CPLWO function
$m_g(\varepsilon)$	Gradient mapping function
P	Pressure in hPa
φ	Latitude
h	Height
p_{w0}	Pressure of water vapour
T_0	Surface temperature
$S-G$	Bending effect
$a_{h,w}, b_{h,w}, c_{h,w}$	Hydrostatic and wet coefficients
xp, yp	Polar coordinates
dφ, dε	Celestial pole offsets
G	Geometric path that can be defined as the part of a signal in vacuum
S	Slant radio wave path beteen the geodetic instrument and the highest part of the troposphere, plus bending effect
$Q(t)$	CIO based transformation matrix between CIRS and GCRS arising from the motion of the CIP at the epoch t in GCRS

$R(t)$	Rotation matrix with $-ERA$ at epoch t around the CIP pole or the rotation between TIRS and CIRS around their third axis (CIP axis)
$W(t)$	Transformation between ITRS and TIRS arising from the motion of the CIP in TRS at the epoch t in GCRS

Abbrevation

AGN	Active Galactic Nucleus
BCRS	Barycentric Celestial Reference System
BIH	Bureau International de l'Heure
BTS	BIH Terrestrial Reference System
CIP	Celestial Intermediate Pole
CIRS	Celestial Intermediate Reference System
CIO	Celestial Intermediate Origin
CPWLO	Continuous Piece-wise Linear Offset
CRF	Celestial Reference Frame
CRS	Celestial Reference System
CTP	Conventional Terrestrial Pole
CW	Chandler Wobble
DAO	Data Assimilation Office
DORIS	Doppler Orbitography and Radiopositioning Integrated by Satellite
EA	Elevation cut-off angle
ECMWF	European Center for Medium-Range Weather Forecasts
EOP	Earth Orientation Parameters
ERA	Earth Rotation Angle
ERP	Earth Rotation Parameters
FCN	Free Core Nutation
FK5	Fifth Fundamental Catalogue
GCRF	Geocentic Celestial Reference Frame
GCRS	Geocentric Celestial Reference System
GEO	Group on Earth Observation

GEOSS	Global Earth Observation System of Systems
GGOS	Global Geodetic Observation System
GHz	Gigahertz
GNSS	Global Navigation Satellite System
GPS	Global Positioning System
GSFC	Goddard Space Flight Center
GST	Greenwich Sidereal Time
HCRF	Hipparcos Celestial Reference Frame
IAA	Institute of Applied Astronomy
IAG	International Association of Geodesy
IAU	International Astromical Union
ICRF	International Celestial Reference Frame
IDS	International Doris Service
IERS	The International Earth Rotation and Reference Systems Service
IGS	International GNSS Service
ILRS	International Laser Ranging Services
IMCCE	Institut de Mécanique Céleste et de Calcul des Ephémérides
IMF	Isobaric Mapping Functions
ITRF	International Terrestrial Reference Frame
ITRS	International Terrestrial Reference System
IUGG	International Union of Geodesy and Geophysics
IVS	International VLBI Service
JPL	Jet Propulsion Laboratory
LLR	Lunar Laser Ranging
LOD	Length of Day
MF	Mapping function
MJD	Modified Julian Date
MTT	MIT Temperature Mapping Function
NCEP	National Centers for Environmental Prediction
NMF	Niell Mapping Function
NNR	No Net Rotation
NRO	Non Rotating Origin
NWM	Numerical Weather Model
SSB	Barycentre of Solar System

TEC	Total Electron Content
TIO	Terrestrial Intermediate Origin
TIRS	Terrestrial Intermediate Reference System
TRF	Terrestrial Reference Frame
TRS	Terrestrial Reference System
UT	Universal Time
VLBI	Very Long Base Interferometry
VieVS	Vienna VLBI Software
TCB	Barycenric Coordinated Time
TCG	Geocentric Coordinate Time
TEC	Total Electron Content
WVR	Water Vapour Radiometer
VMF	Vienna Mapping Function
ZHD	Zenith hydrostatic delay
ZWD	Zenith wet delay
ZTD	Zenith total delay

1. INTRODUCTION

VLBI works, basically, with the principle of observing radio wave signals, coming from the celestial bodies (of which coordinates are defined in celestial reference frame (CRF)), with the antennas on the Earth (of which coordinates are defined in terrestrial reference frame (TRF)) so that e.g. EOP, station positions and velocities are estimated (Schuh and Böhm, 2013). The signals are exposed to delay during the passage through the solar system bodies due to gravitation as well as when propagating through ionosphere and troposphere which should be modeled with VLBI sessions analysis (Sovers, Fanselow and Jacobs, 1998).

The biggest error source affecting the space geodesy techniques observations is the troposphere mainly due to its wet component. The signals coming from the space-fixed sources to the Earth-fixed stations are exposed to delay effects during their passage through the troposphere. While these effects are less in the zenith direction of the antenna, it increases as towards the horizon. While the dry part of the troposphere can be modelled accurately, the wet part of the troposphere is difficult to model and has a grave impact on the station coordinates, source coordinates and EOP (Fleagle and Businger, 1980). On the other hand, since the troposphere is rapidly varying in time and in space, modelling of troposphere wet part with Earth surface based measurement seems not possible. Thus, the ZWD is estimated from the measurements of the radio wavelength space geodetic techniques e.g. VLBI. As the elevation angle (EA) decrease, the stratified troposphere mapping function (MF) value increases. This would result in also an increase in the erorr of the MF. The readers are referred to several troposphere delay MF based studies, among others, e.g. Marini (1972), Herring, Gwinn and Shapiro (1986), Herring (1992), Davis et al. (1985); Ma, Ryan and Caprette (1992); Argus (1996), and Sovers, Fanselow and Jacobs (1998).

One of the biggest contributions of VLBI is that it contributes to the realization of several space reference systems, so-called as terrestrial and celestial. For instance, ICRF3 celestial catalogue (Fey et al. 2015) were prepared constitutes of the coordinates of about 5000 celestial sources (defining and candidate) (Ma et al. 1998). Source positions can be estimated using global VLBI solutions using large data sets, but situations such as jet anomalies caused by the structure of quasars have a restrictive effect on source position accuracy. However, continuous observations with the same VLBI data can be considered an effective mechanism to correct these effects. As a result of each session with VLBI sessions, comparative coordinates of the sources are determined with some biases. In this way, the position components obtained for the same source as a result of different sessions are associated with each other and the source positions are determined with the accuracies at μas level. ICRF is one of the most momentous VLBI products. The effect of the troposphere delays on the source coordinates is one of the main research topics in recent years in space geodesy (Charlot et al., 2018). Tropospheric effects should be taken into consideration to advance the accuracy of space geodetic observations as well as the crustal (linear) and tidal (harmonic) displacements on the positions of the stations. Precise estimation of the crust-fixed station coordinates at the level of millimeters as well as their velocities at sub-millimeter per year level contribute significantly to the determination of accurate ITRF solutions (Boucher et al., 1996; Elgered et al., 1991; Fallon and Dillinger, 1992; Teitelbaum et al., 1996; Schlüter and Behrend, 2007; Altamimi et al., 2016).

The EOP are monitored by the four-space geodesy techniques as referenced in geodesy scientific field. The official combined set of EOP parameters, e.g. the IERS 14 C04 daily combined EOP series as observed by the aforementioned four space geodesy techniques and updated two times in a week with one-month latency, is maintained by the IERS (Bizouard, et al. 2018). One of these space geodesy techniques, VLBI observes the advent time difference of the radio wave signals coming from quasar to the crust-fixed radio telescopes. In this technique, contrary to GNSS continuous observation cannot be performed but pre-scheduled 1 to 2-hour intensive sessions and 24-hour sessions are carried out by the IVS (Schuh and Behrend, 2011), as of 1999. On the other hand, the very first intercontinental VLBI experiments go back much earlier, almost half a century ago.

The purpose of this thesis is to assess the effects of using various troposphere delay MFs, i.e. VMF1, VMF3, GMF3, as well as EAs, i.e. 5, 7, 10, 15 degrees, on the estimated daily coordinates of the VLBI stations, the daily coordinates of the radio sources, the daily EOP and the ZTD at 20-minute intervals. The (WM) differences (mean biases) and the WRMS differences between the estimated parameters in addition to the (WRMS) repeatabilities of the parameters are used as the assessment criteria when various tropospheric delay MFs and EAs are introduced in the analysis. In this thesis; the effects of the troposphere delay estimation on station positions, source positions and EOP are examined. At first, a rough process list is created by processing the daily sessions from 2000 to 2018. The sessions of which a posteriori standard deviation of unit weightexceeds 2 cm are assumed to be not accurate enough for our purpose so these sessions were removed from our process list. As a result, 2483 daily sessions were obtained that ensure our accuracy criteria of unit weight a posteriori standard deviation. In order to eliminate the outlier observations a simple outlier test is introduced. As an objective and unbiased criteria the (WRMS) repeatabilities were calculated for each set of the estimated parameters such as the troposphere ZTD, station positions, source positions and EOP. Finally, the (WRMS) of the estimated parameters as the repeatabilities were interpreted.

This thesis comprises in total 7 chapters. Each of them is briefly explained as follows: Chapter 2 covers the basics of the VLBI technique, the delay (observation) model, the differentiation of the estimated parameters according to the delay model as used in the analysis, and the piecewise linear offset functions for the estimation of sub-daily parameters. Chapter 3 explains the modeling of the radio wavelength signal delays when propagating through the troposphere, the linear troposphere delay model employed during the radio wavelength space geodesy techniques analysis, the azimuthally symmetric and asymmetric delay models, and the MFs considered in this study. Chapter 4 describes the CRS, TRS, and the EOP in brief. Besides, following the IERS Conventions 2010, the equations which are used in VLBI observations analysis for the conversion between the GCRS and the ITRS are presented (Petit and Luzum 2010). In Chapter 5, the IVS daily sessions, the global VLBI network and methodology considered in this study are introduced. Chapter 6 involves the results of the effects of using various troposphere MFs (VMF1, VMF3, GMF3) and EAs (5, 7, 10, 15 degrees) on the estimates of the ZTD, the EOP, the CRF and the TRF positions of the quasars, and the VLBI stations, respectively. Chapter 7 includes some conclusions drawn from the results.

2. VERY LONG BASELINE INTERFEROMETRY (VLBI)

2.1. VLBI basics

The differences between the arrival time of the signals in S and X band emitted from distant radio sources to more than one station on the crust of the Earth are measured by space geodetic technique, namely VLBI. Separate terms for extragalactic radio sources are used in different literature such as radio quasars or quasi-stellar radio sources. The target of the VLBI antennas as radio sources are to determine as the centers of the galaxies (AGN: active galactic nucleus) at distances expressed in billions of light-years (5 to 8 billions of light-years) from our galaxy. AGN of a galaxy emits very strong radio signals containing random noise which is called jet stream. Among those galaxies that consist of AGN and of which jet stream is rotating towards our galaxy are called blazars and these are selected as geodetic VLBI radio sources (Ma and Feissel, 1997; Schuh and Böhm, 2013).

VLBI technique utilizes from the propagation of the radio signals thus like the other space geodesy techniques affected by the atmosphere i.e. troposphere and ionosphere. VLBI is the peerless method that is used to observe the Universal Time (UT1), coordinates of the CIP in a coordinate system which is Earth-fixed i.e. polar motion components as well as in a space-fixed system in short nutation components. Besides, VLBI is the peerless for the realization of the ICRF, among the space geodetic techniques and atmospheric, geodynamic and astronomical parameters are produced using the measurements of VLBI technique. The history of the IVS has begun towards the end of the 1970s, but the year when it has been recognized by the IAG and IAU was 1999. From that day forward the VLBI has made significant progress in every sense (Schlüter and Behrend, 2007; Schuh and Böhm, 2013).

VLBI radio telescopes (antennas) are the basic equipment needed to detect the radio signals emitted from radio sources. They are constructed at long distances to each other to form a global network that covers the Earth as much as possible to identify the Earth orientation and to better determine the coordinates of the sources (Schuh and Böhm 2013; Campbell, 1979; Sovers, Fanselow and Jacobs, 1998; Campbell, 2000; Schuh, 1987; IVS, 2020). Since VLBI antennas are at different distances from the sources, the duration of the arrival of the radio signals to each station is different. State of the art technology detection systems and computers are needed to handle and process such weak signals coming from far sources. Hydrogen masers are used at each station to accurately monitor the time in atomic time scale. This time information and radio signals are transmitted electronically to the correlator in suitable formats. In the IVS analysis centers, the positions of the telescopes and sources as well as the EOP are estimated using the arrival time differences of the radio wavefronts of the signals coming from quasars to at least two telescopes i.e. the delay observable. But before to produce the delay observation a cross-correlation between the group phases in S and X band signals are performed in the correlators where several phases are detected at several frequencies. Then, the fringe fit process is carried out to fit a line to the scattered phases at different frequencies in least-squares sense. The rate of the fitted line is the so-called delay observable used for the analysis. In other words, the delay observable is the mean ratio of the observed phases to their frequencies (Carter and Robertson, 1986).

The measurement period of the VLBI is mostly 24-hours. The integration time of the VLBI antennas to these weak and hard-to-process signals coming from radio sources usually ranges from 2 minutes to 13 minutes. The frequencies of these radio signals are received X and S band, at 8.2-8.6 GHz and 2.25-2.35 GHz, while the wavelengths are 13 and 3.5 centimeters. The signals from the quasars reach the stations in the form of a plane wavefront. The right triangle formed to define the baseline vector is reduced to a rectangular shape to form a direct relationship between the source and the baseline vector. If the signal reception instant of the first antenna is t_1 and the second antenna is t_2, then the difference between these epochs is the observed delay $\tau = t_1 - t_2$ at the proper time (Campbell, 2000; Schuh, 2000). The basic VLBI observation equation is

$$\tau = -\frac{\underline{b} \cdot \underline{s}_0}{c} = t_2 - t_1 \tag{2.1}$$

where b, s and c indicates the baseline and source vector and the light velocity in an environment which is vacuum. To accurately measure the angle between baseline and the source, these two vectors should be transformed to a common coordinate system to be used in the observation equation (see e.g. Figure 2.1.) (Schuh, 2000).

A time tag is added to the recorded data using absolute and accurate atomic clocks then this data is sent to the corresponding correlation center to obtain the group delay by cross-correlation. Using these delays, the baselines and other geodetic parameters can be obtained at the level of centimeter accuracy.

The radio signal coming from the sources towards the antennas participating in the sessions is already being interfered by the intergalactic space, the sun, and the atmosphere surrounding the Earth until it reaches the first antenna. The time of the difference between the time spent by the first signal on the path and the signal arrival time to the second antenna, the Earth continues its natural course and all these variables must be taken into consideration during the analysis of the observation (Sovers, Fanselow and Jacobs, 1998).

Once these signals are received, processed and registered by each participating antenna, the analysis of the VLBI session can be started. The recorded signals in the attendant antennas are correlated in pairs to generate the interference pattern. Correlators are composed of special hardware that is created to connect and process signals. In this way, arrival time difference of radio signal between multiple stations is obtained by comparing recorded data streams. The correlation progression is performed in many frequency channels and the phases are generated mainly every few seconds in these channels (Thomas, 1980; 1981; 1987; Moran, 1976). The results obtained from this process are recorded by post-correlation software for later analysis. Post-correlation software enables to acquire phase samples from diverse times and frequency channels. During the software, phase calibration and fitting these parameters are applied. As a result, delay of group and phase, and phase delay rate and amplitude can be produced by interferometer (Sovers, Fanselow and Jacobs, 1998). Observation of VLBI process requires a complete interdisciplinary study such as the effect of the internal structure of Earth dynamics, plate kinematics of the Earth, tides, atmosphere, relativity effects on signals. Thus, like the other space geodesy techniques, VLBI is a sophisticated technique for the creation of a global Earth model due to this multidisciplinary structure.

A lot of small tidal effects of periodic and nearly periodic should also be regarded in the space geodesy observations analysis in case millimeter level accuracies are desired on any indirectly observed quantity. The atmospheric effect of the ionosphere delays are easily modeled utilizing on two well-distributed frequencies, while the troposphere delays are more difficult to remove from the observations which makes it as the main source of error in the radio wave length observations (Böhm, Werl and Schuh, 2006; Teke, 2011).

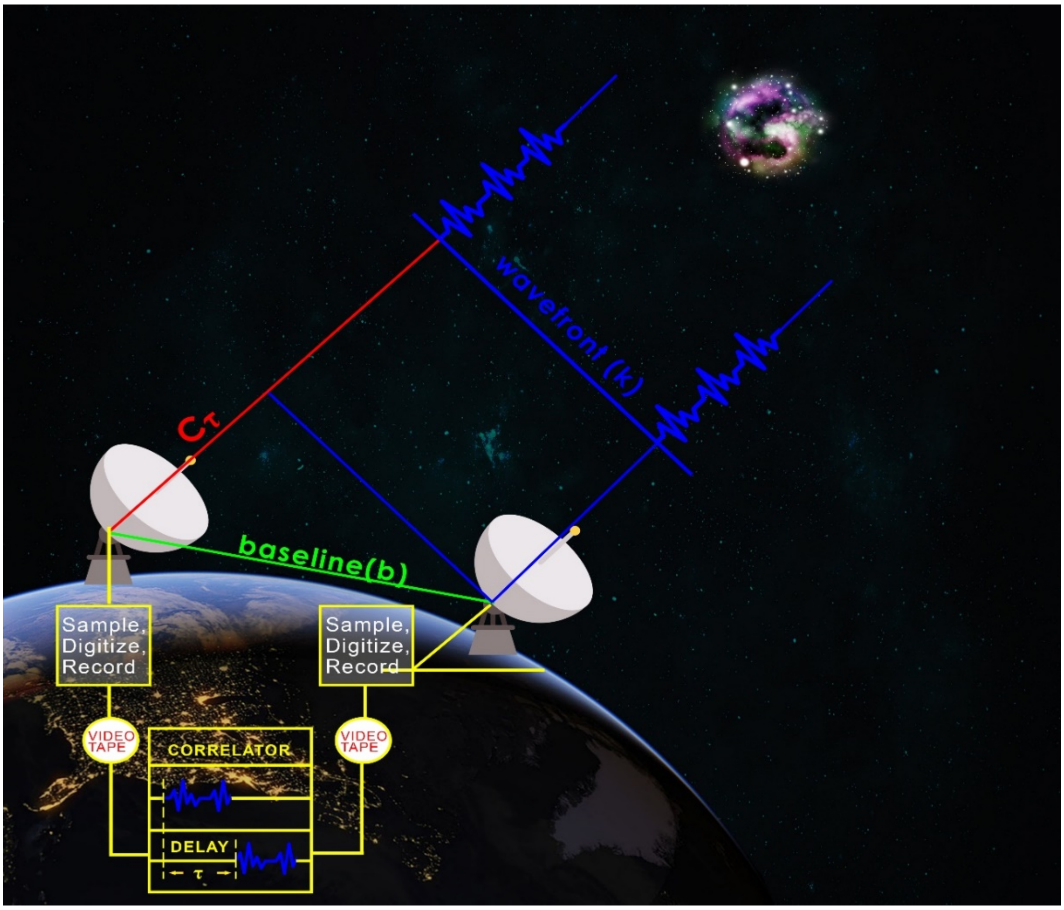

Figure 2.1. Observation session design, data collection and process steps (Sovers, Fanselow and Jacobs, 1998)

2.2. VLBI delay model

VLBI, which operates with the measurement principle of the difference between the arrival times of the wavefront from the quasars to the multiple Earth-fixed antennas, is a geometric technique.

The VLBI identifies the inertial reference frame defined by the source coordinates using multiple time difference observed by a network composed of several antennas at various locations spread around the Earth and also determines the exact positions of the antennas in the TRF synchronically.

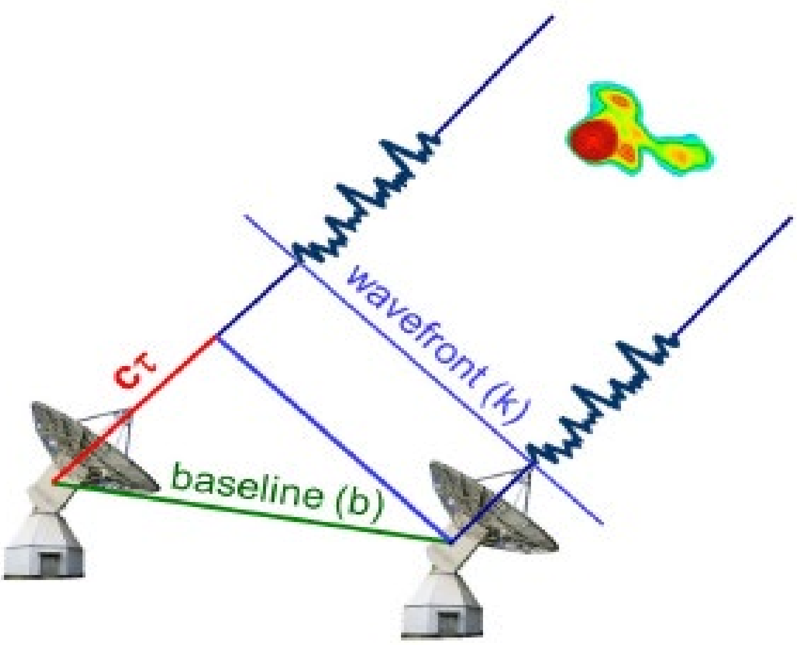

Figure 2.2. VLBI observation principle (Teke, 2011)

The observation equation used for parameter estimation with VLBI is stated as (McCarthy and Petit, 2004);

$$-c \bullet \tau = \vec{b} \bullet \vec{k} + \Delta\tau_{retarded\ baseline} + \Delta\tau_{clock} + \Delta\tau_{trop} + \Delta\tau_{iono} + \ldots \qquad (2.2)$$

$\vec{b}$ is the Earth-fixed baseline vector defined in GCRS, c is the light velocity, $\vec{k}$ is the wavefront propagation direction vector in BCRS (Sovers, Fanselow and Jacobs, 1998). $\Delta\tau_{retarded\ baseline}$ is used to define the correction of the delay at the second antenna's motion in GCRS during the transmission time of the signal between the first and second antenna, $\Delta\tau_{clock}$ is the correction of the delay due to the synchronization of the atomic clocks and the frequency differences in the first station and the second station (Atomic clock readings are set to UTC), $\Delta\tau_{trop}$ the troposphere delay correction and $\Delta\tau_{iono}$ the ionosphere delay correction (Böhm et al., 2010; Teke et al., 2012).

ICRF sources coordinates defined in BCRS which is space-fixed. The mass center of solar system is the origin of BCRS and first axis passes through about the mean vernal equinox of the fundamental epoch, J2000 (1st of January 2000, 12UT). The Earth-fixed international ITRS of which origin is designated to Earth-centred, provides the definition of the positions of the VLBI antennas. Additionally, the other coordinate system in use is GCRS, which accepts the mass center of the Earth as its origin and does not kinematically rotate. The delay is obtained in GCRS by subtracting the arrival times between the second and first station. The delay, which is the difference between the arrival time of the second and first antenna, is reckoned in GCRS. Besides, arrival time of the first antenna is considered as the default reference time for use in all processes. The clocks on the VLBI antennas run on a UTC time scale and arrival time of the first antenna contains the tropospheric effects so UTC time tag is added. First, for each observation, the velocity corrections due to the plate motions, eccentricities and the tidal effects are taken into the a priori coordinates of the stations (ITRF catalogue) as usually done for all VLBI observations analysis. Hence, the antenna ITRF coordinates at the observation epoch are created as X_{ITRS} and the conversion from ITRS to GCRS at an observation epoch expressed as (Petit and Luzum, 2010):

$$X_{GCRS} = Q(t) \cdot R(t) \cdot W(t) \cdot X_{ITRS} \tag{2.3}$$

the CIP motion in TRS is denoted by $W(t)$, the Earth rotation around the CIP and the CIP motion in GCRS is indicated by $R(t)$ and $Q(t)$ transformation matrices, respectively. The observation epoch t used in Equation 2.3 is the equivalent of t_1 which is the elapsed time in TT from the standart (fundamental) epoch in Julian centuries can be derived as follows (McCarthy and Petit, 2004):

$$TT = t_1 + (32.184 + leap\,\mathrm{sec}onds)/86400 \tag{2.4}$$

where $TT = TAI + 32.184$ seconds and leap seconds is so called as TAI-UTC. Representation of the transformation matrix resulting from polar motion, independently of Equinox-based or CIO based transformation procedures:

$$W(t) = R_3(s') \cdot R_2(xp) \cdot R_1(yp) \tag{2.5}$$

the coordinates of CIP in ITRS are polar coordinates, xp and yp. s' is the TIO locator involves the rotation of Earth about the CIP:

$$s' = -47 \cdot 10^{-6} \cdot t \tag{2.6}$$

which gives the TIO position on the equator. The subscripts of the transformation matrices 1, 2 and 3 are the values indicating which axis to rotate with a positive angle. s' is only affected by the most predominant changes in polar motion. Chandlerian and annual oscillations use instant average amplitude (Lambert and Bizouard, 2002; Capitaine, Guinot and Souchay, 1986).

$$R(t) = R_3(-ERA(t_u)) \tag{2.7}$$

ERA is defined on the CIP equator, so called Earth rotation angle, observed between CIO and TIO and as shown:

$$ERA(t_u) = 2\pi(ERA_0 + ak \bullet t_u) \tag{2.8}$$

ak and ERA_0 constants are 1.00273781191135448 and 0.7790572732640, and t_u is UT1 epoch in modified Julian days (MJD) when observation is performed as follows:

$$UT1 = t_1 + \Delta UT1 / 86400 \tag{2.9}$$

The matrix involves nutation/precession resulting from the CIP's movement in GCRS (rotates from CIRS to GCRS) shown as follows:

$$Q(t) = R_3(-E) \cdot R_2(-d) \cdot R_3(E) \cdot R_3(s) \tag{2.10}$$

$$E = \arctan \frac{Y}{X} \tag{2.11}$$

E is derived from the GCRS coordinates of the CIP as well as d shown as:

$$d = \arccos(\sqrt{1 - X^2 + Y^2}) \tag{2.12}$$

and where the s gives the CIO position on the equator of CIP and so called CIO locator when the CIP and GCRS move together in accordance with the NRO explication in the GCRS.

$$s = s_0 - \frac{XY}{2} \tag{2.13}$$

CIO locator is the quantity from the standart epoch to the date, t, exposed by the nutation/precession (McCarthy and Petit, 2004; Capitaine, Guinot and McCarthy, 2000; Capitaine et al., 2002). After estimating the VLBI antenna coordinates at observation time of, delays acting on the observations are calculated at the relevant observation time.,

2.2.1. Gravitational delay model

As explained by Einstein (1911, 1916) in the Theory of General Relativity, temporal difference occurs between the propagation of a microwave signal in the gravity and vacuum field. The signal propagated in the gravitational field lags in comparison of the propagation time in the vacuum field and affects VLBI. Because the difference value in the arrival time of the signal to the VLBI stations must be corrected in terms of gravitational effects. In addition, considering the effects of general relativity, not just a time delay but also a delay caused by a deflection from the plain path owing to the relativity effect of the signal shall be taken into account (Shapiro, 1964, 1967).

The theory of general relativity causes the delay for the gravitating body, J^{th}, can be computed as,

$$\Delta T_{gravJ} = 2\frac{GM_J}{c^3}\ln\frac{|\vec{R}_{1J}|+\vec{K}\cdot\vec{R}_{1J}}{|\vec{R}_{2J}|+\vec{K}\cdot\vec{R}_{2J}} \tag{2.14}$$

where the absolute length of vector between the antenna and gravitating body is symbolised as $\vec{R}_{iJ}$. $|\vec{x}|=\sqrt{\sum x_i^2}$. $\vec{K}$ defined in vacuum environment from the barycenter to the source,

$$\vec{K} = \left[\cos\delta\cos\alpha \;\; \cos\delta\sin\alpha \;\; \sin\delta\right] \tag{2.15}$$

where the right ascension and declination are the components defined in the BCRS, those are used for denoting the quasar positions and depicted by α and δ. The Earth-caused signal gravitational delay is calculated,

$$\Delta T_{grav\oplus} = 2\frac{GM_\oplus}{c^3}\ln\frac{|\vec{x}_1|+\vec{K}\cdot\vec{x}_1}{|\vec{x}_2|+\vec{K}\cdot\vec{x}_2} \tag{2.16}$$

$M_\oplus$ is the Earth mass and $\vec{x}_i$ represents the antenna coordinates defined in GCRS in t_1. (McCarthy and Petit, 2004; Kopeikin and Schafer, 1999). Not only the Sun and the Earth but also the all solar system planets must be taken into account. In very close observations to some massive planets, additional unknowns shall regard to obtain the ambiguity of the 1 picoseconds (Klioner, 1991).

While the passage of ray nearest to the gravitating body the vector, $\vec{R}_{iJ}$, and time correction to t_1 should be calculated as,

$$t_{1J} = t_1 - \frac{\vec{K}(\vec{X}_J(t_1)-\vec{X}_1(t_1))}{c} \tag{2.17}$$

$$\vec{X}_J(t_{1J}) = \vec{X}_J(t_1)+\vec{V}_J(t_{1J}-t_1) \tag{2.18}$$

where $\vec{X}_J$ and $\vec{V}_J$ symbolize the barycentric coordinate and velocity vector of J^{th} gravitating body. X_J and t_{1J} can be found by an iterative approach. The difference vector from the gravitating body to the first antenna can be shown as,

$$\vec{R}_{1J}(t_1) = \vec{X}_1(t_1) - \vec{X}_J(t_{1J}) \tag{2.19}$$

where the barycentic coordinates of the i^{th} antenna $\vec{X}_i$ at epoch t_1 can be obtained from barycentric coordinates of the geocenter $\vec{X}_{\oplus}(t_1)$ and the GCRS coordinates of the antenna, $\vec{x}_i(t_1)$ is given by,

$$\vec{X}_i(t_1) = \vec{X}_{\oplus}(t_1) + \vec{x}_i(t_1) \tag{2.20}$$

the signal arrival time difference between the first and second antenna is regarded in the vector from the any other planet in the solar system to second antenna as,

$$\vec{R}_{2J} = \vec{X}_2(t_1) - \frac{\vec{V}_{\oplus}}{c}(\vec{K}\cdot\vec{b}) - \vec{X}_J(t_{1J}) \tag{2.21}$$

$V_{\oplus}$ and $\vec{b}$ are the barycentric geocenter velocity vector and the baseline vector on GCRS at t_1, the sum of all gravitational delays of the planets in solar system including the Earth, is the total gravitational delay.

$$\Delta T_{grav} = \sum_{j} \Delta T_{gravJ} \tag{2.22}$$

2.2.2. Geometric delay model

In the observed delay, the largest part belongs to the geometric component. The total geocentric geometric vacuum delay is formed as

$$t_{\upsilon_2} - t_{\upsilon_1} = \frac{\Delta T_{grav} - \dfrac{\hat{K}\cdot\vec{b}}{c}\left[1 - \dfrac{(1+\gamma)U}{c^2} - \dfrac{\left|\vec{V}_{\oplus}\right|^2}{2c^2} - \dfrac{\vec{V}_{\oplus}\cdot\vec{\omega}2}{c^2}\right] - \dfrac{\vec{V}_{\oplus}\cdot\vec{b}}{c^2}(1+\hat{K}\cdot\vec{V}_{\oplus}/2c)}{1+\dfrac{\hat{K}\cdot(\vec{V}_{\oplus}+\vec{\omega}_2)}{c}} \tag{2.23}$$

where VLBI antenna regarding the gravitational but ignoring the atmospheric propagation delay and variation in geometric delay due to atmospheric propagation delay. $\hat{K}$ is the unit source vector, which neglects the gravitational bending effects, $\vec{b}$ the baseline vector at the arrival time in the GCRS. $\vec{V}_{\oplus}$ and $\vec{w}_i$ are the velocity, w.r.t. the geocenter and barycenter, of related antenna. γ is 1 in general relativity and U is a geo-centered gravity potential created as a result of ignoring the Earth mass effects (Soffel et al., 1991; Kopeikin, 1990).

$$U = \frac{GM_{\odot}}{\left|\vec{R}_{\oplus\odot}\right|} \tag{2.24}$$

remaining Earth mass and the vector from the Sun to the Earth centre are denoted by $M_{\odot}$ and $\vec{R}_{\oplus\odot}$ (Eubanks, 1991; Sovers and Jacobs, 1994; Treuhaft and Thomas, 1991). The vectors used in the gravitational and vacuum parts of the delay model such as $\vec{X}_{\oplus}$ and $\vec{X}_J$ can be obtained from the planetary ephemeris. While the signal is passing through the troposphere exposed to propagation delay. By means of geometric part of this delay the vacuum delay is collected and then the geometric delay is attained,

$$\vec{k}_i = \vec{K} + \frac{\vec{V}_{\oplus} + \vec{\omega}_i}{c} - \vec{K}\frac{\vec{K}\cdot(\vec{V}_{\oplus} + \vec{\omega}_i)}{c} \tag{2.25}$$

where δt_{atm1} is the troposphere hydrostatic delay at at the t_1 observation epoch:

$$\delta t_{atm1} = \frac{\Delta L_h^{st(1)}(t_1)\cdot m_h^{st(1)}(\varepsilon, t_1)}{c} \tag{2.26}$$

where $\Delta L_h^{st(1)}(t_1)$ indicates troposphere dry delay for receiver first in epoch t_1 and m_h is the dry MF and ε the EA. To obtain the total delay $(t_2 - t_1)$, other delays are added and then can be obtained as,

$$t_2 - t_1 = t_{g2} - t_{g1} + \tau_{thermdef12} + \tau_{axisoffset12} + \tau_{trop12} \tag{2.27}$$

where the azimuth of the observation and after transforming to TRF the zenith distance is reckoned from the deviated source vector. Hence, MFs, wet and dry delays and gradients of troposphere are fixed for the aberration effect. The VLBI observation also includes an ionospheric delay as well as the observation delay therefore the delay of the ionosphere (oc) is considered to be created from the observed delay and shown (Böhm et al, 2010; McCarthy and Petit, 2004)

$$oc = \tau_{observed} - (t_2 - t_1) \tag{2.28}$$

where the oc vector contains the delays caused by the troposphere wet part (Teke, 2011; Sovers, Fanselow and Jacobs, 1998; Titov, Tesmer and Böhm, 2004).

2.2.3. Partial differentiation of the VLBI delay model w.r.t. EOP, as well as the antenna and source coordinates

The simple observation model calculated:

$$\tau = \vec{K} \cdot Q \cdot R \cdot W \cdot \vec{b} \tag{2.29}$$

where $\vec{K}$ denotes the unit source vector without aberrational or gravitational bending in BCRS. $\vec{b}$ the baseline vector at the arrival time in TRS.

The partial differentiations of the simplified VLBI delay model (Equation. 2.29) according to the x_p:

$$\frac{\partial \tau}{\partial x_p} = \vec{K} \cdot Q \cdot R \cdot \frac{\partial W}{\partial x_p} \cdot \vec{b} \tag{2.30}$$

and

$$\frac{\partial W}{\partial x_p} = R_3(s') \cdot \begin{bmatrix} -\sin x_p & 0 & -\cos x_p \\ 0 & 0 & 0 \\ \cos x_p & 0 & -\sin x_p \end{bmatrix} \cdot R_1(y_p) \tag{2.31}$$

according to the y_p :

$$\frac{\partial \tau}{\partial y_p} = \vec{K} \cdot Q \cdot R \cdot \frac{\partial W}{\partial y_p} \cdot \vec{b} \tag{2.32}$$

where

$$\frac{\partial W}{\partial y_p} = R_3(s') \cdot R_2(x_p) \cdot \begin{bmatrix} 0 & 0 & 0 \\ 0 & -\sin y_p & \cos y_p \\ 0 & -\cos y_p & -\sin y_p \end{bmatrix} \cdot \tag{2.33}$$

and according to the Earth's rotation phase, UT1, is:

$$\frac{\partial\tau}{\partial(UT1)}=\vec{K}\cdot Q\cdot\frac{\partial R}{\partial(-ERA)}\cdot\frac{\partial(-ERA)}{\partial(UT1)}\cdot W\cdot\vec{b} \tag{2.34}$$

where

$$\frac{\partial R}{\partial(-ERA)}=\begin{bmatrix}-\sin(-ERA) & \cos(-ERA) & 0\\ -\cos(-ERA) & -\sin(-ERA) & 0\\ 0 & 0 & 0\end{bmatrix} \tag{2.35}$$

and

$$\frac{\partial(-ERA)}{\partial(UT1)}=-ak=-1.00273781191135448 \tag{2.36}$$

according to the X:

$$\frac{\partial\tau}{\partial X}=K\cdot\frac{\partial Q}{\partial X}\cdot R\cdot W\cdot\vec{b} \tag{2.37}$$

The celestial pole offsets matrix Q for the CIP motion in CRS involves four matrices which are shown in Equation 2.10.

$$\begin{aligned}\frac{\partial Q}{\partial X}&=\frac{\partial R_3(-E)}{\partial(-E)}\cdot\frac{\partial(-E)}{\partial X}\cdot R_2(-d)\cdot R_3(E)\cdot R_3(s)\\ &+R3(-E)\cdot\frac{\partial R_2(-d)}{\partial(-d)}\cdot\frac{\partial(-d)}{\partial X}\cdot R_3(E)\cdot R_3(s)\\ &+R3(-E)\cdot R_2(-d)\cdot\frac{\partial R_3(E)}{\partial(E)}\cdot\frac{\partial(E)}{\partial X}\cdot R_3(s)\\ &+R3(-E)\cdot R_2(-d)\cdot R_3(E)\cdot\frac{\partial R_3(s)}{\partial s}\cdot\frac{\partial s}{\partial X}.\end{aligned} \tag{2.38}$$

Equations (2.11, 2.12, 2.13) demonstrate the formulas of E, d and s.

$$\frac{\partial(-E)}{\partial X}=\frac{Y}{X^2+Y^2} \tag{2.39}$$

$$\frac{\partial(-d)}{\partial X}=\frac{X}{\sqrt{1-(X^2+Y^2)}\sqrt{X^2+Y^2}} \tag{2.40}$$

$$\frac{\partial s}{\partial X}=\frac{-Y}{2} \tag{2.41}$$

according to the Y:

$$\frac{\partial\tau}{\partial Y}=\vec{K}\cdot\frac{\partial Q}{\partial Y}\cdot R\cdot W\cdot\vec{b} \tag{2.42}$$

where

$$\frac{\partial Q}{\partial Y}=\frac{\partial R_3(-E)}{\partial(-E)}\cdot\frac{\partial(-E)}{\partial Y}\cdot R_2(-d)\cdot R_3(E)\cdot R_3(s)$$

$$+R3(-E)\cdot\frac{\partial R_2(-d)}{\partial(-d)}\cdot\frac{\partial(-d)}{\partial Y}\cdot R_3(E)\cdot R_3(s) \tag{2.43}$$

$$+R3(-E)\cdot R_2(-d)\cdot\frac{\partial R_3(E)}{\partial(E)}\cdot\frac{\partial(E)}{\partial Y}\cdot R_3(s)$$

$$+R3(-E)\cdot R_2(-d)\cdot R_3(E)\cdot\frac{\partial R_3(s)}{\partial s}\cdot\frac{\partial s}{\partial Y}.$$

In Equation (2.43),

$$\frac{\partial(-E)}{\partial Y}=\frac{-X}{X^2+Y^2} \tag{2.44}$$

$$\frac{\partial(-d)}{\partial Y}=\frac{Y}{\sqrt{1-(X^2+Y^2)}\sqrt{X^2+Y^2}} \tag{2.45}$$

$$\frac{\partial s}{\partial Y}=\frac{-X}{2} \tag{2.46}$$

according to the α right ascension of a quasar:

$$\frac{\partial\tau}{\partial\alpha}=\frac{\partial\vec{K}}{\partial\alpha}\cdot Q\cdot R\cdot W\cdot\vec{b} \tag{2.47}$$

where

$$\frac{\partial K}{\partial\alpha}=\begin{bmatrix}-\cos\delta\sin\alpha & \cos\delta\cos\alpha & 0\end{bmatrix} \tag{2.48}$$

and δ declination:

$$\frac{\partial\tau}{\partial\delta}=\frac{\partial\vec{K}}{\partial\delta}\cdot Q\cdot R\cdot W\cdot\vec{b} \tag{2.49}$$

where

$$\frac{\partial\vec{K}}{\partial\delta}=\begin{bmatrix}-\sin\delta\cos\alpha & -\sin\delta\sin\alpha & \cos\delta\end{bmatrix} \tag{2.50}$$

The partial differentiations of the model according to the TRF coordinates of an antenna, for example the X coordinate of the first station:

$$\frac{\partial \tau}{\partial X_{st1}} = \vec{K} \cdot Q \cdot R \cdot W \cdot \frac{\partial \vec{b}}{\partial X_{st1}} \tag{2.51}$$

where

$$\frac{\partial \vec{b}}{\partial X_{st1}} = \begin{bmatrix} 1 \\ 0 \\ 0 \end{bmatrix} \tag{2.52}$$

2.2.4. PLO parameter estimation functions for sub-daily

In VLBI observations analysis by using the VieVS (Böhm et al. 2018), ZWDs are generally estimated in every 20-60 minutes. In VieVS, only the piecewise linear offsets (PLO) are used which means that offsets-based functional model and conjectured at UTC integer hours (such as 09, 14, 00, …), at fractions (such as 15.20 UTC, 00.40 UTC, …) or multiples of UTC integer hours (such as 18, 00, 6, …). The piecewise linear offset functions are formed as follows:

$$x_i = x_1 + \frac{t - t_1}{t_2 - t_1}(x_2 - x_1) \tag{2.53}$$

where x_1 and x_2 are the estimated parameters at epochs t_1 and t_2, x_i are the functional values at epoch t which are the values of the corresponding parameters at the observation epochs.

In "vie_lsm" which is the parameter estimation module of VieVS, it is possible to estimate parameters as PLO, such as quasar CRF and station TRF coordinates, EOP, zenith wet delays and errors of clock. The partial differentiations of the simplified delay mode1 according to the parameter x_i

$$\frac{\partial \tau(t)}{\partial x_1} = \frac{\partial \tau(t)}{\partial x_i} \cdot \frac{\partial x_i}{\partial x_1} \tag{2.54}$$

$$\frac{\partial \tau(t)}{\partial x_2} = \frac{\partial \tau(t)}{\partial x_i} \cdot \frac{\partial x_i}{\partial x_2} \tag{2.55}$$

the partial differentiation of PLO according to the x_1 and x_2 sequential offsets are:

$$\frac{\partial x_i}{\partial x_1} = \left[1 - \frac{t - t_j}{t_{j+1} - t_j}\right] \tag{2.56}$$

$$\frac{\partial x_i}{\partial x_2} = \left[\frac{t - t_j}{t_{j+1} - t_j}\right] \tag{2.57}$$

In Figure 2.3. the presentation of the PLO functions is illustrated.

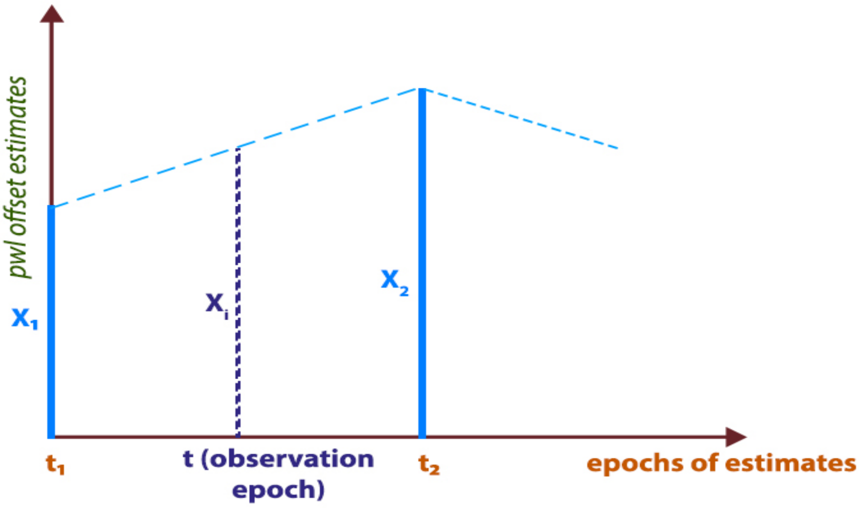

Figure 2.3. PLO function representation (Teke, 2011)

It should be taken into account that the t may provide the following condition: $t_j < t < t_{j+1}$.

For instance, the partial differentiation of mode1 according to the $UT1$ can be derived at t

$$\frac{\partial \tau(t)}{\partial (UT1)_{x_1}} = \frac{\partial \tau(t)}{\partial (UT1)} \cdot \frac{\partial (UT1)}{\partial x_1} \tag{2.58}$$

$$\frac{\partial \tau(t)}{\partial (UT1)_{x_2}} = \frac{\partial \tau(t)}{\partial (UT1)} \cdot \frac{\partial (UT1)}{\partial x_2} \tag{2.59}$$

The partial differentiation of the mode1 according to the coordinates of first antenna ($st1$), as the X coordinate:

$$\frac{\partial \tau(t)}{\partial (X_{st1})_{x_1}} = \frac{\partial \tau(t)}{\partial (X_{st1})} \cdot \frac{\partial (X_{st1})}{\partial x_1} \tag{2.60}$$

$$\frac{\partial\tau(t)}{\partial(X_{st1})_{x_2}}=\frac{\partial\tau(t)}{\partial(X_{st1})}\cdot\frac{\partial(X_{st1})}{\partial x_2} \tag{2.61}$$

2.3. VLBI Clock Error

VLBI modeling utilizes the all numerical values, such as the radius and velocity vectors of the station and celestial coordinates of the bodies which cause the gravitation on the signal, as the function of time. The most significant step here is to transform the UTC time tag which is added for each observation to the appropriate time scale is used to calculate the all VLBI model constituents. Therefore, types of time and the connection between them are of great importance. Time systems can be examined in two main topics: astronomical (universal and sidereal) and dynamic systems. While astronomical predicates on the Earth motions, dynamic follows the law of gravity and predicate on the orbital motions of solar system bodies, independent from the Earth rotation. And the other time kind is the atomic which predicates on the time taken by a Celsium atom in the ground state to make a certain number of oscillations (Teke, 2011).

2.3.1. Modeling and estimating VLBI clock errors based on PLO functions

One of the most important components in the VLBI signal delay is the clock error. The observables performed by the VLBI are saved signals with the attached time readings of the antenna clock. The quality of the clock are determined by the accuracy, frequency stability and its sensitivity to environmental factors. Frequency stability and accuracy measurements are made to determine the quality of the clock readings. Frequency stability is a metric that shows the frequency variations between two different time periods. Even if there is a very grave error of frequence accuracy within the clock, it can continue to be stable. Although the elapsed time to complete a minute is inaccurate in frequency, the completion time of two different time periods would be the same (Holman, 2005).

The differences in the frequencies of the clocks, the positions of the quasars and receivers in CRF and TRF cause the VLBI signal delay. Accurate clock error estimation and modeling due to VLBI measurements frequency irregularities are of great importance. In principle, the reference clock for VLBI sessions analysis must be selected with high frequency consistency so as to derive minimum residuals according to the modelled part of the clocks (Herring, Davis and Shapiro, 1990; Schuh, 1987).

2.3.1.1. Clock Error Model

VLBI session analysis, mainly clock errors are estimated as an offset and a rate for each clock w.r.t. a reference clock as PLO using e.g. Gauss Markov least-squares adjustment. For producing more certain VLBI parameter, Herring, Davis and Shapiro (1990) suggested using Kalman Filter to estimate associated clock errors. In "vie_lsm", mainly parameters to be predicted for the VLBI analysis are modeled with the PLO functions using least square at the integer hours, fractions or multipliers of integer hours. Two steps least-squares adjustment is carried out for clock error fixing in VieVS (Böhm et al., 2018) At the initial, ZWD and clock polynomial coefficients offsets are estimated for the all participant stations in the session using the simple polynomial. Then, in the second step PLO functions are used. β_i the polynomial coefficients, x_1 the PLO of clocks at the integer estimation epoch t_1 and x_2 the PLO of clocks at the integer estimation epoch t_2 . Total error at observation epoch calculated as:

$$\Delta\tau_{clk}(t) = \Delta\tau_{clk}^{POLY}(t) + \Delta\tau_{clk}^{CPWLOF}(t) \tag{2.62}$$

The partial differentiations of the Equation (2.62) according to the polynomial coefficients, β_i are:

$$\frac{\partial\Delta\tau_{clk}(t)}{\partial\beta_0} = 1 \tag{2.63}$$

$$\frac{\partial\Delta\tau_{clk}(t)}{\partial\beta_1} = t - t_0 \tag{2.64}$$

$$\frac{\partial\Delta\tau_{clk}(t)}{\partial\beta_2} = (t - t_0)^2 \tag{2.65}$$

The partial differentiations of the Equation (2.62) according to the PLO (x_1 and x_2) are:

$$\frac{\partial\Delta\tau_{clk}(t)}{\partial x_1} = 1 - \frac{t - t_1}{t_2 - t_1} \tag{2.66}$$

$$\frac{\partial\Delta\tau_{clk}(t)}{\partial x_2} = \frac{t - t_1}{t_2 - t_1} \tag{2.67}$$

2.3.1.2. Determining and correcting for the clock breaks

Since clock jumps (breaks) are usually occurs randomly in the analysis of VLBI observations two-step least squares adjustment is carried out in VieVS. In the first least squares adjustment, the epochs of the clock jumps are determined and used as the boundaries of the intervals for spline polynomial fits. For each of these intervals, the clock jumps are fixed through forming a separate clock polynomial for each interval (see Figure 2.4.).

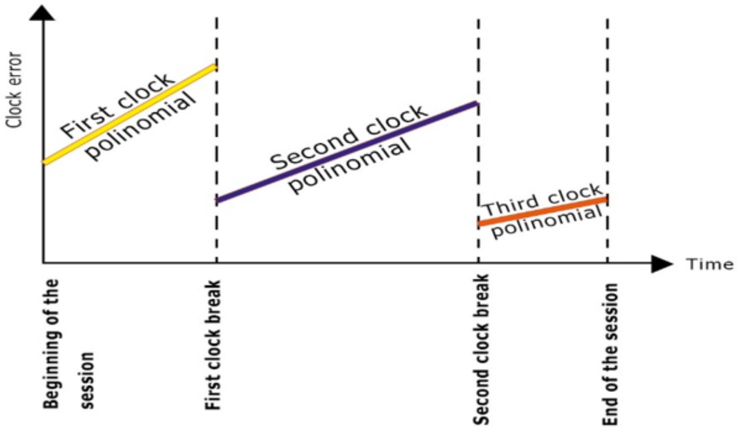

Figure 2.4. A polynomial is fitted for each interval deliminated by the epochs of the clock breaks (Teke, 2011)

Also in the first least squares solution, the clock polynomial types can be selected discretionary. The solution is operated for reducing offsets and fixing jumps as well as for investigating the small errors of clock (Teke, 2011).

3. TROPOSPHERE SIGNAL DELAYS AT RADIO WAVELENGTH FREQUENCIES

For the space geodesy, the atmosphere is mainly examined under two main headings, ionosphere and troposphere. Atmosphere has an influence upon the Earth arising out of the motion of gases and stratified structure with different properties. Clouding, properties of Earth surface, dispersed spreading of land and ocean, the partial heating in the troposphere due to the latitude creates the atmospheric mass model that changes with the variations of temperature and the circulatory system (Salstein, 1995).

Ionosphere starts 100 km from surface of the Earth, extends up to 1000 km. Ionosphere is a dispersive environment for the wavelength signals of radio source and contains free electrons which are due to ionization of solar radiation of neutral molecules. Delay effects of ionosphere on GPS, VLBI and DORIS signals depend on the electron density. An electromagnetic signal passing through ionosphere is affected in two ways. While phase velocity is accelerating, group velocity is decelerating and both effects are same in size but opposite sign. In other words, e.g. GPS code measurements are delayed but carrier phase measurements are accelerated. Therefore, code pseudoranges are longer and phase pseudoranges are shorter compared to geometric length between satellite and receiver. Both are in same size due to the same frequencies they have. The variation in length, which is caused by ionospheric refraction can be limited by determining total electron content (TEC), TEC is varying rapidly both in space and in time. The reason for this is that TEC varies depending on sunspot's movement, seasonal and diurnal variation, azimuth and inclination of signal coming from satellites and position of the receiver (Hofmann-Wellenhof, Lichtenegger and Collins, 1994). At the same time there are several global and local ionosphere models for reducing the ionosphere delays from single frequency measurements. These models can not produce accurate results relatively to those derived from the linear combination of the observations at distinct frequencies (Alizadeh et al., 2013).

Troposphere which is approximately spherical shell, starts from the Earth surface and reach up to 100 km. The lower part of troposphere, up to 50 km from the topography of the Earth constitutes %99 of the whole atmospheric mass (Kertz, 1971). This lower part consists of troposphere where temperature increases with a decrease of altitude. The delay which the signal is exposed to while the passage through the troposphere is usually named as ‘tropospheric delay’ (Hopfield, 1971).

The troposphere is the neutral part, with regard to the electrically, of the atmosphere. Total troposphere delay comprises of hydrostatic and wet parts. There is no significant change of dry air depending on latitudes and heights (Smith and Weintraub, 1953). The water vapor varies widely with both height and latitude. In the meantime, after 10 km, the size of the water vapour goes down to zero (Hopfield, 1971). Dry part of the troposphere delay can be accurately determined using the insitu total pressure observations and the latitude of the site using an analytic function e.g. Saastamoinen (1972). The wet part is difficult to model because of the rapidly varying water vapour in the troposphere both space and time. Although 10% of the total delay is resulted from the delay of wet part (Janes, Langley and Newby, 1989), it causes a restricting ambiguity about finding an accurate solution for total delay.

The tropospheric delay reaches a very large size and becomes more difficult to model when the EA of the observation is less than 10 degrees. The total troposphere delay of the signal in the zenith of the receiver is around 2 meters, and it can be more than 20 meters when the EA is close to 5 degrees. There are several determining methods for the total tropospheric delay owing to the wet component. The most common of these are surface models (eg, Saastamoinen and Hopfield models), radiosonde profiles, water vapour radiometer (WVR) and tropospheric parameter estimation (Standard atmosphere model) (Mekik, 1999).

3.1. Neutral Atmosphere

The electromagnetic microwave signals when propagating through the troposphere are bended and delayed. These retardations are named as troposphere slant path delays, ΔL_{trop}. Slant path delay is also formulised as $\Delta L_{trop} = c \cdot \Delta \tau_{trop}$. If the electromagnetic microwave signals are not exposed to any effect along the troposphere and the light velocity in vacuum environment is the same as the light velocity in the troposphere, the electromagnetic microwave signals could be defined as geometric path, G, also the shortest path by the means of length. The main propagation path of the signal from the top of troposfer (H_{trop}) to the receiver is defined as slant path, S, also the shortest path by the means of time. The skewness of the delay is resulted from the refractivity. Space geodesy researches the refractivity ($N_{h,w}$), through using the refractive index (n), in two principal branch: hydrostatic and wet. The slant path delays can be calculated as (Nilsson et al., 2013):

$$\Delta L = \int_s (n - 1)\, ds = 10^{-6} \int_s N\, ds = 10^{-6} \int_0^{H_{trop}} \left[N_h(s) + N_w(s) \right] ds + S - G \tag{3.1}$$

where the bending effect, $S - G$, is obtained from MFs. Refractivities are considered to compute the delay of wet and hydrostatic and if these delays are projected through the zenith direction (Nilsson et al., 2013):

$$ZHD = 10^{-6} \int_{h_0}^{\infty} N_h(z) \mathrm{d}z \tag{3.2}$$

$$ZWD = 10^{-6} \int_{h_0}^{\infty} N_w(z) \mathrm{d}z \tag{3.3}$$

where h_0 is the station altitude

Equation (3.1) consists of spherical part and non-spherical part. When we look at the contents of these parts, we see that the spherical part is dependent on the EA and non-spherical part is an azimuthally asymmetric part (Davis et al. 1993)

$$\Delta L = \Delta L_{spherical}(\varepsilon) + \Delta L_{non\text{-}spherical}(\alpha, \varepsilon) \tag{3.4}$$

where ε is the EA from local horizon and α the azimuth. Spherical and non-spherical parts of the total slant delay is derived as follows

$$\Delta L_{spherical}(\varepsilon) = ZHD \cdot m_h(\varepsilon) + ZWD \cdot m_w(\varepsilon) \tag{3.5}$$

$$\Delta L_{non\text{-}spherical}(\alpha, \varepsilon) = S - G = m_g(\varepsilon) \left[G_n cos(\alpha) + G_e sin(\alpha) \right] \tag{3.6}$$

G_e and G_n are the troposphere total horizontal gradients (wet plus hydrostatic) in the direction of east-west and north-south. The gradient MF, $m_g(\varepsilon)$ according to MacMillan (1995),

$$m_g(\varepsilon) = m_h(\varepsilon) \cdot \cot(\varepsilon) \tag{3.7}$$

ZHD is determined from the receiver insitu the latitude, the height and the total pressure p , as the input of the (Saastamoinen 1972) function as

$$ZHD = 0.0022768 \frac{p}{(1 - 0.00266 \cdot cos(2\varphi) - 0.28 \cdot 10^{-6} \cdot h)} \tag{3.8}$$

In normal meteorological conditions, ZHD measured at sea level is approximately 2.3 m and 1 mbar error at the surface pressure generates an error about 2 millimetres (Davis et al. 1985).

Pressure values are taken in space geodesy techniques with three ways: empirical, from NWM and making records at the site. However, pressure measurements from local stations are not suitable for use in general (Böhm, Heinkelmann and Schuh; 2009). On the other hand, we can use empirical models for all epochs but in terms of spatial resolution, empirical models are limited due to it is represented by e.g. using the spherical harmonics function degree and order up to 9 (Berg, 1948) so NWM is preferred to obtain a priori values (Böhm, Kouba and Schuh, 2009).

ZWD is more complicated to model than ZHD. Unlike ZHD, the observations of Earth surface measurements are not sufficient for determining the ZWD. ZWD values take different values at the poles and humid regions e.g. the equator, ranges from several millimeters up to 40 centimeters (Nilsson et al., 2013). According to Saastamoinen (1972), ZWD can be associated with the amount of integrated water vapor, temperature by applying ideal gas laws

$$ZWD = 0.0022768(1255 + 0.05T_0)\frac{p_{w0}}{T_0} \tag{3.9}$$

T_0 and p_{w0} denotes surface temperature and water vapour pressure, respectively. Likewise, equation of Hopfield (1969) is

$$ZWD = \frac{10^{-6}}{5} N_w(h_0)h_w \tag{3.10}$$

N_w is the refractivitiy of wet air, h_0 is the height and h_w, equals to 11000m, is the mean height of troposphere. Another formulation given by Mendes (1999) is

$$ZWD \approx \frac{0.217 p_w}{T} \tag{3.11}$$

Generally, by means of the VLBI and GPS observations analysis, the zenith delay is estimated. The MF values are used as the partial differentiations in the design matrix when estimating the e.g. ZWD. The partial differentiations calculated according to the station heights and clocks are clearly known, 1 and $\sin(\varepsilon)$ respectively, while the partial differentiations of the observation delays calculated by the station height depend only on the EA. In the meantime partial differentiations of the zenith delays, e.g. MFs, are known to be of limited accuracy. Nevertheless, any inadequacy and error in the MFs should propagate into the station heights. The errors in ZHDs or MFs have effects on receiver heights to some extent (Böhm, 2004; Niell et al., 2001).

3.2. Troposphere Mapping Function

The troposphere MF is the ratio between the troposphere slant delays at an EA above the local horizon and troposphere zenith delay. The purpose of the MFs is to project zenith delays to the direction of a radio source, or vice versa. If the atmosphere had a flat, smooth and evenly layered structure, the MF would be $1/\sin(\varepsilon)$.

MFs, which are not associated with the azimuth angle of observation, are determined by the coefficients a, b, c in the form of continuous fraction form Marini (1972) produced the continuous fractional form as follows

$$m_{h,w}(\varepsilon)=\frac{1+\dfrac{a_{h,w}}{1+\dfrac{b_{h,w}}{1+c_{h,w}}}}{\sin(\varepsilon)+\dfrac{a_{h,w}}{\sin(\varepsilon)+\dfrac{b_{h,w}}{\sin(\varepsilon)+c_{h,w}}}} \tag{3.12}$$

where the hydrostatic and wet coefficients are indicated as $a_{h,w}$, $b_{h,w}$ and $c_{h,w}$ (Davis et al. 1993). MFs might use the standart atmosphere model (Chao, 1974), or numerical weather models (Niell, 2000; Böhm and Schuh, 2004) for providing the input for the estimation of the MF coefficients.

Herring (1992) produced coefficients for MIT Temperature MF (MTT) in latitude, altitude, and corresponding point temperature. Instead of the standard atmospheric data used by Davis et al. (1985), the radiosonde data was used. The MTT is the MF that is based on a slightly modified type of the widely accepted form recently. Niell (1996) has developed a new MF because the MTT is highly dependent on the surface temperature (Herring, 1992). Initially this MF was called New MF but later and nowadays it is being called Niell MF.

Niell Mapping Function (NMF)

The day of year, latitude and height of the station are input parameters. The standard atmosphere data at different latitudes is used by the NMF to determine hydrostatic and wet MFs and it was verified using radiosonde data while the ray tracing method is used to determine the coefficients a, b and c similar to Herring (1992) and Davis et al. (1985). NMF path delays are computed from 90 degrees up to 3 degrees with 9 different EAs and latitudes of (15, 30, 45, 60 and 75) degrees using standard atmosphere profiles. NMF uses the sine function to express temporal changes of coefficients, and the period of this function is 365.25 days.

Isobaric Mapping Function (IMF)

IMF (Niell, 2000) is the first model to determine the MF coefficients based on the 6-hourly profiles of numerical weather model. The IMF uses empirical functions to determine the b and c coefficients and re-assessment of meteorological parameters, which are on 2.0 degrees latitude by 2.5 degrees longitude grid (Schubert, Pjaendtner and Rood, 1993). The formulas of these functions use radiosonde data to determine the "true" MFs at 28 locations. Hydrostatic IMF (IMFh) uses height data at 200 hPa pressure. This pressure (height) level can be easily found in many models and the atmospheric thickness can be well illustrated by this pressure (height) level. For each of the 28 locations, the profiles were ray traced from 90 degrees up to 3 degrees for 9 EAs. The coefficients a, b, c for each profile are estimated by least squares 9 EAs. The isobaric elevation information required for the IMFh, the height and the water vapor information required for the wet IMF (IMFw) can be achieved with a 6 hour time interval from many meteorological analysis centers. For the IMFh, only the height of the isobaric level at each grid point is needed, while the IMFw requires data such as height, pressure and relative humidity.

Vienna Mapping Function 1 (VMF1)

Niell proposed the use of a coarse ray tracing in numerical weather models at 3.3 degree initial EA for the wet IMF (IMFw) models, but various restrictions during the calculation of IMFw led to the creation of VMF by Böhm and Schuh (2004). For this reason, the VMF can be said to be free of some weaknesses of IMFw. The same method is used for wet and hydrostatic MFs. The hydrostatic and wet MFs in the outgoing EA are calculated along with the ZHD and ZWD determined by the ray tracing. As in the IMF, the VMF uses empirical functions for the b and c coefficients, while the coefficient a in Equation (3.12) is calculated by the least squares according to the ray traced MFs. Therefore, the coefficients are highly correlated, small errors in b and c can readily be compensated by the coefficient a. However, the b and c have been improved by Böhm et al. (2006) and as a consequence a had to be recalculated. This model is called as VMF1. The VMF1 is operative for EAs above 3 degrees and the largest deviation in other heights occurs at 5 degrees of EA. The ray tracing is based on ECMWF data in 2.5 by 2.0 degree grids and 6 hours resolution. The geometric bending effect is also taken into account in the hydrostatic VMF1. 2.5 degree in longitude times 2.0 degree in latitude with 6 hours resolution for selected IVS (Böhm, Werl and Schuh, 2006).

Global Mapping Function (GMF)

The aim of GMF is to create a MF, synchronized with numerical weather model (NWM), which is admitted and can be readily applied in geodetic data analysis softwares. The GMF is based on MF, VMF1 (Böhm, Werl and Schuh, 2006; Böhm et al., 2006). The coefficients of GMF are derived from the spherical harmonic expansion of VMF parameters in a global grid. The continuous fractional equation with the parameters has been improved to include the latitude dependence. The a_h and a_w coefficients were determined by using 15°x15° grids obtained by re-analysis of ECMWF data, using the same method of data in the period of September 1999 to August 2002 and using the same b and c coefficients of VMF1. In this way, the 36-month, a, values were achieved for the hydrostatic and wet MFs at each of the 312 grid points. The hydrostatic coefficients were projected to mean sea level as a result of the height correction presented by Niell (1996). The mean values (a_0) and the annual amplitudes (A) of the sinusoidal function,

$$a = a_0 + A \cdot \cos(\frac{doy - 28}{365.25} \cdot 2\pi) \tag{3.13}$$

were placed to the " a " parameter in the time series of a_h and a_w at each grid point, with the phases based on January 28 and corresponding to the NMF. According to the values obtained from the Equation (3.13), the standard deviations of monthly values at a single grid point increase as they go from the equator to the poles and are seen in Siberia with a maximum of 8 mm. For the wet component, these values are slightly smaller and different. It is seen on the equator with maximum 3 mm.

Vienna Mapping Function 3 (VMF3)

VMF2 has been evolved to overcome the deficiencies, such as station heights, orbital altitudes and about determining the a values in 3 degree EA, in VMF1 model. However, since VMF2 could not improve the data acquired from VMF1 to the desired extent so a new model has been drawn on. Afterwards, VMF3 has been designed in such a way that the deficiencies in the coefficients (b and c) obtained by using empirical functions and the deficiencies mentioned above are also set aside. During the VMF3 studies, two different models are used under the names of VMF3$_{3\text{deg}}$ and VMF3$_{\text{LSM}}$. The basic difference between these models is the method used to determine the coefficient, a , by the virtue of ray-trace. It is called VMF3$_{3\text{deg}}$ if it is obtained by using 3 degrees EA, and VMF3$_{\text{LSM}}$ if it is obtained via least-square adjustment. VMF3 reduced the obvious disruption of VMF1 especially in high areas and hydrostatic part. VMF3$_{\text{LSM}}$ produces superior results for EAs of 5 degrees and above, while VMF3$_{3\text{deg}}$ gives better results because of generating the coefficient a using 3 degrees of EAs.

VMF3 uses monthly mean values obtained through ECMWF in total 120 epoch between 2001-2010 with 1°x1° horizontal resolution. The coefficient a (hydrostatic and wet) is stemmed from using 3 degree EA at 1°x1° grid and 3.3, 5, 15, 30 degree EAs at 5°x5° degree grid. Since both VMF1 and VMF3 concepts get b and c coefficients from empirical models, these coefficients are similar. Therefore, in order to develop the VMF3 concept, coefficient a is used rather than b and c coefficients. VMF3 is designed by supporting b and c coefficients of VMF1 with the components of the coefficient a specific to VMF3. For both b and c coefficients, for example bh:

$$b_h = A_0 + A_1 \cdot \cos\left(\frac{doy}{365.25} 2\pi\right) + B_1 \cdot \sin\left(\frac{doy}{365.25} 2\pi\right)$$

$$+A_2 \cdot \cos\left(\frac{doy}{365.25} 4\pi\right) + B_2 \cdot \cos\left(\frac{doy}{365.25} 4\pi\right) \tag{3.14}$$

where mean value (A_0), annual amplitudes (A_1 - B_1) and semiannual amplitudes (A_2 - B_2) of the coefficients. The coefficients could then be saved as a grid that could generate new values by the user, but at this time the system would consume excessive processing time. For this reason, a discrete grid is formed with the spherical harmonic functions of the empirical coefficients and amplitudes then the least-square adjustment is applied for adapting to the spherical harmonic coefficients. As a result, much more advanced empirical coefficients are obtained compared to VMF1.

The slant delays are reckoned using MFs show that the ability of VMF3 to estimate reason of ray-traced delays, which is the basis for determining MF coefficients, is higher than VMF1. For this reason, especially in low EAs, VMF3 can be more preferable in terms of sensitivity than VMF1. It is already mentioned above that MFs are gravely effective on the height component and constitute one-fifth of the delay occurring at 5 degree EA (Böhm, 2004). As a result of using the VMF3LSM, the station height of the VMF1 model has been evolved by approximately 0.25 mm. In addition, GPT3 provides an empirical comprehensive troposphere model compatible with VMF3 as it generates hydrostatic and wet coefficients (b_h, c_h , b_w, c_w) from VMF3 specific data and contains meteorological data used by GPT2 (Landskron and Böhm, 2018)

Niell (2006) compared MFs i.e. GMF, VMF1, IMF and NMF to those obtained from the ray-tracing method to the radiosonde data. As a result, the best fit is provided by VMF not just for the hydrostatic delays but also for the wet delays. On the other hand, errors in the wet MFs due to almost no moisture in the poles are not very critical in estimating the station height and zenith wet delays. Again, the best fitting results for the wet MF values are provided by VMF1. However, it should be noted that radiosonde data may be adapted to the NWM used to determine VMF and IMF. Numerous studies have been conducted to accurately determine the parameters of the troposphere delay such as MacMillan and Ma (1994); Emardson, Elgered and Johansson (1998); Behrend et al. (2000, 2002); Niell et al. (2001); Kouba (2009); Cucurull et al. (2000); Schuh and Böhm (2003); Gradinarsky et al. (2000).

3.3. Azimuthal Asymmetric Troposphere Delays (Gradients)

Troposphere delays on the vertical direction above a station are sufficient to determine azimuthally symmetric path delays at any EA. However, path delays are not constant when the EA is fixed and azimuths are changing e.g. the path delays are larger along south azimuths then in the north when the observer is located in the northern hemisphere. In earlier studies, the difference between path delays with or without gradients were neglected. Therefore, gradients are considered as a set of parameters that can cause changes in slant path delays. The azimuthal symmetric part is modeled by MFs and is only EA dependent. Horizontal total (wet plus hydrostatic) gradients should therefore be taken into account. The Equation (3.1) can be examined in two main parts; azimuthally symmetrical part and gradient delays (Davis et al., 1985, 1993):

$$\Delta\tau_{trop} = ZHD \cdot m_h(\varepsilon) + ZWD \cdot m_w(\varepsilon) + m_{h,w}(\varepsilon)cot(\varepsilon)[G_N cos(\alpha) + G_E sin(\alpha)] \tag{3.15}$$

where ε denotes the EA, $m_{h,w}(\varepsilon)$ is the hydrostatic and wet MFs, ZWD the zenith wet delay and ZHD the zenith hydrostatic delay which is calculated using station coordinates and total pressure at the site (Saastamonien, 1972; Marini, 1972; Niell, 1996; Böhm, Werl and Schuh, 2006). Gradient delays are the azimuth dependent part which is described using troposphere gradient vectors in the east (G_e) and north (G_n) directions and projected by the azimuth angle (α) and the gradient MF ($m_g = m_{h,w}(\varepsilon)\cot(\varepsilon)$). The representation of the gradient model shown in Equation (3.15) is illustrated in Figure 3.1 and Figure 3.2.

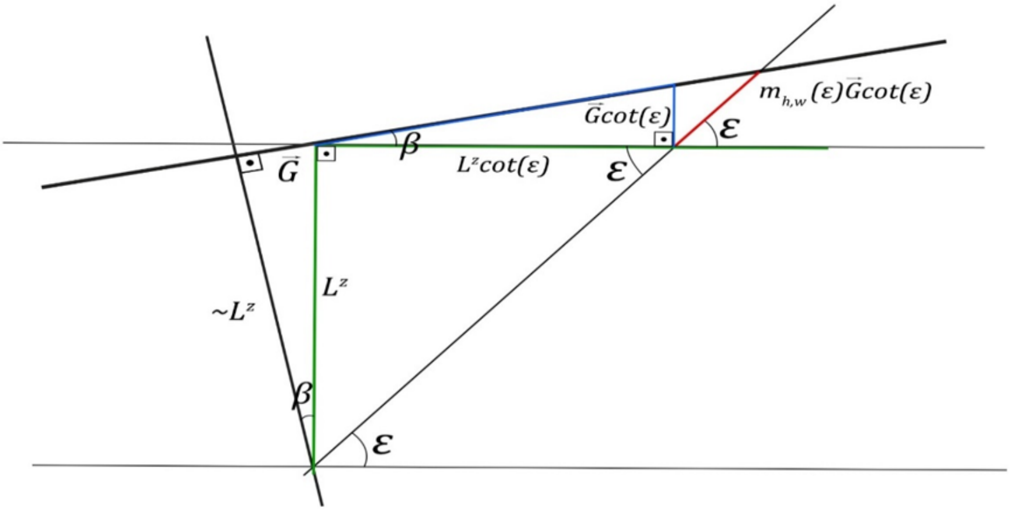

Figure 3.1. Projecting gradient vector from zenith to slant direction. β is the tilting angle of the MF assuming a horizontally stratified atmosphere (Böhm, 2009).

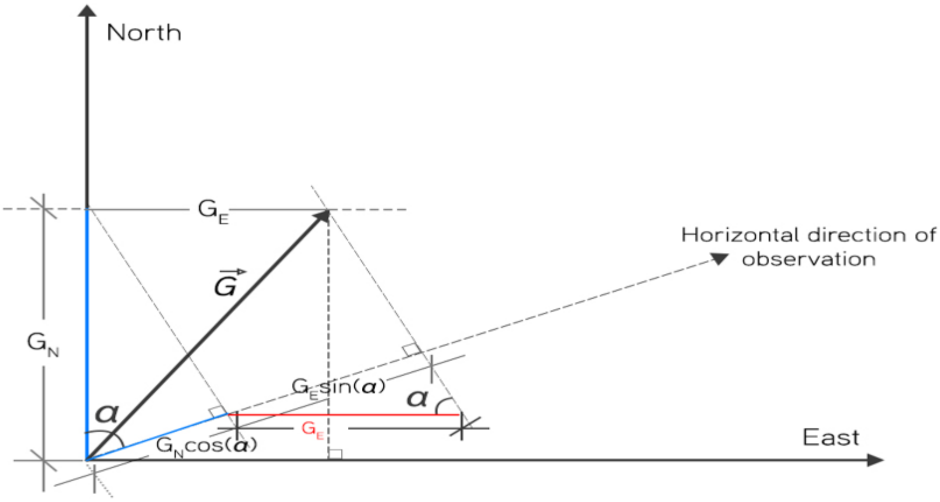

Figure 3.2. Projecting the gradient vector at the slant direction to the azimuth of observation (Teke, 2011).

The gradient part of the Equation (3.15) was developed by MacMillan (1995). Besides, their analysis revealed that when the gradient model is included in the observation equations. MacMillan and Ma (1997) studied the TRF and CRF gradient estimation effects. Interferometric group delay data (observations) of the VLBI daily sessions from 1980 to 1994 were used for TRF determination. In their studies, a sequence of TRF standard solutions is carried out in which quasar positions, as well as station positions and velocities, are estimated. Their research has shown that when gradients are estimated, adjusting the celestial source positions produced systematic effects in TRF (Ma and Feissel, 1997). Two methods were developed by Chen and Herring (1997) to determine the propagation delay of troposphere originating from gradients. Both methods showed a similar atmospheric gradient delay of about 30 mm at a 10-degree EA. According to Böhm and Schuh (2007) and Davis et al. (1993), NWM can produce linear horizontal gradients as the vertical constituent of refractive index. They searched the effects of gradients on repeatabilities of baselines. ECMWF gradients when creating a priori value or estimated at intervals of 6 and 24 hours.

4. THE TRANSFORMATION BETWEEN GCRS AND ITRS FOLLOWING CELESTIAL INTERMEDIATE ORIGIN BASED IERS CONVENTIONS

The Earth does not have a uniform rotation, so the Earth rotation axis deviations in time is being monitored. Geodynamic effects cause angular momentum changes between the solid and fluid parts of the Earth. The atmosphere, ocean, and hydrology are the fluid envelope of the Earth create internal torques (Schindelegger et al., 2013).

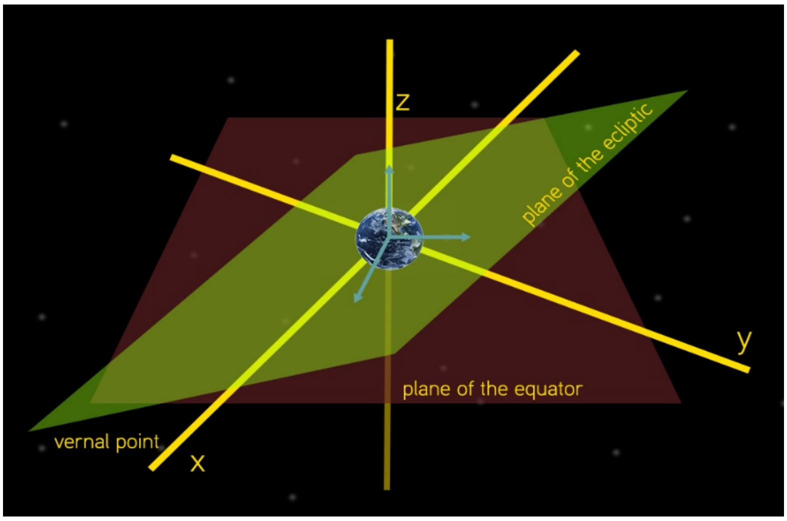

Figure 4.1. Simple relation between the TRF and the CRF axes (McCarthy and Seidelmann, 2009).

The reference systems consist of a specific origin, axes directions and a number of conventional models, procedures and coefficients. By means of these parameters, reference systems are realized. The methods and models required to establish a relationship between TRS and CRS are developed and maintained by the IERS (Petit and Luzum, 2010). In Figure 4.1. red and yellow axes ilustrate TRF and CRF, respectively. The CRS is determined by astronomically defined origins and directions. Global reference systems are considered its origin as the barycenter of the solar system and the polar axis is somehow related to the rotation axis of the Earth. The second axis is perpendicular to the pole axis and extends on the equatorial plane, oriented towards a reference point which is vernal equinox in the equinox-based conventions and NRO in the CIO-based conventions. The right handed orthogonal system is used to determine the third axis required for the completion of the system (Perryman et al., 1997; Boucher et al., 2004).

As a result of advancing technology and developing systems after 1 January 2000, the CEP was regulated as CIP. In addition to its definition, the direction and motion of the CIP in GCRS are formulated (Capitaine, 2000). The precession was used to obtain the mean positions of stars at certain times, while the theory of nutation was used to switch to instant positions of the celestial objects. In 1992, independent of the epoch, ICRS, which consist of defined directions to remote radio sources, were appointed by the IAU (Ma and Feissel, 1997). Hipparcos Catalog is used to get information about the location of ICRF-related optical stars (Perryman et al., 1997).

In 1884, Greenwich longitude was defined astronomically to form the second axis. However, the developments in the field of accuracy in geodesy after this date left the Greenwich longitude in the background. Despite all this, the origin of the longitudes are used today is very close to the location defined in 1884. The third axis is determined using the right-handed orthogonal system (Boucher et al., 2004). The solar system barycentre is regarded as the origin of the ICRF, in which case the ICRS appears as a specific implementation of the BCRS. However, the terrestrial system which considers geocenter as an origin, is used for observations. At this stage we use GCRS that does not rotate kinematically w.r.t. BCRS, so GCRS and ICRS are in the same orientation. In transformations involving BCRS, a deviation effect is produced which can be explained by relative theory.

The terrestrial system moves within the celestial system and this movement is influenced by a lot of complications. CIRS is used to facilitate the transformation between the CRF, which takes the barycenter of the solar system as the origin, and the geocentric TRF. CIRS, is obtained by taking into account the precession and nutation motions of the CIP in GCRS, is an instantenous geocentric celestial reference system. It is determined for a certain (observation) epoch using the intermediate CIP equator. According to the Nutation theory, CIP is used as the reference pole for many space geodesy techniques, thus defining axes. CIP is an intermediate pole that enables us to separate the pole motion of ITRS on the GCRS into terrestrial and celestial parts. CIO is the NRO within the GCRS and was located very close to the GCRS meridian, and is set to remain within 0.1 arc second of the deviation from this alignment from 1900 to 2100. For an ICRS at time t, the CIP is the third axis and the CIO is the first axis (Schuh and Böhm, 2011; McCarthy and Seidelmann, 2009; Kaplan, 2005).

All the motions of CIP in the terrestrial frame out of the range of -1.5 and -0.5 cpsd are so called as the polar motion. The minus sign indicates a retrograde motion and the plus sign indicates a prograde motion. The 2-day arbitrary division which is used to classify these terms is determined in accordance with IAU-Resolutions 2000/2006 B1.7.

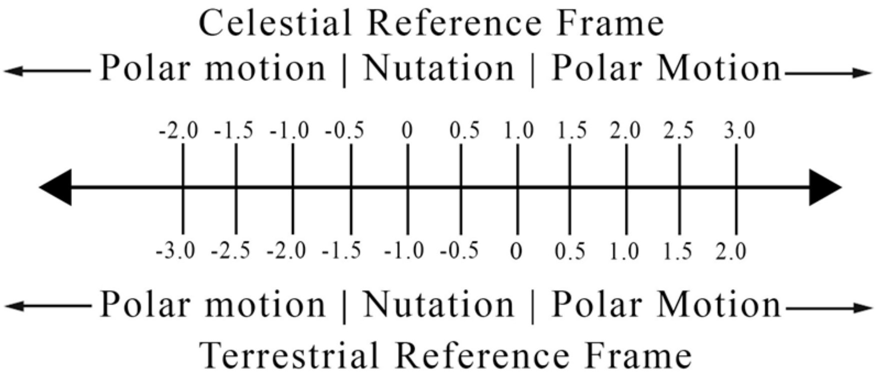

Figure 4.2. Relationship between the frequencies of the CIP motion as viewed from the celestial reference frame and the corresponding frequencies of the same motion as observed from the terrestrial reference frame (Gross, 2007).

The connection between these frequencies is made through the Equation (4.1) presented below.

$$\sigma_c = \sigma_t + \Omega \tag{4.1}$$

The classification of precession-nutation and polar motion in terms of frequencies replaces the distinction between geophysical and astronomical Earth rotation. Similar to CIRS, TIRS is a geocentric reference system, used to transform between terrestrial and celestial frames. It is identified by the TIO and the CIP intermediate equator.

4.1. Earth Orientation Parameters

The orientation of the rotating Earth w.r.t. space can be defined with the three Euler angles to transform between the earth-fixed the space-fixed coordinate systems. However, as Eubanks (1993) points out that when the rotation of the Earth is desired to be examined in geophysical point of view, five angles are required. Two angles define the orientation of the earth rotation axis relative to the TRF (polar motion), an angle defines the rotation of the earth around the rotation axis (UT1-UTC), and the other two angles define the orientation of the earth rotation axis within the space-fixed system (precession and nutation) (Schuh and Böhm, 2011; McCarthy and Seidelmann, 2009).

The atmosphere affecting the three basic components that shape the rotation of the Earth has been studied for more than a century. Although the whole air mass is 1/300 of the ocean mass, the atmosphere has more impact on the Earth than the oceans and the core at semi-annual and annual periods (Schuh and Böhm, 2013; Lambeck, 1980; Eubanks, 1993). Wind friction and atmosphere pressure changes during the year generate significant seasonal excitation signals within the ERP. The regional winds chiefly affect only the axial component, especially when the isobaric pressure level is below 10hPa (Gross et al., 2003 and 2004, Madden and Julian, 1971). Although ocean tides have a 30-times greater impact on both Earth rotation and polar motion than the effect of the atmosphere, the effect of the high-frequency atmosphere on the EOP can be calculated using NWM data (Chao et al., 1996; Brzeziński, Bizouard and Petrov, 2002; Ray et al., 1994). The ocean periodic mass motions triggered by surface pressure and wind changes are used by the atmosphere to have an indirect effect on Earth rotation (de Viron and Dehant, 1999).

Two different methods, which appear to be different from each other, but are essentially equivalent, can be used to evaluate the effetcs of the fluid envelope of the Earth. In first approach, the solid Earth, atmosphere, ocean, and hydrology are handled independently of the other variables to preserve the angular momentum. The other method is known as the torque approach which is the differentiations of the angular momentum w.r.t. direction. It is necessary to calculate the torque magnitude directly between e.g. the atmosphere and the solid Earth (Brzeziński, Bizouard and Petrov, 2002; Iskenderian and Salstein, 1998; de Viron and Dehant, 1999).

Polar motion observations were first obtained by Friedrich Küstner as a result of measuring latitude changes. Space geodesy techniques such as VLBI, SLR, LLR, DORIS, GNSS have been utilized effectively as history progresses to the present day and it is seen that the measurement accuracy obtained as a result of the improvements and projected to the Earth surface are better than 0.6 cm. GNSS is the most accurate method for determining polar motion, while VLBI is the only way to measure UT1-UTC and nutation (Schuh and Böhm, 2011).

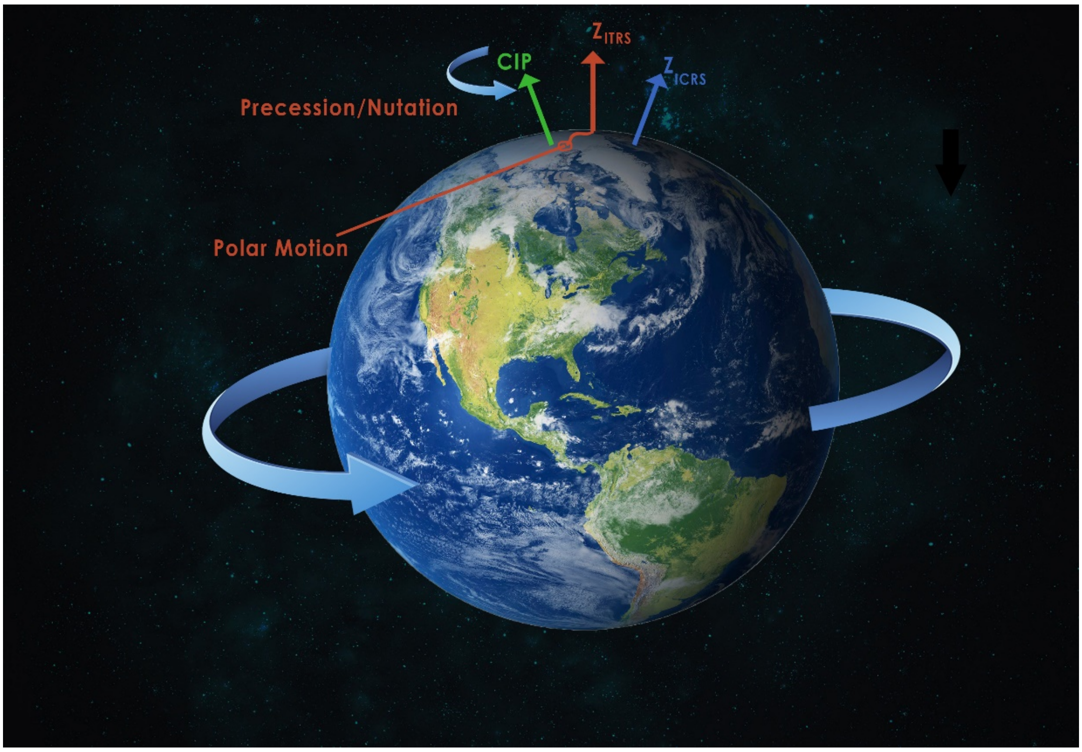

Figure 4.3. Motion of the Z axes of the reference systems according to the orientation of the Earth (McCarthy and Seidelmann, 2009).

The forced motion of the CIP according to the space-fixed system is caused by the gravitational effects of the moon, sun and the solar planets. Secular and long-term motion of the CIP w.r.t. space is called precession. Hipparchus' invention that the equinox positions move westward in relation to time compared to the stars made him known as the person who discovered the precession in the second century BC. The precession motion has a period of about 26000 years in a cone-like manner with an angle equal to 23.5 degrees, and covers a distance of 50 arc-seconds per year in space. The period of precession is, 26000 years, called the Platonic year. The main reason for the mean obliquity of the ecliptic, 23.5 degrees, is the permanent tidal effect of the moon and the sun.

Nutation is the small tidal periodic motions of the CIP superimposed to the secular precession motion. The swerves that occur on the conic like movement of the rotation axis direction as a result of the Earth moving like a gyroscope are called nutation. Nutation is the periodic motion of the CIP in a space fixed frame with a period from 2 days to 18.6 years (McCarthy and Seidelmann, 2009). Precise modeling and prediction of the precession and nutation is possible through time-dependent harmonic series expansions. The most precise precession-nutation model currently applied is IAU2006/2000A (Mathews, Herring and Buffet, 2002).

The parts of the Earth's rotation axis motion considered according to the space-fixed system, which are not covered by the precession-nutation model, can be measured through VLBI and are so called as CPO. These residuals CPO consists of mostly free core nutation (FCN) signals in addition to a small part coming from the signals due to the inadequacy of the geophyscial models. The FCN results from the fact that the rotation axes of the core and the mantle are not aligned (Sasao and Wahr, 1981). Initial calculations for FCN showed a period of 460 days, while measurements with VLBI showed a period of 430 days (Herring, Gwinn and Shapiro, 1986) and its amplitude is in between about 0.1 and 0.3 mas (Petit and Luzum, 2010).

The CIP motion in the terrestrial reference system is called polar motion. The magnitude of the polar motion, which CIP forms, within this terrestrial reference system is expressed in mas and these variations are regularly published by IERS under the name of pole coordinates. The polar motion component, x_p is oriented towards the Greenwich meridian, while the y_p takes positive values along the 90-degree west longitude.

In the presumed times when the Earth was thought as a rigid oblate spheroid, Leonhard Euler calculated the circular motion of the pole with a 304-day period. But by the end of the nineteenth century, it became clear that the Earth was not as simple as predicted and that pole movement, motion of the CIP, is mainly consisted of a linear drift and two periodic movements which are the annual variation and Chandler wobble (CW). Although the establishment of the reality of the polar motion phenomenon is associated with Karl Friedrich Küstner, it is Seth C. Chandler (1891a, 1891b, 1892) who first determines the major periodic components under the name of Chandler oscillation or Chandler wobble (Brosche, 2000; Küstner, 1888, 1890; Carter and Carter, 2000). The Chandler wobble which is the main component of polar motion, cause to quasi-circular counter-clock-wise motion as seen from the north pole with a period of almost 14 months equal to about 433 days. Chandler wobble causes the true latitudes and longitudes of the Earth to vary of about 9 to 21 meters in a year. Besides the annual motion of the CIP in TRF has an amplitude of about 90 mas, which corresponds to a distance of 2.7 meters (Schuh and Böhm, 2011).

CW is the first, main, component of polar motion and the proper eigenmode of the Earth. The track which CW follows is very similar in shape to the circle. On the other hand, this wobble motion is a damped oscillation, and it would have been a movement that would have ended in the coming years due to the friction in the internal dynamics of Earth if it had not been a driving factor that was in constantly cycling excitation.

Besides, although more than a hundred years have passed since the invention of Chandler wobble, the mechanism underlying the dynamics that have led to this movement of Chandler wobble is still under investigation. In addition, the broad consensus in recent years is that the energy required for the continuity of the Chandler wobble comes from irregular processes between the atmosphere and the ocean (Schuh and Böhm, 2011; Gross, 2000; Brzeziński, Dobslaw and Dill, 2012). The second main component of the pole motion, the annual motion that occurs as a result of the redistribution of atmospheric and water bodies on the earth. Moreover, sub-daily changes caused by ocean tides and gravitational torques which have less than two days periods also contribute to polar motion, but the effect is about one percent of the Chandler wobble (McCarthy and Seidelmann, 2009). The dynamic coupling between the core and the mantle results in a significant change in the analysis of long-term pole motion for about ten years. Postglacial rebound causes the pole to move straight to 76--78 degrees west with a size of 3.3 mas/year (Schuh, Nagel and Seitz, 2001).

UT1 is the measurement of the rotation angle of the Earth, expressed in units of time. It is considered an astronomical time scale defined by the Earth's rotation w.r.t. the mean Sun. In fact, UT1 was defined by a traditional formula until 1 January 2003 (Aoki et al., 1982). ERA is a linearly increasing angle for a smoothly rotating Earth that moves positively in the retrograde direction. In the Equation (4.1) of UT1 which conventionally adopted. The time derivative of UT1 is the LOD. UT1 is determined using VLBI observations and can be considered as the time-dependent rotational motion of the Earth by IERS (McCarthy and Seidelmann, 2009). Optical observations were first used to reveal the presence of polar motion. Many observation devices were used until modern observation techniques. Nowadays, information about polar motion can be obtained mainly by GPS and VLBI. Geodetic VLBI is unique in providing UT1 as well as being the only space geodesy technique in which all EOP can be obtained (Böhm et al. 2011).

4.2. Celestial Reference System (CRS)

The CRS utilizes the location of extragalactic objects measured by the geodetic VLBI. Actually an ideal CRS consists of fixed space coordinates and a time scale. Needless to say that it took some time before the system was established on such a fixed and inertial basis. In celestial systems used in the past, general relativity was considered to be an input that only had a deviation effect on Newton mechanics and needed to be corrected and the systems were based entirely on Newton's mechanical principles. The fundamental deficiency of the old systems was that the axes refer to the moving equatorial and ecliptic planes, and that movement based on these planes was required. But sometimes the equinox provided by the theory had to be changed by the observations and this was misleading in terms of the epoch definition and caused three different equinoxes to emerge (two different dynamical and the fifth fundamental catalogue (FK5) equinox).

The CRS was defined using the planetary equations of the motion without coriolis effect and was theoretically dynamic. The planets were not precisely linked to the positions of the base points to define the frame. All these factors led to uncertainties between FK5 and those based on dynamical theories. For all these reasons, in 1991, the IAU revealed a CRS whose axis was determined using sources and based on the barycenter of solar system as origin. This system was formed by IERS and IAU adopted in 1997, and in 1998 it was replaced by FK5 under the name of ICRS.

CRS realizations i.e. CRF were carried out using the same conventions for each year between 1989 and 1995 and the number of sources observed from year to year increased from 23 to 212. In this process, the realization of IAU defined CRS showed that the deviation magnitudes declined over the years. As a result, IERS proposed the adoption of the system in 1995 as ICRS, and was officially accepted by the IAU in 1997 (Arias et al., 1995). After that, the stability of the axes gradually improved and decreased below 10 µas value, e.g. ICRF2 (Fey et al., 2015). The CRS is based on a kinematic basis that can provide fixed axis information relative to distant galaxies. The realization of this system is provided by a frame with the accurate coordinates of the stable and point like quasars. The main plane of the ICRS system is chosen as close as possible to the mean equator at the fundamental epoch (Lieske et al., 1977; Seidelmann, 1982). The IAU decided that the traditional reference pole and FK5 should be compatible. The uncertainty about the direction of the FK5 pole is predicted in two steps: (1) the systematic part governed by the correction to construct and (2) considering the accuracy of the FK5 equator of Fricke's (1982) and the residual rotation boundary of Schwan's (1988) are estimated by obtaining the observation epochs from Fricke, Schwan and Lederle (1988). For all these reasons, ICRS celestial pole is compatible with the FK5 (Petit and Luzum, 2010).

The frame for realizing the ICRS is the ICRF. This realization includes the precise coordinates of a group of dense sources outside the galaxy. These sources used for ICRS realization should include several observations of sufficient and long data width to assess position accuracy. The first ICRF realization, ICRF1, was performed by observing 212 "defining" radio sources using VLBI method and as a result, uncertainty was obtained below 0.01 mas value. The second ICRF realization, ICRF2, was performed in 2009 using 295 new "defining" radio sources. In the selection of these new sources, the spatial stability and the lack of intensive internal source structure were taken into account (Fey et al., 2015). ICRF2 which contains more additional resources than ICRF1 so provides more accurate information by means of the more additional resources. The noise floor of the ICRF2 is much better than the ICRF1 and is about 40 µas. As a result, due to the spatial consistency of 295 defining sources in ICRF2 and the homogeneous distribution of these sources, the two main weaknesses in ICRF1 are eliminated.

VLBI observations on sources, solar system probes or other astrometry projects establish the connections with celestial frames. Links to the other celestial reference frames with the catalogs of different radio wavelengths are also provided by the ICRS center of the IERS (Petit and Luzum, 2010).

In cases such as lunar laser ranging and interplanetary satellite navigation, the best ephemerides should be chosen because the accuracy of the ephemerides affects the quality of the results, but it is not essential to use the latest version ephemerides to model the gravity of the celestial bodies for the tides and nutations. Ephemerides constantly remain up to date employing the using of more data. The ephemerides DE421 from the JPL (Folkner, Williams and Boggs, 2009), are expected to be up-to-date and of close quality. The ephemeris were aligned with the ICRF using VLBI observations (Petit and Luzum, 2010).

4.3. Terrestrial Reference System

The reference coordinate systems are used for many scientific and engineering fields, among others, e.g. precision navigation, construction projects as well as atmosphere, sea level and crustal deformation monitoring (Angermann, Seitz and Drewes, 2013). The accuracy of the geodetic parameters in global scale has increased substantially with the usage of the space geodetic techniques. However, due to the changing nature of the Earth which is caused by internal and external dynamics of the Earth e.g. due to ocean and atmosphere, the progresses required to determine the reference system and its evaluation in time in sub-millimeter accuracies have become more complicated.

Reference systems and frames have been established and maintained by many national and international organizations. The terrestrial reference system is needed in conjunction with the celestial system to identify, analyze and present the results of the movement of bodies (Rothacher, 2000; Plag and Pearlman, 2009). The origin of the reference system is geocenter, the direction of rotation is equatorial (perpendicular to the equator at the center of mass) and the z-axis passes through the mean pole. ITRS which is based on IERS conventions was accepted by IUGG in 2007 (Petit and Luzum, 2010).

ITRS realizations i.e. ITRF of which parameters publicly available are the catalogue station coordinates at a given epoch and the linear velocities. The identification of the reference coordinate system, the realization of the system i.e. the frame and the determination of the datum must be consistent. The realization of the system by the frame and the allocation of the datum must not change the definition. The datum definition must be made independent of the measurements of the reference frame.

ITRS is realized and maintained by the IERS. The center of mass is calculated by considering all the masses of the Earth including the atmosphere. The time scale is TCG and the variation of orientation over time is achieved by using the no net rotation (NNR) condition for horizontal tectonic movements (Petit and Luzum, 2010). ITRS is basically metric, equatorial, and geocentric. The z axis is close to the variable Earth rotation axis, and the x and y axes are on the equatorial plane (Drewes, 2009).

The orientations of the all ITRS realizations are constantly alligned to BIH Terrestrial System (BTS) at the 1984.0 epoch by convention using NNR conditions on the estimated coordinates. Thus, the orientation definition is completely geometric and does not depend on the physical Earth parameters unlike to the origin of the ITRS which should always overlaps with the mean center of mass. By applying the NNR condition, the consistency between successive ITRF solutions is ensured. This means that the orientation cannot be independently generated from scratch and is always dependent on the former ITRF realization. It is not desirable that uncertainties and errors spread in this way to subsequent realizations. During the transfer of orientation from one particular epoch to other epochs, time-dependent evolution is an issue that needs to be resolved. ITRS asserts that the NNR requirement for horizontal movements on Earth shall be used to ensure this evolution. The scale of the ITRS is determined by the SLR and VLBI observations whereas the origin is dominantly determined by the SLR observations.

The points on the Earth are exposed to many geophyscial effects such as gravitational tides and mass loads which are mainly tidal periodic in nature, tectonic motions which are linear as well as volcanic and seismic deformations that are episodic events. However, the realization of ITRS, ITRF consists of the coordinates and linear velocities of the crust-fixed reference points that are free from the effects of any tide and periodic as well as episodic deformations (Petit and Luzum, 2010). In the first realization by BTS84, the global network of geodetic reference stations was identified by BIH (then IERS) (space, then IERS) using other space geodetic techniques (Boucher and Altamimi, 1985). Each station is identified by a property called a DOMES number. By the virtue of advances in space geodetic techniques and efforts, GPS, SLR, VLBI, DORIS have contributed to the ITRS (Angermann, Seitz and Drewes, 2013).

IERS was founded in 1988 by IUGG and IAU and has since published 13 ITRF realizations, excluding the release scheduled for 2020, each replacing the previous one (Petit and Luzum, 2010). The regular release of realizations within 1-3 years is due to the development of the monitoring network of developing space techniques, increasing data and modeling over time, the continuous development of combination methods and data analysis methods.

The number of stations belonging to ITRF realizations from 1988 to 2000 and the solutions obtained by using these stations are shown in the Table 4.1. it is easily understood that both the number of stations as well as the type and number of solutions have increased with the advancing time.

Table 4.1. Overview of the ITRF realizations between ITRF88 and ITRF2000 compiled by the IERS TRF section

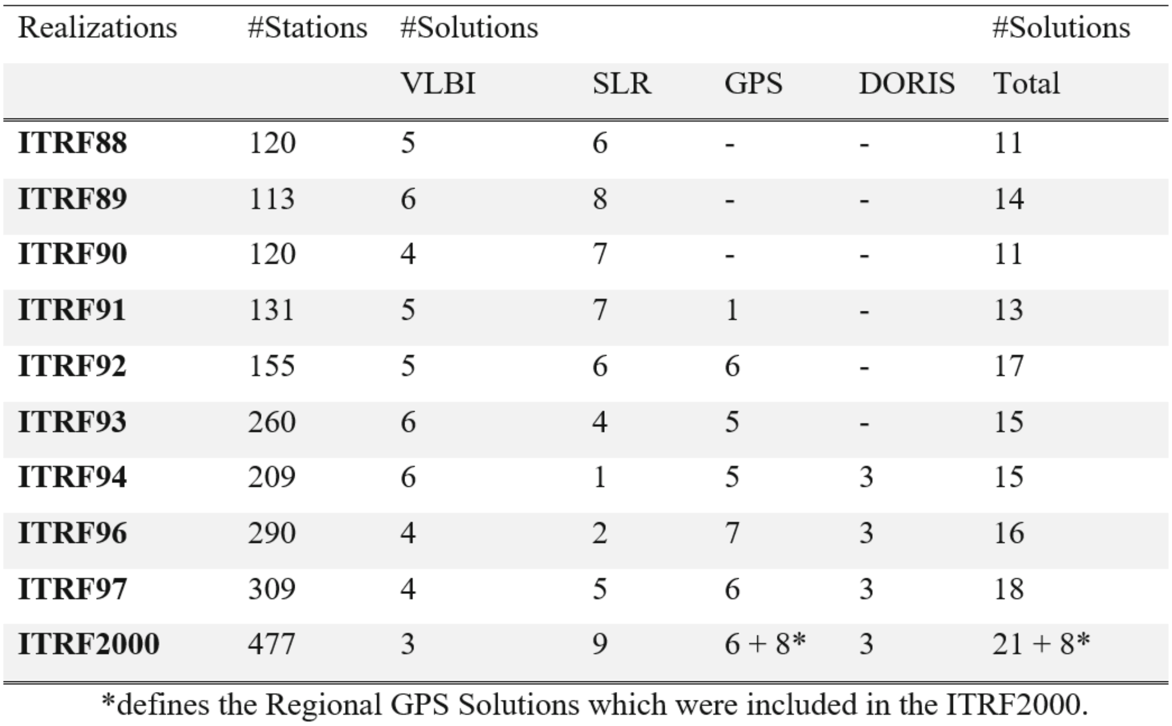

Realizations	#Stations	#Solutions				#Solutions
		VLBI	SLR	GPS	DORIS	Total
ITRF88	120	5	6	-	-	11
ITRF89	113	6	8	-	-	14
ITRF90	120	4	7	-	-	11
ITRF91	131	5	7	1	-	13
ITRF92	155	5	6	6	-	17
ITRF93	260	6	4	5	-	15
ITRF94	209	6	1	5	3	15
ITRF96	290	4	2	7	3	16
ITRF97	309	4	5	6	3	18
ITRF2000	477	3	9	6 + 8*	3	21 + 8*

*defines the Regional GPS Solutions which were included in the ITRF2000.

After 200, all of institutions contributed to the terrestrial reference frame calculations by developing the refined combination strategies. The geodetic co-location sites are settled with more than one space geodesy technique instruments in the same location or in close proximity to each other. The tie between these geodetic instruments located in the vicinity are generally measured by the leveling, trilateration or GPS local networks. The so called local ties required precision magnitude of the ties between these terrestrial reference points (local tie vectors) is expected to be even less than 1 mm which cannot be attained during most applications. The availability of sufficient number of co-located sites, and the quality of local tie vectors is extremely important for ITRF calculations and there are over 100 stations suitable for this purpose (Seitz et al. 2012; Krügel and Angermann 2007; Angermann et al. 2004). These local tie vectors are used to form the constrain equations, e.g. in normal equation level, to combine the station coordinates of each space geodetic technique at the geodetic colocation sites. On the other hand, it is also important to determine the specific errors of space techniques and to compare them with other techniques. In this way, they provide the basis for combining common parameters to techniques that will enhance reference frame realizations (Angermann, Seitz and Drewes, 2013).

The first realization created with the new strategy obtained after these developments in ITRF calculations is ITRF05 and then postulated to establish ITRF08 and these are based on the Earth orientation parameters and station position of different space techniques. Moreover, the Earth orientation parameters in the ITRF05 and ITRF08 calculations provide important information for all techniques to work together with different space techniques as common parameters (Angermann et al., 2007, 2009; Altamimi et al., 2007).

ITRF08 model was established as a result of continuous improvement of the data analysis models and standards of different observation techniques in the ITRF05 model. ITRF08 realization is the result of a two-step analysis. First, the ITRF08 require the time series data of the daily EOP obtained by means of four space geodesy technology services, velocities and station positions at reference epoch are combined to estimate long-term solution. While performing the operations in this two-step method, it takes advantage of the variance-covariance information generated in the SINEX format. Since the estimation of conversion parameters is performed between weekly and long-term frames, it is of great importance to determine the time evolution of the long-term frame, origin, scale and orientation. The unique constraints created by Altamimi et al. (2007) with ITRF05 were used for this purpose, thereby preserving origin and scale. Depending on the space geodesy technique, the data is generated in the relevant IAG services. IGS, ILRS, IDS and IVS in SINEX format (Altamimi, Collilieux and Métivier, 2012). With ITRF2008 realization, for the first time, consistent in itself time series was produced for each of the techniques involved in realization process.

The SINEX observation files temporal resolution is weekly for GPS, SLR, DORIS and daily for VLBI. VLBI data is generated for GPS, SLR, DORIS, the satellite observation technique, is produced with solutions with loose and minimal constraints as shown in Table 4.2.:

Table 4.2. Overview of Submitted Solutions to ITRF2008 (Altamimi, Collilieux and Métivier, 2012)

TC	Data Span	Solution Type	Constraints	EOPs
IVS	1980.0-2009.0	Normal Equation	None	Polar Motion, rate, UT1-UTC, LOD
ILRS	1983.0-2009.0	Variance-Covariance	Loose	Polar Motion, LOD
IGS	1997.0-2009.5	Variance-Covariance	Minimum	Polar Motion, rate, LOD
IDS	1993.0-2009.0	Variance-Covariance	Minimum	Polar Motion, rate, LOD

The ITRF08 network consists of 934 stations located on 580 different sites 84 of which are co-location sites and besides 463 of which are in the northern and 117 of which are in the southern hemisphere. The local ties all of which are available on http://itrf.ign.fr/local_surveys.php. Hence, the GPS is of great importance for ITRF combinations thanks to a total of 137 tie vectors between these three techniques, 44 with VLBI, 48 with SLR, 45 with DORIS (Altamimi, Collilieux and Métivier, 2012).

ITRF14, presented as the highest quality among the published implementations, proves this situation with two basic innovations related to the modeling of the non-linear station movements it contains. These innovations consist of annual signals in the time series of station locations and seismic deformations for 124 points exposed to major earthquakes. The time series of station positions and EOP produced by the IVS, ILRS, IGS, IDS technique centers of IERS are obtained by collecting time series and combining them with co-located sites together with long term solutions. This two-step system utilizes the full variance-covariance information presented in SINEX format. Since IERS technical centers solutions are independent of any external constraints, actual space geodesy estimates of station positions and EOP are maintained. The ITRF14 origin is defined as the null translation parameter in the 2010.0 epoch and the null translation rate relative to the mean origin of the ILRS SLR time series. The scale of ITRF14 is defined as the null scale factor in the 2010.0 epoch and the null scale rate according to the mean scale and scale rate of the VLBI and SLR time series. The ITRF14 orientation is defined so that there are no rotation parameters at 2010.0 epoch or rotation rates between ITRF14 and ITRF08. ITRF14 orientation and ratio are aligned to ITRF08 using 127 geodetic reference stations settled in 125 sites. The temporal resolution of SINEX observation files is daily for GPS, weekly and fortnightly for SLR, weekly for DORIS and daily for VLBI (see also Table 4.3).

Table 4.3. Overview of Submitted Solutions to ITRF2008 (Altamimi et al., 2017)

TC	Data Span	Sampling	Solution Type	Constraints	EOPs
IVS	1980.0-2015.0	Daily	Normal Eq.	None	Polar Motion, rate, UT1-UTC, LOD
ILRS	1983.0-1993.0	Fortnightly	Var-Cov	Loose	Polar Motion, LOD
	1993.0-2015.0	Weekly	Var-Cov	Loose	Polar Motion, LOD
IGS	1994.0-2015.1	Daily	Var-Cov	Minimum	Polar Motion, rate, LOD
IDS	1993.0-2015.0	Weekly	Var-Cov	Minimum	Polar Motion

ITRF14 has velocity and position information of 1499 stations at 975 sites. In ITRF14, GNSS is of great importance as it has 33 co-located stations with SLR, 40 with VLBI, and 46 with DORIS. As with other ITRF solutions, it is based on the links between collocation sites as well as space geodesy solutions.

The ITRF structure, starting with ITRF05 and continuing with ITRF08 and ITRF14, takes advantage of the time series of EOP and station locations. In addition to nonlinear motions and irregularities occurring in stations, it is important to evaluate the change of origin and scale over time, which is critical for earth science. Thus, the ITRF forms an EOP series that is consistent in itself, including polar motion obtained using VLBI and other space geodesy techniques, and UT and LOD derived from VLBI. Although ITRF14 is more advanced than previous solutions, some problems have been identified especially in the modeling of nonlinear station motions caused by large earthquakes. The deformation of events such as glacial rebound, major earthquakes and the commissioning of new stations increased the need for a new solution. Since the release of ITRF14, many improvements have taken place, such as have been added new stations and collocation sites and local ties to the network of the ITRF, periodic signals observed in the station position time series will be modeled to estimate station speeds and will eventually be combined in co-location sites. ITRF2020 is planned to be released in order to benefit from all these developments and innovations.

4.4. Transformation equations between GCRS and ITRS

The transformation between GCRS and ITRS based on IAU 1976 Precession Model and the IAU 1980 Theory of Nutation (ecliptic/equinox based) was renewed into the IAU 2000/2006 precession-nutation model (CIO-based). The main equation of the transformation from terrestrial to celestial in any epoch is given as follows:

$$\left[GCRS\right] = Q(t)R(t)W(t)\left[ITRS\right] \tag{4.2}$$

wherein $W(t)$ is the rotation matrix for polar motion; $R(t)$ is for Earth rotation angle, between CIO and TIO, about the CIP axis and $Q(t)$ stands for precession/nutation, namely CIP motion in the GCRS. The t used in the Equation (4.2) is

$$t = (\mathrm{TT} - 2000\ \mathrm{January}\ 1\mathrm{d}\ 12\mathrm{h}\ \mathrm{TT})\ \mathrm{in\ days} / 36525 \tag{4.3}$$

where

$$2000\ \mathrm{January}\ 1,\ 12\mathrm{h}\ \mathrm{TT} = \mathrm{Julian\ Date}\ 2451545.0\ \mathrm{TT} \tag{4.4}$$

The $W(t)$, $R(t)$ and $Q(t)$ transformation matrices provide a coordinate transformation between the reference frames with a positive angle around the 1st, 2nd and 3rd axes by using the R_1, R_2 and R_3 rotation matrices. The equation of s' in x_p and y_p is written as

$$s'(t) = \frac{1}{2}\int_{t_0}^{t} (x_p \dot{y}_p - \dot{x}_p y_p)\, dt \tag{4.5}$$

If this equation is shortened for present-century, it is approximated by (Lambert and Bizouard, 2002)

$$s' = -47\,\mu\mathrm{as}\, t \tag{4.6}$$

The $W(t)$ converts from ITRS to TIRS which uses the CIP as the z axis and the TIO as the x axis. $W(t)$ can be written as follows

$$W(t) = R_3(-s') \cdot R_2(-x_p) \cdot R_1(y_p) \tag{4.7}$$

CIRS uses the CIP direction as the z axis and the CIO direction as the x axis. The $Q(t)$ transformation matrix is used to convert from GCRS to CIRS. The $Q(t)$ transformation matrix is produced by using the CIP coordinates of the GCRS, E and d, and the s value called the "CIO Locator". These inputs to be used in the matrix are obtained as follows

$$X = \sin d \cos E, \qquad Y = \sin d \sin E, \qquad Z = \cos d \tag{4.8}$$

and can be shown as

$$E = \arctan \frac{Y}{X}, \quad d = \arccos Z = \arccos(\sqrt{1 - X^2 + Y^2}), \quad s = s_0 - \frac{XY}{2} \tag{4.9}$$

herein X and Y represent the angular coordinates of the CIP in GCRS.

$$s(t) = -\int_{t_0}^{t} \frac{X(t)\dot{Y}(t) - Y(t)\dot{X}(t)}{1 + Z(t)} dt - (\sigma_0 N_0 - \Sigma_0 N_0) \tag{4.10}$$

where σ_0 represents the position of the CIO in the epoch of $J2000.0$, Σ_0 represents the $x-$ origin of the GCRS and N_0 represents the ascending node of the $J2000.0$ equator.

When the CIP moves according to GCRS due to precession and nutation, between the J2000.0 reference epoch and t, CIO locator serves to determine the position of the CIO on the CIP equator relative to the NRO in the GCRS (Capitaine, Guinot and McCarthy, 2000). $Q(t)$ can be written as follows

$$Q(t) = R_1(-E) \cdot R_2(-d) \cdot R_3(-E) \cdot R_3(s) \tag{4.11}$$

In order to obtain the X and Y, the celestial pole offsets, δX and δY, obtained by astronomical observations should be added to the X_{MODEL} and Y_{MODEL} derived from IAU 2000/2006 precession-nutation model as follows:

$$X = X_{\mathrm{MODEL}} + \delta X \tag{4.12}$$

$$Y = Y_{\mathrm{MODEL}} + \delta Y \tag{4.13}$$

The transformation matrix $R(t)$ to be used for the rotation applied at any t epoch in the CIP equator as well as the angle (ERA) between these points to overlap the CIO and TIO.

$$R(t) = R_3(-ERA) \tag{4.14}$$

In brief, TIRS uses the CIP as z axis and TIO as x axis. CIRS uses the CIP as z axis and CIO as x axis. Using $W(t)$ matrice, TIRS is realized from ITRS at the t epoch and through using $Q(t)$ matrice, CIRS is realized from GCRS. Then, by using $R(t)$ matrices, CIO and TIO are overlapped.

5. APPLICATION

5.1. IVS daily sessions and the global VLBI network considered in this study

VLBI sessions are scheduled, carried out, and analyzed by the IVS (Schlüter and Behrend, 2007) routinely to provide the EOP series, the TRF, and the CRF to the scientific and industrial community worldwide. These sessions are handled as two categories so-called as the intensive sessions (1-2 hours long) and the standard, i.e. 24 hours long, sessions. The VLBI sessions cannot be carried out every day due to operational difficulties. This causes gaps in the estimated parameter time series which is not the case e.g. GNSS. Nevertheless, Intensive sessions of IVS are conducted every day with the participation of at least 2 to 4 stations for the only purpose of UT1 monitoring, while 24 hour sessions are held with the participation of at least 5 stations e.g. EOP monitoring, TRF and CRF determination, densification and constraining the datums of the other space geodetic techniques and called as, among others, e.g. IVS-R1, IVS-R4, RDV, APSG, EUROPE, IVS-T2, IVS-CRF, and CONT (Schuh and Behrend, 2011).

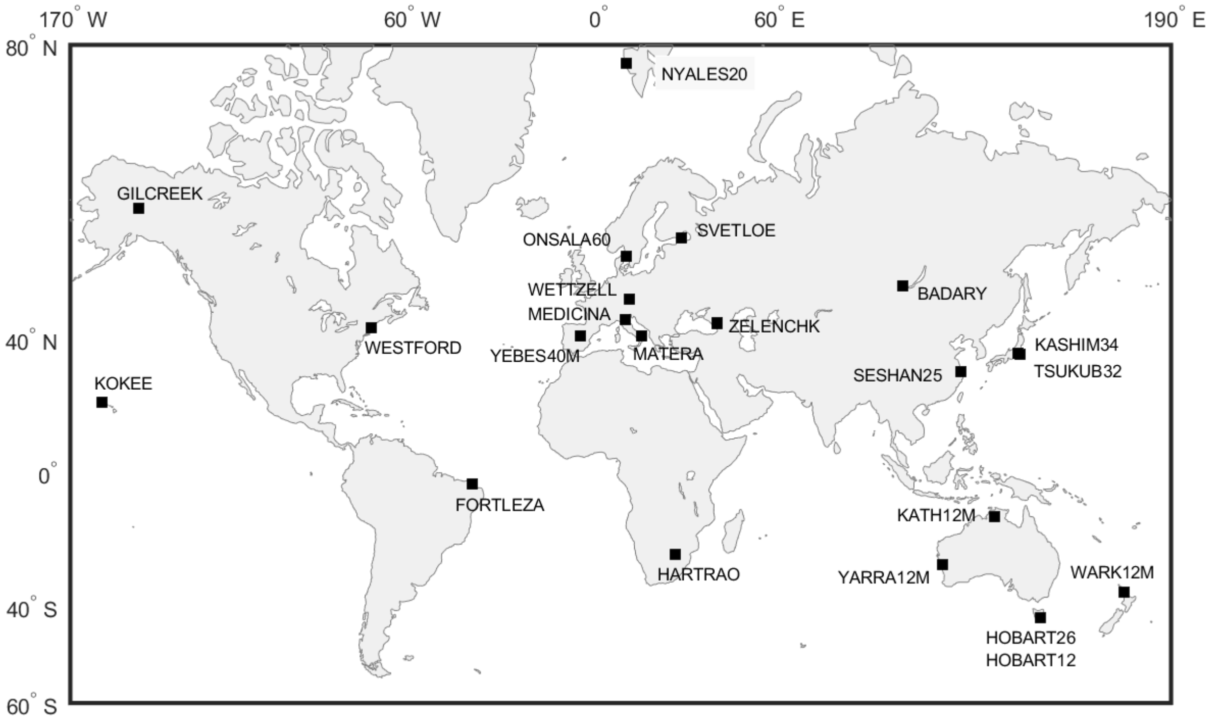

Figure 5.1. Global distribution of the VLBI stations considered in this study

5.2. Methodology

In this thesis, 24 hour sessions observed from 04.01.2000 to 30.09.2018 were analyzed. In the analysis, Vienna VLBI and Satellite Software, VieVS (Böhm et al., 2018) was used which is based on estimating the parameters with the classical Gauss-Markov least-squares method. NNR (no-net-rotation) condition equations were imposed w.r.t. ICRF3sx (Charlot et al., 2018) for estimating the source coordinates, as well as both NNT (no-net-translation) and NNR (no-net-rotation) conditions, were imposed w.r.t. ITRF2014 (Altamimi et al., 2016) for estimating the station coordinates while the velocities of the stations are fixed to ITRF20014. We used FES2004 (Lyard et al., 2006) as the ocean tide loading model, the (Petrov and Boy, 2004) model as the atmosphere loading, and the IERS pole model (Petit and Luzum, 2010) for the geophysical displacement corrections to the a priori coordinates of the stations. The daily celestial pole offsets (CPO) in addition to the precession/nutation model, IAU 2006/2000A plus IERS 14 C04 series (Bizouard et al., 2018) were estimated. Polar motion and UT1-UTC coordinates are estimated daily w.r.t. the IERS 14 C04 series plus semi-diurnal and diurnal high-frequency variations calculated from the IERS model (Petit and Luzum, 2010).

Piecewise linear offset (PLO) functions were used in the troposphere delay estimation. ZWD were estimated at 20-minutes intervals as PLO, i.e. at UTC integer hours but the gradients need longer observation intervals due to their slowly varying nature, so the north and east gradients were estimated at every 6 hour, as PLO. 1.5 cm after 20 minutes, relative constraints were imposed on the ZWD as well as 0.05 cm after 6 hour relative constraints plus 0.1 cm absolute constraints were imposed on the estimated troposphere gradients.

The stations that participate in the sessions have atomic clocks, and these clocks occasionally exposed to atomic frequency jumps, instant energy shifts, or energy changes, also so-called as clock breaks. After correcting the clock breaks using spline quadratic polynomials, the clock errors due to synchronization and frequency instabilities were estimated at 60-minute intervals as PLO on which 1.3 cm after 1 hour relative constraints are imposed. EOP were estimated as daily offsets with tight relative constraints as 10^{-4} mas after 1 day.

In this thesis; the effects of the troposphere delay estimation on station positions, source positions, and EOP are examined. At first, a rough process list is created by processing the daily sessions from 2000 to 2018. The sessions of which a posteriori standard deviation of unit weight (m_0) exceeds 2 cm are assumed to be not accurate enough for our purpose so these sessions were removed from our process list. As a result, 2483 daily sessions are obtained that ensure our accuracy criteria of a posteriori standard deviation of unit weight. To eliminate the outlier observations a simple outlier test is introduced.

As an objective and unbiased criteria, the repeatabilities were calculated for each set of the estimated parameters such as the troposphere ZTD, station positions, source positions, and EOP. The weighted root-mean-square (WRMS) of the estimated parameters as the repeatabilities were calculated by

$$WRMS = \sqrt{\frac{\sum_{i=1}^{n} \frac{\left(x_i - WM\right)^2}{\sigma_{x_i}^2}}{\sum_{i=1}^{n} \frac{1}{\sigma_{x_i}^2}}} \tag{5.1}$$

where x_i denotes the ith estimated parameter and σ_{x_i} is the formal error (standard error) of the concerning parameter calculated from e.g. $\sigma_{x_i} = \sigma_0 \sqrt{Q_{x(diag)}}$ and the weighted mean is

$$WM = \frac{\sum_{i=1}^{n} \frac{x_i}{\sigma_{x_i}^2}}{\sum_{i=1}^{n} \frac{1}{\sigma_{x_i}^2}}. \tag{5.2}$$

To assess the agreement between two sets of parameters, the weighted mean (WM) and the weighted root-mean-square (WRMS) of the differences were computed as follows

$$WM_{diff} = \frac{\sum_{i=1}^{n} \frac{x_i - y_i}{\sigma_{x_i}^2 + \sigma_{y_i}^2}}{\sum_{i=1}^{n} \frac{1}{\sigma_{x_i}^2 + \sigma_{y_i}^2}} \tag{5.3}$$

The WRMS of the difference vectors were calculated as

$$WRMS_{diff} = \sqrt{\frac{\sum_{i=1}^{n} \frac{\left(x_i - y_i - WM\right)^2}{\sigma_{x_i}^2 + \sigma_{y_i}^2}}{\sum_{i=1}^{n} \frac{1}{\sigma_{x_i}^2 + \sigma_{y_i}^2}}} . \tag{5.4}$$

where n is the number of parameters that should be the same for each of the parameter set.

6. RESULTS

A set of analyses i.e. 12 times (3 mapping functions by 4 elevation cut-off angles), of the 2483 daily VLBI sessions were performed through using the VMF1, VMF3 and GMF3 troposphere mapping functions as well as the elevation cut-off angles of 5, 7, 10, and 15 degrees. The troposphere ZTD, the daily station coordinates, the daily quasar coordinates, and the daily EOP were estimated from these analyses in which the different mapping functions and the elevation cut-off angles were used and all the other parameters were held as fixed. Then the estimated parameter time series were assessed in terms of the repeatability metric.

6.1. Results of the troposphere ZTD estimated from the analysis of VLBI daily sessions when different troposphere mapping functions and elevation cut-off angles are used.

The troposphere ZTD as piece-wise linear offsets (PLO) with 20-minute intervals were derived by adding the estimated ZWD to the calculated ZHD using Saastamoinen (1972) analytical function (e.g. see Figure 6.1 and 6.2 for the Wettzell and Tsukuba sites, respectively). At the Wettzell (Germany) VLBI site, a seasonal variation of the ZWD (black line) with a peak to peak amplitude of about 30 cm is seen. On the other hand, the seasonal variation of the ZHD (red line) is as not that much clear unlike ZWD, and has a seasonal amplitude of about 10 cm. When the Tsukuba (Japan) ZWD (black) is considered, the peak to peak amplitude of the seasonal variation is found about 40 cm and the ZHD (red line) exhibits a more apparent seasonal variation compared with Wettzell. This is a clear indication that the seasonal variations of the atmospheric pressure as well as the humidity are superior at the Tsukuba site than those of the Wettzell.

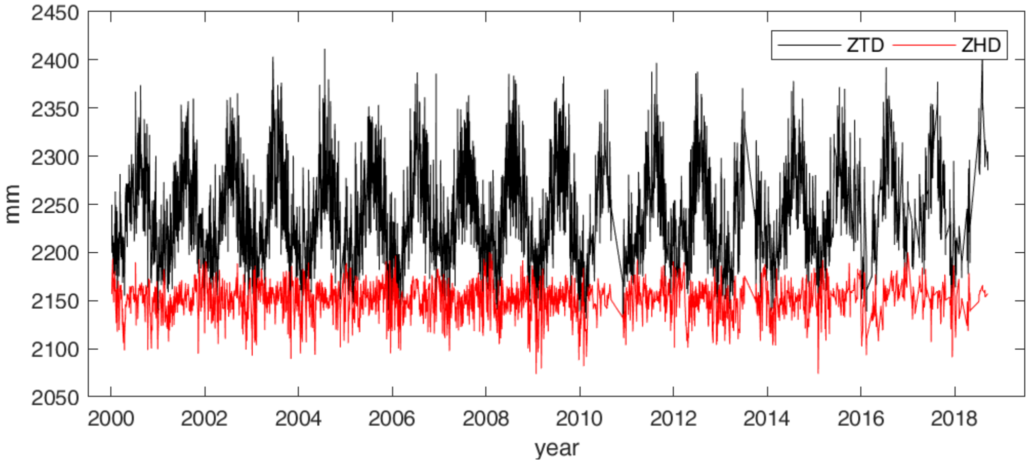

Figure 6.1. ZHD computed from Saastamoinen (1972) and ZTD estimates at 20-minute intervals at Wettzell (Germany) from the analysis of VLBI daily sessions when using the mapping function VMF3 and 5 degrees elevation cut-off angle.

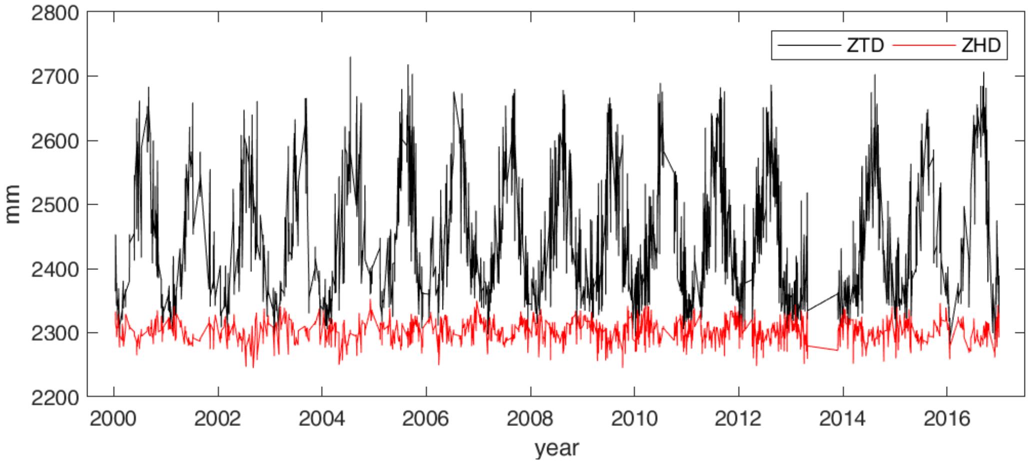

Figure 6.2. ZHD computed from Saastamoinen (1972) and ZTD estimates at 20-minute intervals at Tsukuba (Japan) from the analysis of VLBI daily sessions when using the mapping function VMF3 and 5 degrees elevation cut-off angle.

When different troposphere mapping functions (VMF1, VMF3, and GMF3) and 5 degrees elevation cut-off angle are considered, the following results in terms of the WRMS of the ZTD differences can be inferred: The WRMS differences of ZTD between VMF1 and VMF3 are found smaller than 0.5 mm for most of the sites. However, these WRMS differences at Tsukuba (Japan), Kashima (Japan), and Seshan (China) VLBI sites reach up to 1 mm. This might be most likely due to the higher humidity at these coastal sites. GMF3 mapping function ZTD results exhibit high correlations with VMF1 and VMF3 mapping functions. This is expected since GMF is a global spherical harmonic seasonal approximation of VMF. When the WRMS differences of ZTD between the GMF3 and VMF3 mapping functions are considered, about 2 mm differences are seen at most of the geodetic sites (see Figure 6.3).

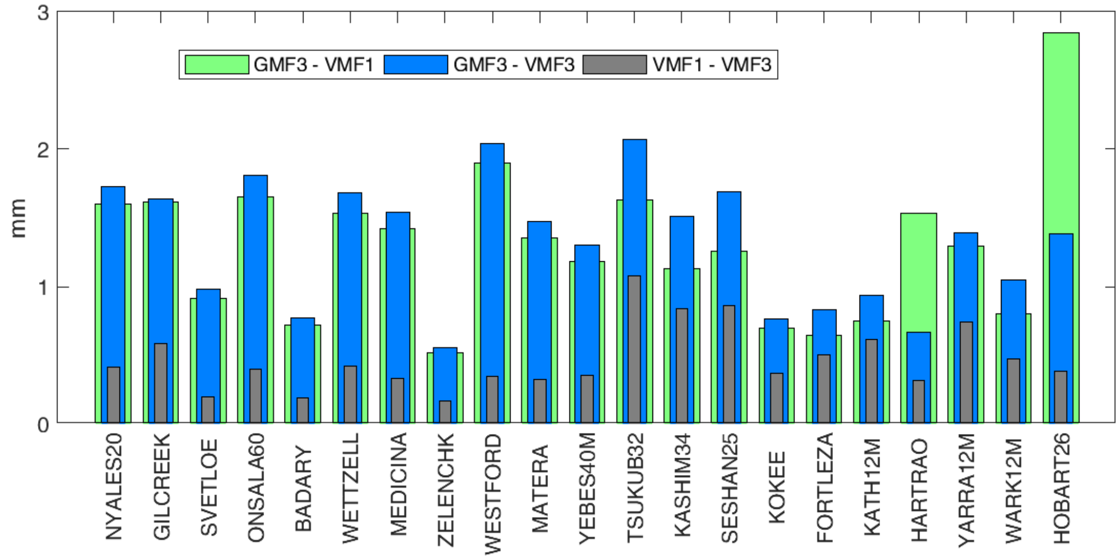

Figure 6.3. The weighted root mean square (WRMS) of the ZTD differences when different troposphere mapping functions and 5 degrees elevation cut-off angle are used in the analysis of the VLBI daily sessions.

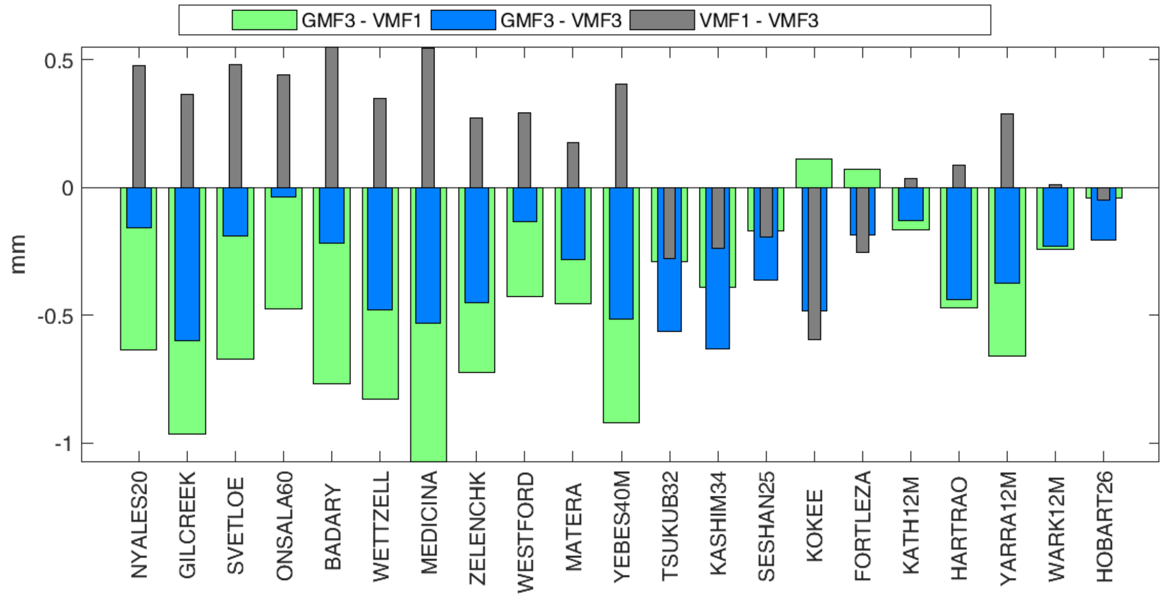

Figure 6.4. The weighted mean (WM) of the ZTD differences when different troposphere mapping functions and 5 degrees elevation cut-off angle are used in the analysis of the VLBI daily sessions.

While the WRMS of the ZTD differences between GMF3 and VMF1 at Hartebeesthoek (South Africa) and Hobart (Tasmania Island, Australia) sites are within 1.5 mm and 2.8 mm, the WRMS of the ZTD differences between GMF3-VMF3 decrease to the range of 0.7 mm and 1.4 mm. In general, considering the WRMS of the ZTD differences between GMF3-VMF1 and GMF3-VMF3, it can be suggested that the ZTD agreement between GMF3-VMF3 is better (Figure 6.3.). As expected, ZTD agreement between VMF1-VMF3 is found to be 2 to 3 times better than GMF3-VMF1 and GMF3-VMF3 agreements in terms of the WRMS differences (see Figure 6.3.).

When different troposphere mapping functions and 5 degrees elevation cut-off angle is considered the following results are found in terms of the WM of the ZTD differences: The largest ZTD biases are found between GMF3 and VMF1 mapping functions at most of the sites that reach up to -1 mm. GMF3-VMF3 WM ZTD biases are negative at all sites and ranges within -0.1 and -0.6 mm. The WM ZTD biases between VMF1 and VMF3 are all positive at the northern hemisphere sites but negative at most of the southern hemisphere sites and ranges within -0.6 and +0.6 mm (see Figure 6.4.).

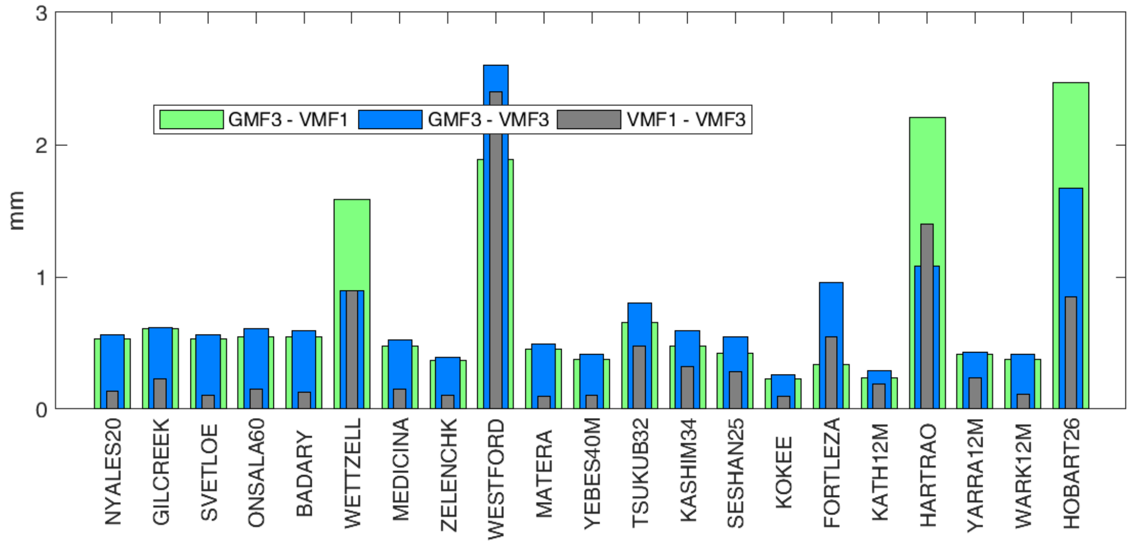

Figure 6.5. The WRMS of the ZTD differences when different troposphere mapping functions and 15 degrees elevation cut-off angle are used in the analysis of the VLBI daily sessions.

When different troposphere mapping functions and 15 degrees elevation cut-off angle are considered the following results are inferred in terms of the WRMS of the ZTD differences: The largest WRMS differences of the ZTD are found between GMF3 and VMF1 at the VLBI sites: Wettzell, Westford (east coast of USA), Hartebeesthoek and Hobart. At 15 degrees elevation cut-off angle the WRMS differences of the ZTD between VMF1 and VMF3 are found below 0.3 mm for most of the sites except the sites: Wettzell, Westford, Hartebeesthoek and Hobart (see Figure 6.5.).

When 5 degrees and 15 degrees elevation cut-off angles are compared it is seen that the WRMS differences between mapping functions reduce substantially with the increase of the elevation cut-off angle. This suggests that there should not be a significant difference between mapping functions above e.g. 15 or 20 degrees elevation cut-off angle. From this result the benefit of using VMF3 is started after reducing the elevation cut-off angle to about 5 degrees.

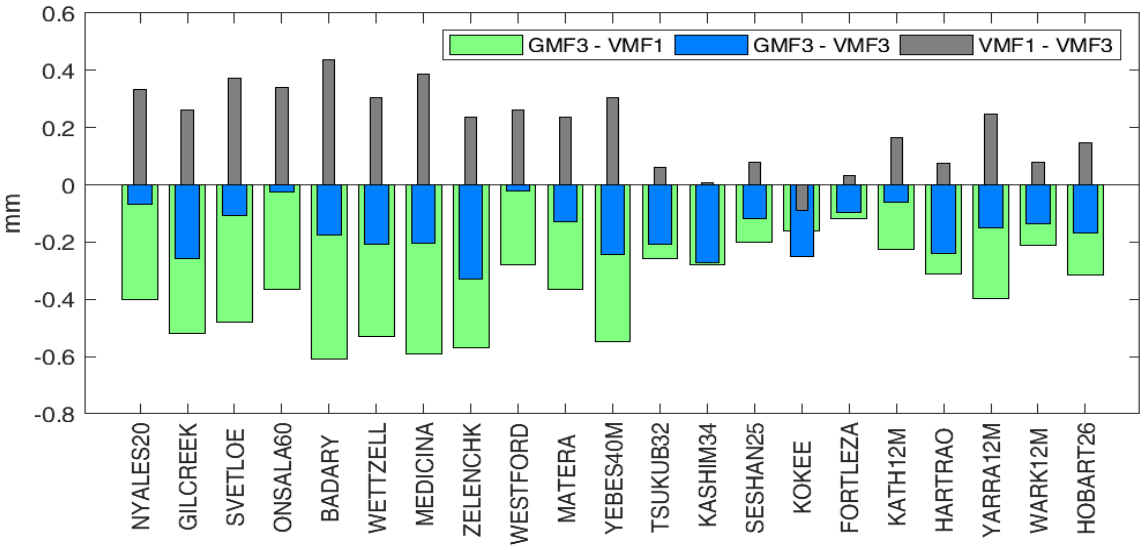

Figure 6.6. The WM of the ZTD differences when different troposphere mapping functions and 15 degrees elevation cut-off angle is used in the analysis of the VLBI daily sessions.

When the WM of the ZTD differences are compared between 5 and 15 degrees, unlike WRMS differences, a significant change in WM biases of ZTD is not detected. On the other hand, for both 5 and 15 degrees, the WM of ZTD differences are positive for most of the sites between VMF1 and VMF3, and negative both between GMF3-VMF3 and GMF3-VMF1 (see Figure 6.6). The largest WM of the ZTD differences (mean biases) are seen both for 5 and 15 degrees between GMF3 and VMF1. These results indicate that when different elevation cut-off angles are used, the biases between ZTD estimates do not reduce. As an inference from these results, changing elevation cut-off angle does not considerably affect the ZTD biases between mapping functions.

The best agreement in terms of the WRMS of ZTD differences is found between 5 and 7 degrees for all stations where the largest value is 6.5 mm at the VLBI site Fortleza (Brazil). The worst agreements, as expected, are seen between 5-15 degrees, 7-15 degrees, and 10-15 degrees elevation cut-off angles when VMF3 is used.

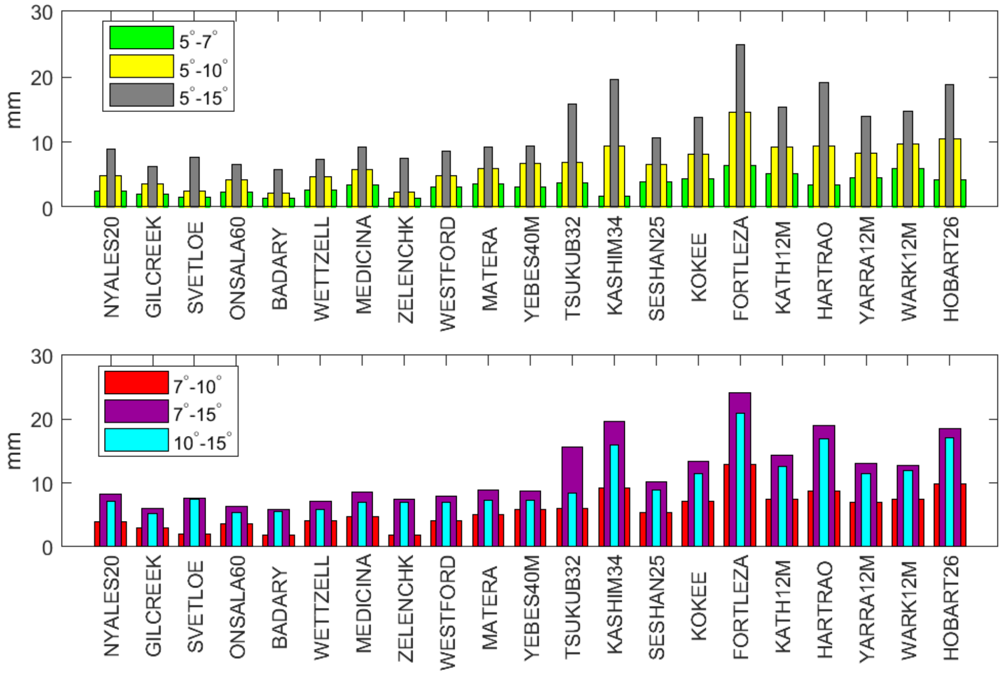

Figure 6.7. The WRMS of the ZTD differences between 5, 7, 10, and 15 degrees elevation cut-off angles when the troposphere mapping function, VMF3 are used in the analysis of the VLBI daily sessions.

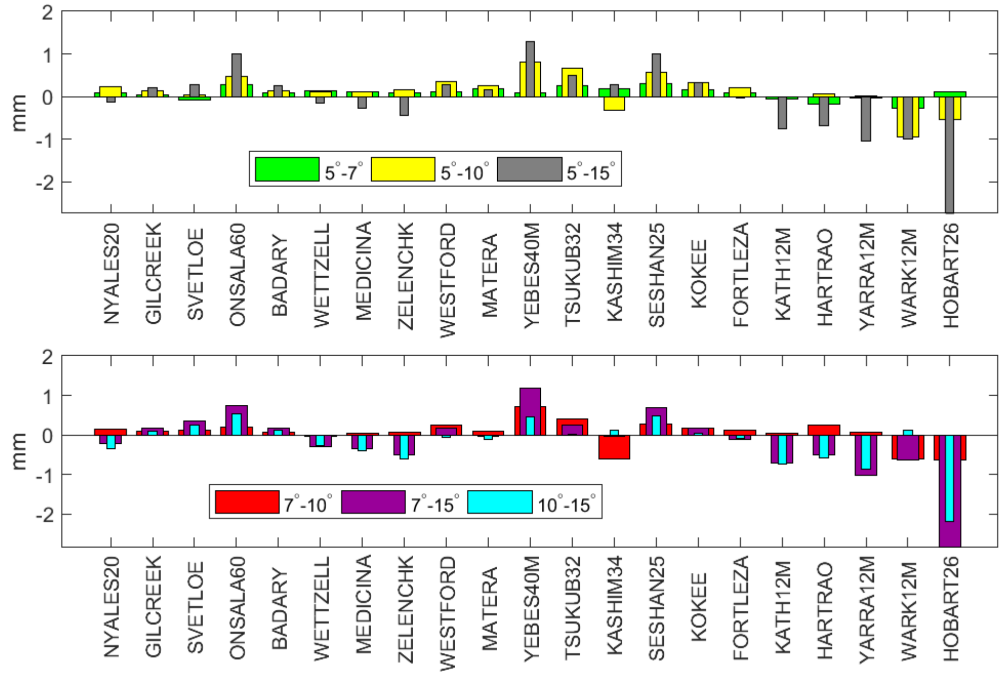

Figure 6.8. The WM of the ZTD differences (ZTD mean biases) between 5, 7, 10, and 15 degrees elevation cut-off angles when the troposphere mapping function, VMF3 are used in the analysis of the VLBI daily sessions.

A latitude dependency is detected in terms of the WRMS of the ZTD differences. From the northernmost VLBI site i.e. Ny Alesund (Svalbard Island, Norway) to Yebes (Spain) site the WRMS of the ZTD differences between 5-7, 5-10, 5-15 elevation cut-off angles range within 2 to 10 mm whereas from Tsukuba (Japan) to Hobart (Tasmania Island, Australia) that is the southernmost located site, the WRMS of ZTD differences varies within 3 to 25 mm. In general, the agreement between elevation cut-off angles is larger at the southern hemisphere than those of the northern hemisphere. This would most probably due to the fewer number of VLBI sites at the southern hemisphere results in less number of observations as well as the relatively inhomogeneous distribution of observations at local skies (see Figure 6.7.).

When the WM of ZTD differences between 5, 7, 10 and 15 degrees elevation cut-off angles are considered, the values do not exceed ± 1 mm at most of the VLBI sites whereas at Yebes, Yarragade (west coast of Australia), and Hobart the WM biases exceed ± 1 mm (see Figure 6.8.).

The reason for the large increase in WRMS of the ZTD differences from 7 to 10 degrees and 7 to 15 degrees relative to 5 to 7 degrees should be the larger number of observations lie in between 7-10 and 7-15 degrees compared to 5 to 7 degrees. Besides, the larger WRMS of ZTD differences at southern hemisphere sites should have resulted from not just less number but also inhomogeneous geometry of the observations and all the sites at the southern hemisphere are near the coast (furthest located about 150km off the coast).

6.2. Results of the daily station positions estimated from the analysis of VLBI daily sessions when different troposphere mapping functions and elevation cut-off angles are used

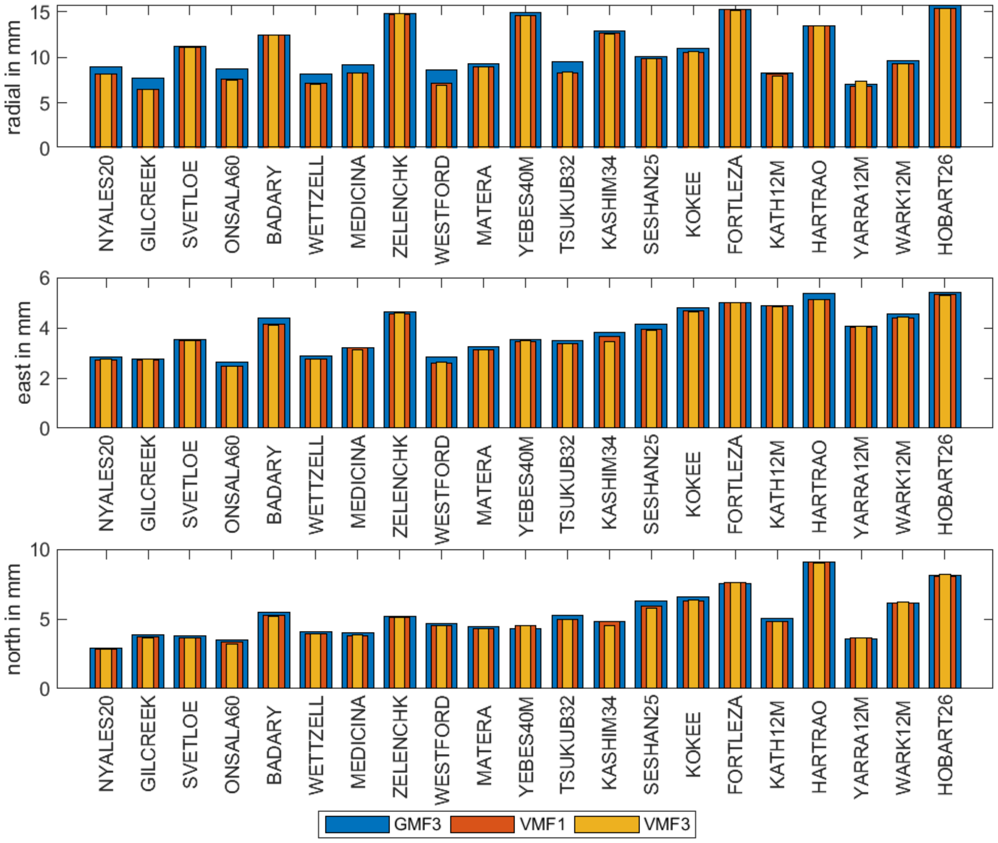

Figure 6.9. The WRMS repeatabilities of the station daily positions when different troposphere mapping functions and 5 degrees elevation cut-off angle are used in the analysis of the VLBI daily sessions.

When different troposphere mapping functions and elevation cut-off angles are used in the analysis of the VLBI daily sessions and all other parameters are held as fixed, the variations in daily station positions are examined. When different mapping functions are used in the analysis at 5 degrees cut-off angle the WRMS repeatabilities of station daily positions vary in 10 to 15 mm in radial, 3 to 5 mm in east, and 3 to 9 mm in north components (see Figure 6.9.).

When different troposphere mapping functions and 5 degrees elevation cut-off angle are used in the analysis of the VLBI daily sessions, the WM of the station daily positions w.r.t. to ITRF2014 changes as much as 0.2 mm at Seshan (Shangai, east coast of China) VLBI site. This suggests that the WM of the stations' daily positions are not sensitive to the change of mapping functions. However, the large WM biases seen in all components of Yebes, Kashima, Warkworth (North Island, New Zealand) and Hobart vary between -4 and 3 mm indicate that a combination of the ITRF2014 catalog errors in addition to a priori unreduced geophysical effects such as non-tidal ocean loading as well as hydrological loading displacements might most probably propagate into these biases (Figure 6.10.).

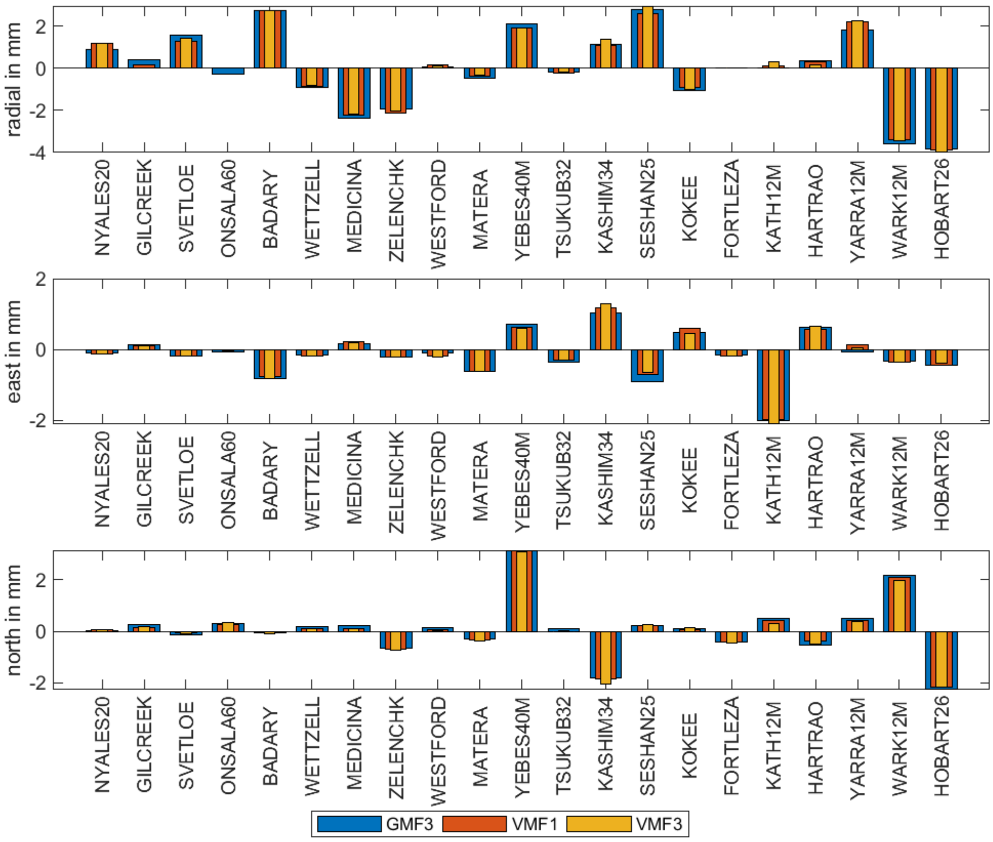

Figure 6.10. The WM (mean biases) of the station daily positions w.r.t. ITRF2014 when different troposphere mapping functions and 5 degrees elevation cut-off angle are used in the analysis of the VLBI daily sessions.

When different mapping functions and 15 degrees cut-off elevation cut-off angle are used in the analysis, the WRMS repeatabilities of station daily positions vary in 10 to 21 mm in radial, 3 to 10 mm in east, and 3 to 12 mm in north components (see Figure 6.11.). Relatively to 5 degrees, the 15 degrees cut-off elevation cut-off angle worsened the WRMS repeatability results up to about 5 mm in radial, 5 mm in the east, and 3 mm in north components at most of the sites.

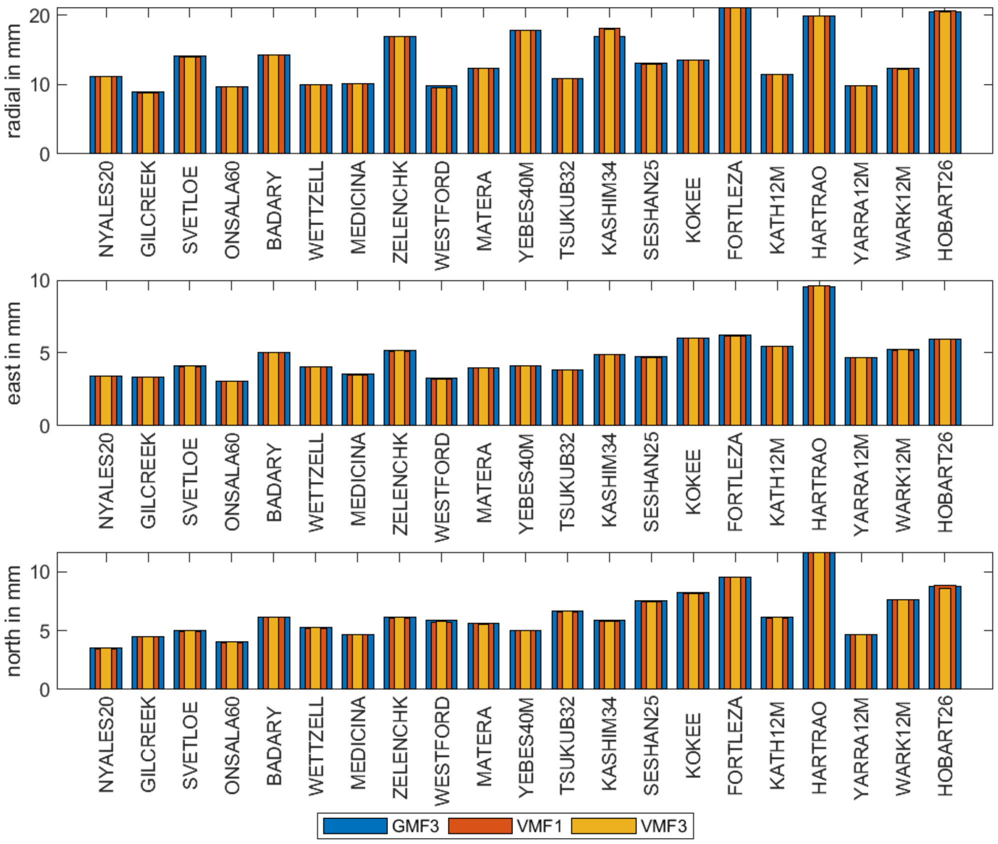

Figure 6.11. The WRMS repeatabilities of the station daily positions when different troposphere mapping functions and 15 degrees elevation cut-off angle are used in the analysis of the VLBI daily sessions.

The WRMS of the station position differences are examined when different troposphere mapping functions are used and elevation cut-off angle is fixed in the analysis of the VLBI daily sessions. Thus, the effects of changing the mapping functions on the station position repeatabilities are figured out. When 5 degrees elevation cut-off angle is used in the analysis, the WRMS of the radial position differences vary in 0.5-1.5 mm between VMF1-VMF3, and 2 - 5 mm between GMF3-VMF1 as well as GMF3-VMF3. In tangential components, the WRMS of the position differences varies in about 0.2-0.5 mm between VMF1-VMF3 whereas larger about 0.8 mm in east component and 1.5 mm in north components between GMF3-VMF1 and GMF3-VMF3 at most of the sites. The radial component is found to be the most variable component and the GMF3 is the mapping function that causes the largest position repeatabilities (see Figure 6.12.). When 5 degrees (Figure 6.12.), 7 degrees (Figure 6.13), 10 degrees (Figure 6.14) and 15 degrees (Figure 6.15) elevation cut-off angles are used in the analysis, the WRMS of the station positions differences gradually decrease and finally the differences reach down to 1 mm in radial and 0.2 mm in tangential components at 15 degrees elevation cut-off angle (see Figure 6.15.). These results indicate that the differences in the station position repeatabilities between the mapping functions decrease when the elevation cut-off angle increases. Finally from 15 degrees upwards mapping functions produce similar (nearly identical) position repeatability results. On the other hand, due to the long baselines of VLBI, most of the observations lie in between the lower elevation cut-off angles i.e. 5 to 30 degrees. Thus, the choice of mapping function in the analysis of VLBI observations has the utmost importance for the estimation of accurate parameters especially the station positions (see Figure 6.12.).

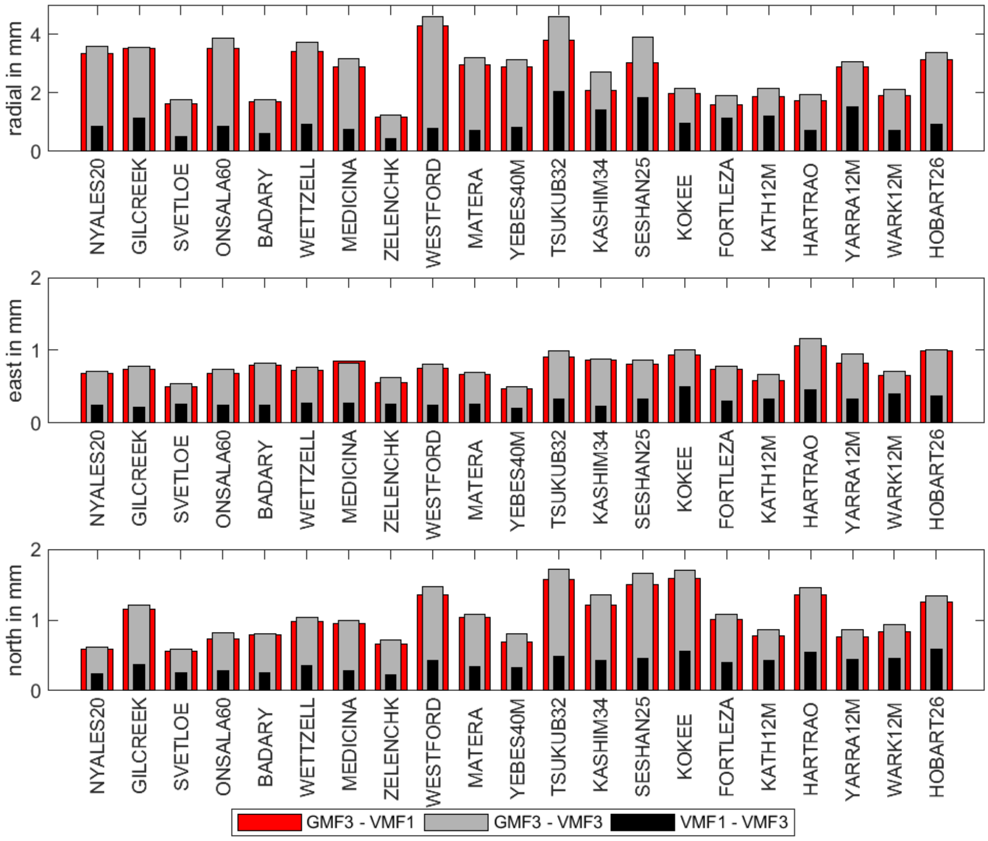

Figure 6.12. The WRMS of the station position differences when different troposphere mapping functions and 5 degrees elevation cut-off angle are used in the analysis of the VLBI daily sessions.

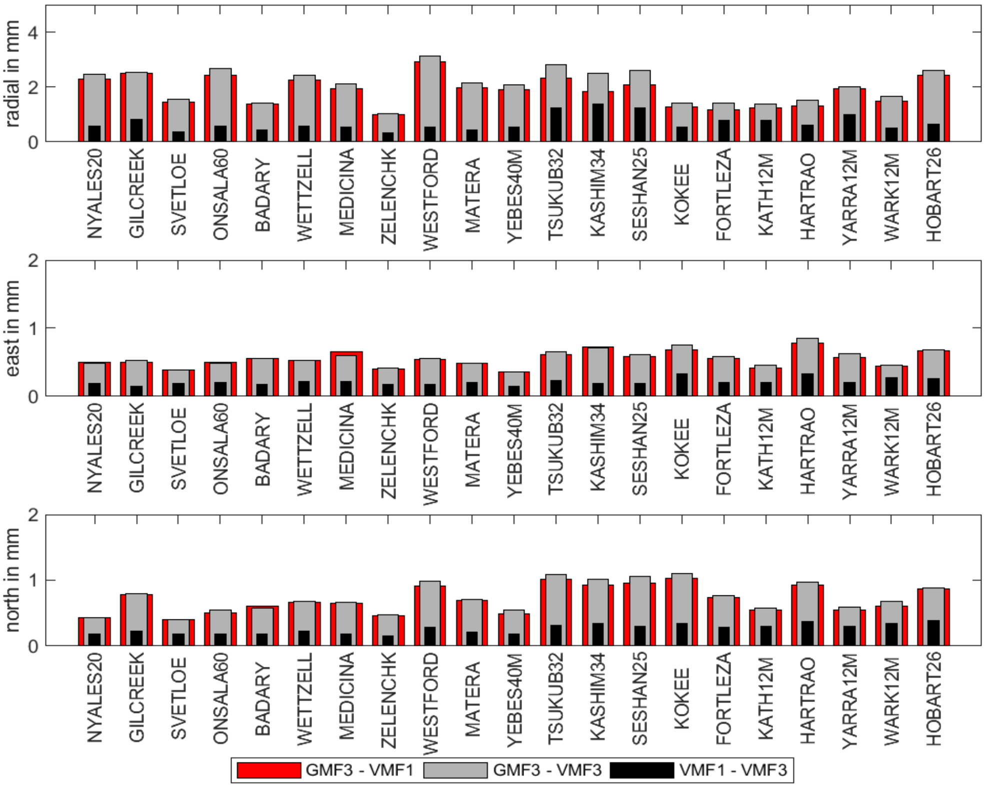

Figure 6.13. The WRMS of the station position differences when different troposphere mapping functions and 7 degrees elevation cut-off angle are used in the analysis of the VLBI daily sessions.

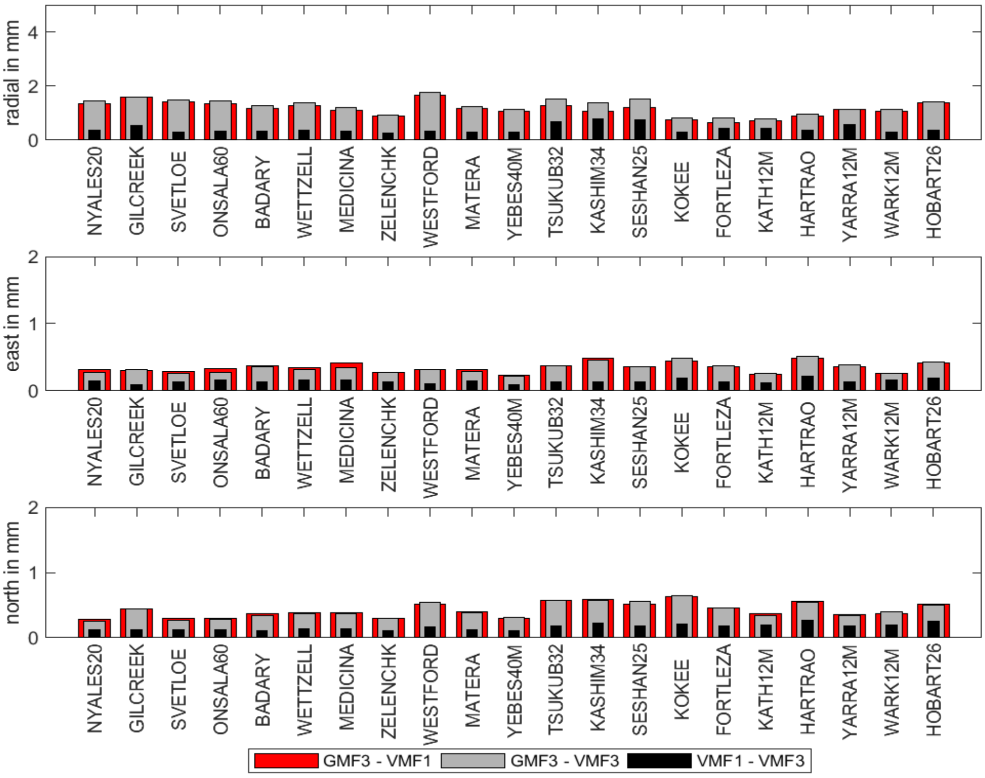

Figure 6.14. The WRMS of the station position differences when different troposphere mapping functions and 10 degrees elevation cut-off angle are used in the analysis of the VLBI daily sessions.

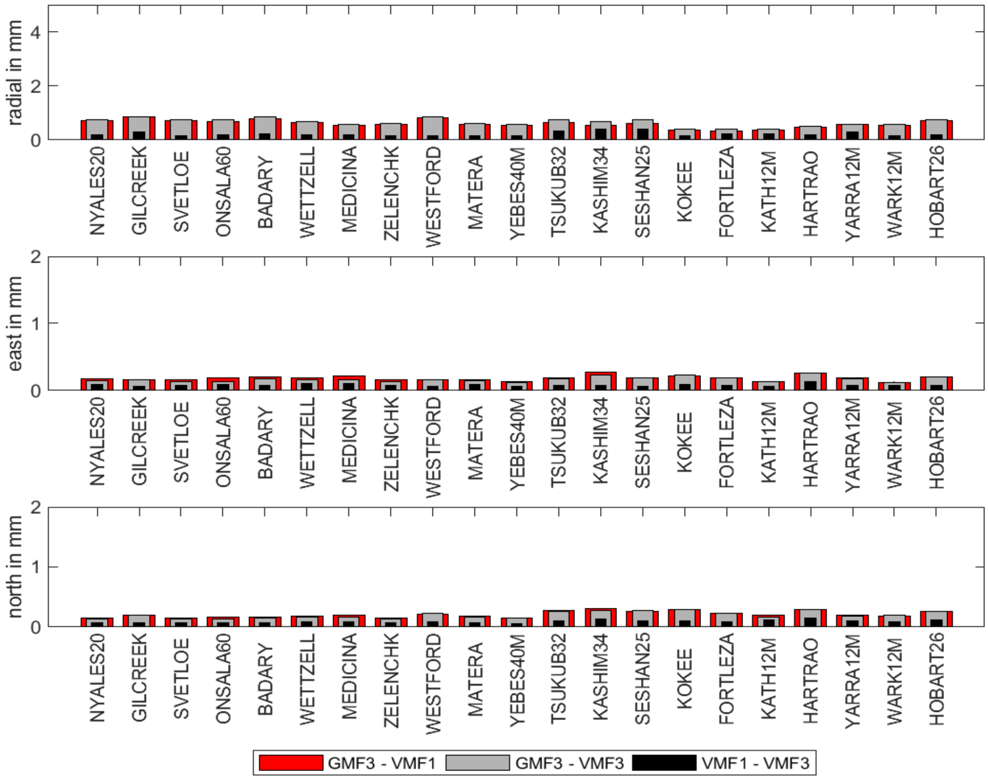

Figure 6.15. The WRMS of the station position differences when different troposphere mapping functions and 15 degrees elevation cut-off angle are used in the analysis of the VLBI daily sessions.

6.3. Results of the daily Earth orientation parameters (EOP) estimated from the analysis of VLBI daily sessions when different troposphere mapping functions and elevation cut-off angles are used.

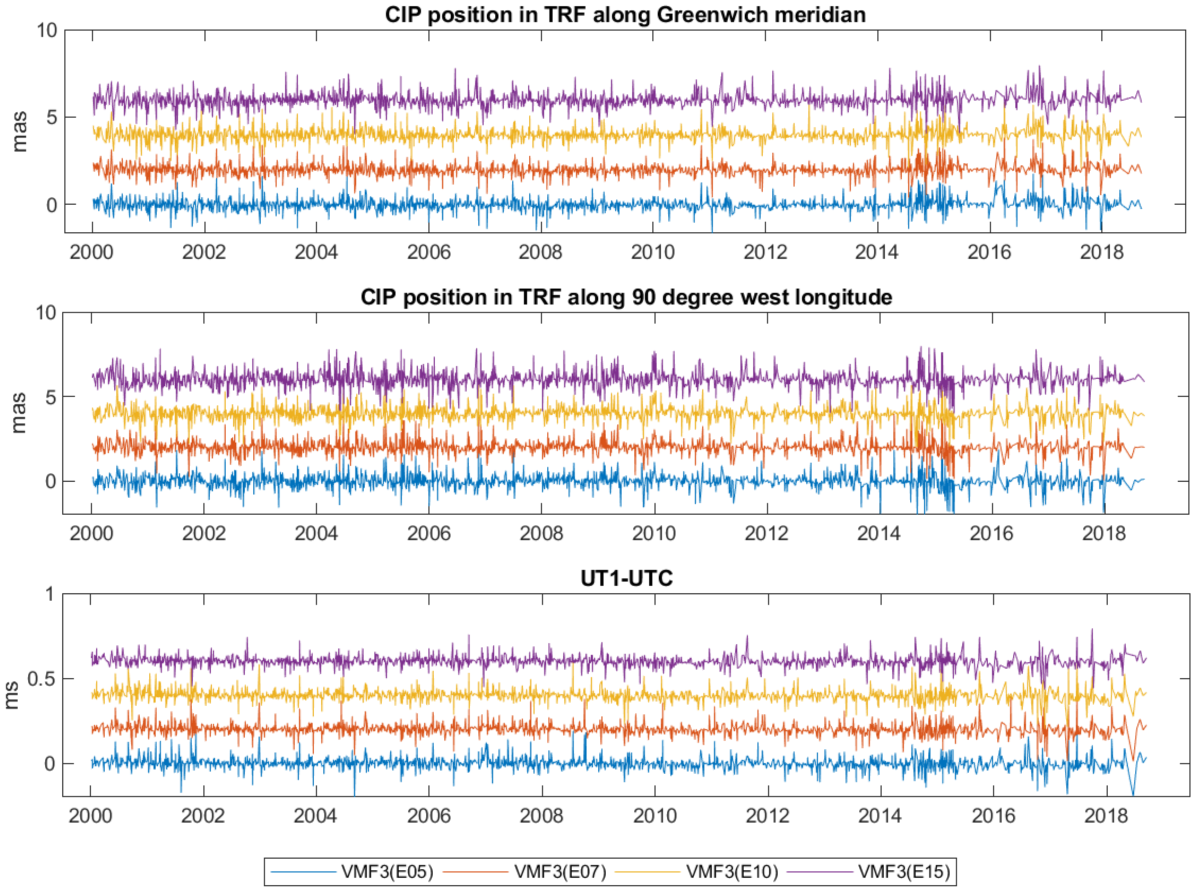

Figure 6.16. The time series of the daily Earth rotation parameters (ERP) estimated w.r.t. IERS 14 C04 combined EOP series when troposphere mapping function VMF3 and different elevation cut-off angles (5, 7, 10, and 15 degrees) are used in the analysis of the VLBI daily sessions. To make the plots more clear polar motion coordinates and UT1-UTC are shifted as 2 mas and 0.2 ms, respectively.

In this section, the effects of using different troposphere mapping functions and elevation cut-off angles on the estimated daily EOP are investigated (see Figure 6.16.). In Figure 6.16, the time series of the daily Earth rotation parameters (ERP), estimated w.r.t. the IERS 14 C04 combined EOP series when troposphere mapping function VMF3 and different elevation cut-off angles (5, 7, 10, and 15 degrees) are used in the analysis of the VLBI daily sessions, are shown. The median formal errors of the xp, yp and UT1-UTC are found as 122 µas, 147 µas and 12 µs when VMF3 and 5 degrees elevation cut-off angle is used in the analysis, respectively.

However, the median formal errors of the xp, yp and UT1-UTC get larger when 15 degree elevation cut-off angle is used as 176 µas, 219 µas and 13 µs, respectively. As for the celestial pole offsets the median formal errors of the X and Y coordinates are found as 161 µas and 152 µas for 5 degrees elevation cut-off angle but 171 µas and 161 µas for 15 degrees elevation cut-off angle and VMF3 are used in the analysis. These median formal errors of the estimated EOP are all in the range of expected values from a standard IVS daily session analyses. However, the EOP formal error differences are significant when different elevation cut-off angles are used.

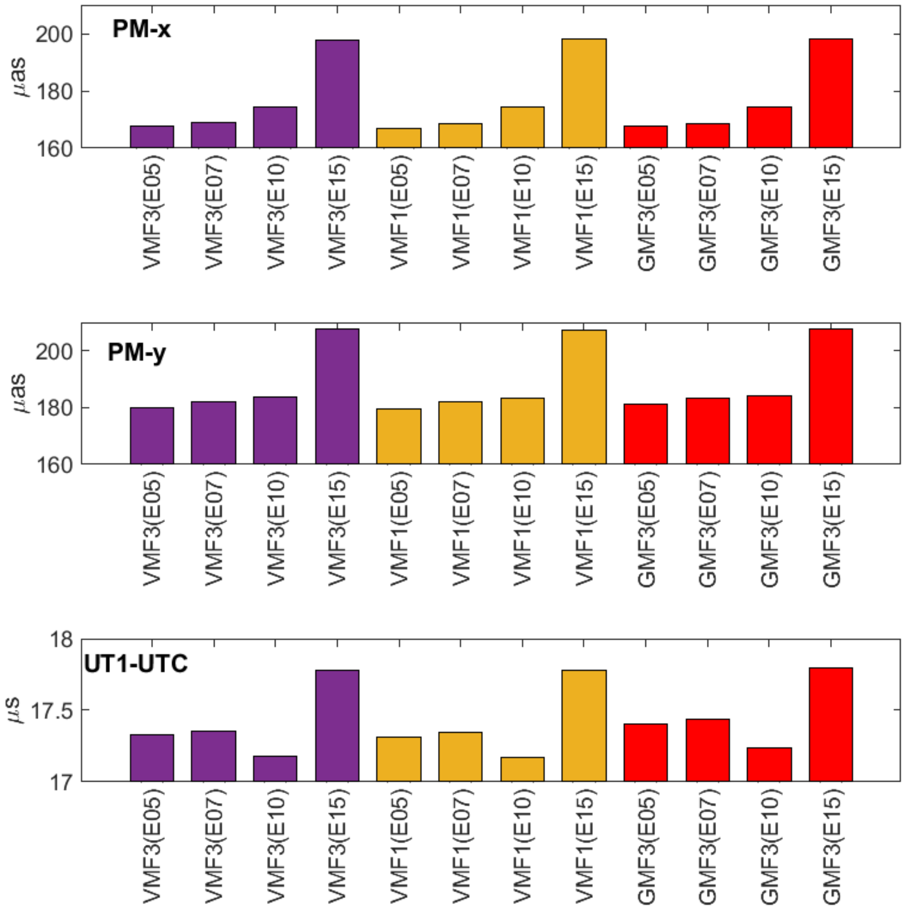

Figure 6.17. The WRMS repeatabilities of the daily ERP estimates w.r.t. the IERS 14 C04 combined EOP series when different troposphere mapping functions (VMF3, VMF1, GMF3) and elevation cut-off angles (5, 7, 10, and 15 degrees) are used in the analysis of the VLBI daily sessions.

In Figure 6.17, the WRMS repeatabilities of the daily ERP estimates w.r.t. the IERS 14 C04 combined EOP series when different troposphere mapping functions (VMF3, VMF1, GMF3) and elevation cut-off angles (5, 7, 10, and 15 degrees) are used in the analysis of the VLBI daily sessions, are shown. It can be clearly seen from Figure 6.17 that the WRMS repeatabilities of daily ERP estimates slightly vary w.r.t. the change of mapping function, but increase substantially w.r.t. the increase in the elevation cut-off angle. It can be inferred from these results that instead of mapping function, the repetabilities of EOP are much more sensitive to the number and the geometry of the observations i.e. the elevation cut-off angle.

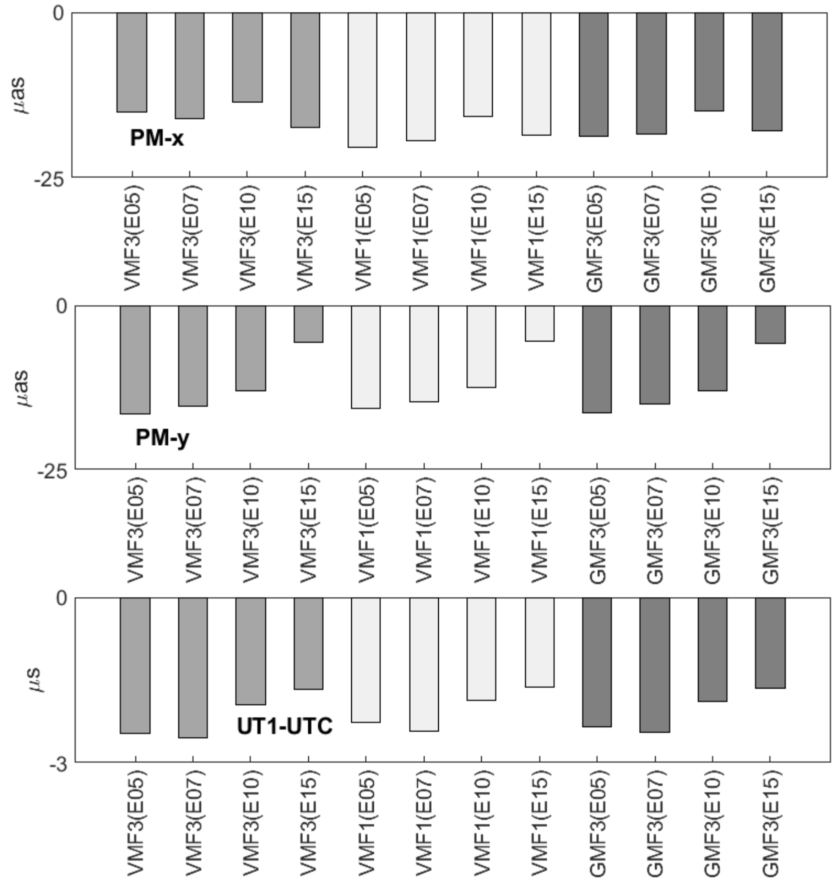

Figure 6.18. The WM (mean biases) of the daily ERP estimates w.r.t. the IERS 14 C04 combined EOP series when different troposphere mapping functions (VMF3, VMF1, GMF3) and elevation cut-off angles (5, 7, 10, and 15 degrees) are used in the analysis of the VLBI daily sessions.

When the WM (mean biases) of the daily ERP estimates w.r.t. the IERS 14 C04 combined EOP series are considered (see Figure 6.18), similar to WRMS differences, WM biases stay nearly invariant to the change of mapping functions (VMF3, VMF1, GMF3). But, slight variations are seen when the elevation cut-off angles (5, 7, 10, and 15 degrees) are used in the analysis of the VLBI daily sessions. All the WM biases of the ERP w.r.t. IERS 14 C04 series are found as negative values range within -14 µas and -20 µas for the polar motion coordinates and within -1.6 µs and -2.5 µs for the UT1-UTC. These all negative biases are resulted from the IERS 14 C04 series. Because, the IERS Earth orientation center (EOC) combines ERP estimates of all four space geodetic techniques at normal equation level using different variance components, i.e. the scaling factor of normal equations, for each technique. Thus, this results in biases in ERP of the IERS 14 C04 series relatively to those of only one technique. When the WM biases of the celestial pole offsets are considered the aforementioned explanation would partly valid since not inter-technique but intra-technique combination of the solutions of different IVS analysis centers are performed. Thus, the solutions of normal equations of different IVS analyis centers are scaled with the corresponding variances at the combination of CPO which finally results in biases when compared to a single solution. When overall EOP repeatabilities are considered, it can be inferred that 5 degrees elevation cut-off angle should be used regardless from which mapping function is introduced in the analysis. It is worth to note that this conclusion can only be drawn for the daily EOP estimation in analysis of the daily sessions.

The WRMS repeatabilities of the daily CPO w.r.t. IAU2000/2006 precession-nutation model plus IERS 14 C04 combined EOP series when different troposphere mapping functions (VMF3, VMF1, GMF3) and elevation cut-off angles (5, 7, 10, and 15 degrees) are used in the analysis of the VLBI daily sessions, are shown in Figure 6.20. From Figure 6.20, one can infer that the sensitivities of Y coordinates of CPO are much larger than those of X coordinates. The WRMS repeatabilities of the daily CPO coordinates vary within 202 µas-205 µas for the X coordinates and 183 µas-197 µas for the Y coordinates.

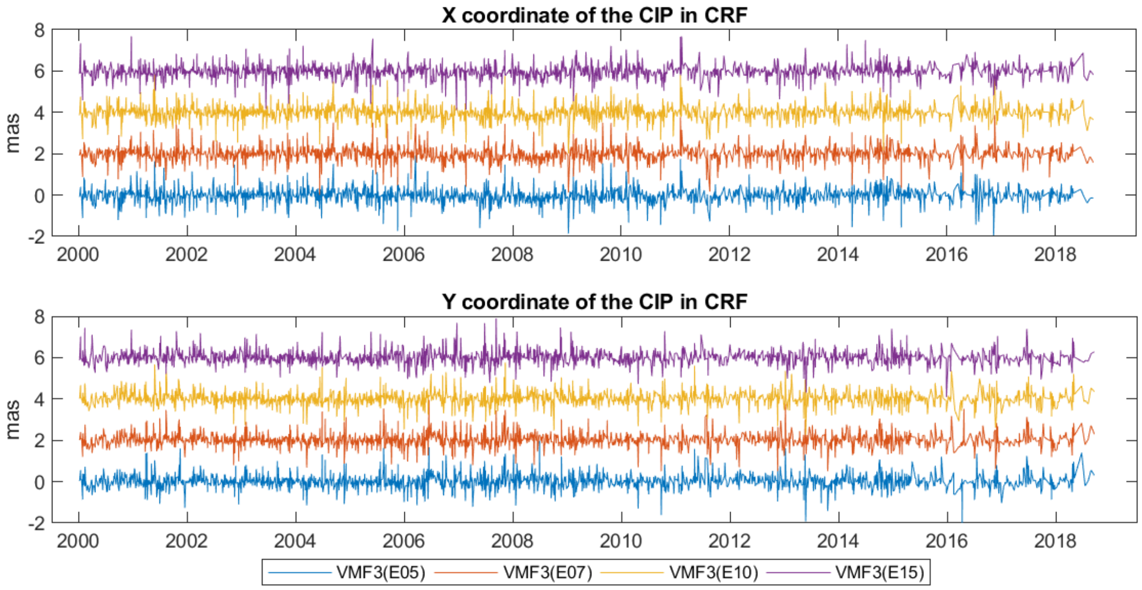

Figure 6.19. The time series of the daily celestial pole offsets w.r.t. IAU2000/2006 precession-nutation model plus IERS 14 C04 combined EOP series when troposphere mapping function VMF3 and different elevation cut-off angles (5, 7, 10, and 15 degrees) are used in the analysis of the VLBI daily sessions.

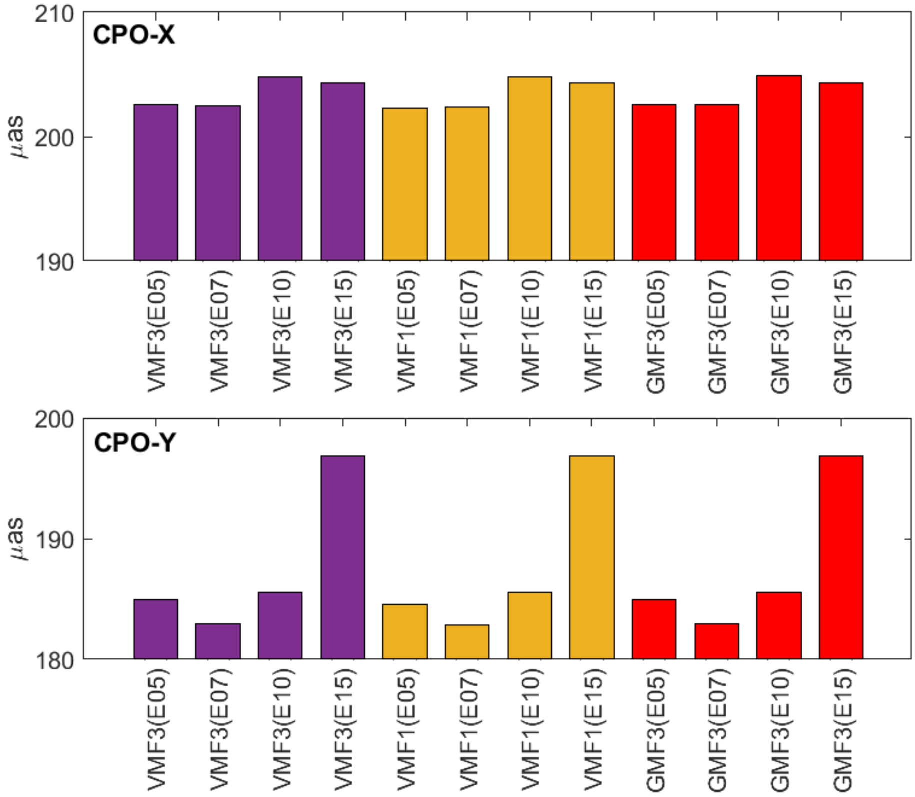

Figure 6.20. The WRMS repeatabilities of the daily celestial pole offsets w.r.t. IAU2000/2006 precession-nutation model plus IERS 14 C04 combined EOP series when different troposphere mapping functions (VMF3, VMF1, GMF3) and elevation cut-off angles (5, 7, 10, and 15 degrees) are used in the analysis of the VLBI daily sessions.

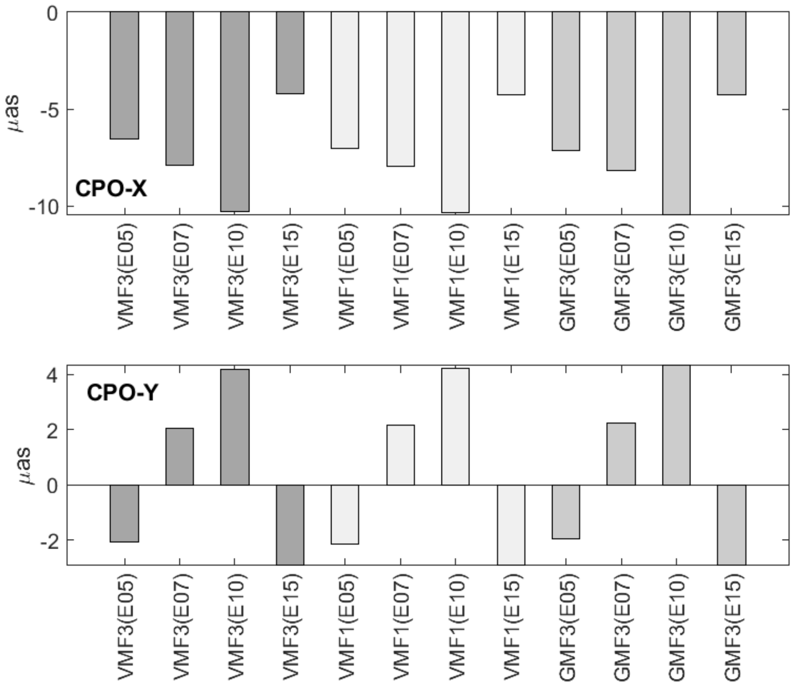

Figure 6.21. The WM (mean biases) of the daily celestial pole offsets w.r.t. IAU2000/2006 precession-nutation model plus IERS 14 C04 combined EOP series when different troposphere mapping functions (VMF3, VMF1, GMF3) and elevation cut-off angles (5, 7, 10, and 15 degrees) are used in the analysis of the VLBI daily sessions.

6.4. Results of the daily radio source positions estimated from the analysis of VLBI daily sessions when different troposphere mapping functions and elevation cut-off angles are used

To see the influence of different mapping functions (VMF1, VMF3, and GMF3) and elevation cut-off angles (5, 7, 10, and 15 degrees) on the daily radio source position estimates w.r.t. ICRF3sx catalog, the WM, and WRMS of the source coordinates are used as a metric. In Figure 6.22, the variations of the daily estimates around the ICRF3sx catalogue coordinates are shown for several sources. The variation of the estimates, as can be seen from the plot of Figure 6.22 exhibits different textures. These quasi-systematic variations formed by the daily source positions (distributions of the grey points) around the WM (green dots) as well as around the ICRF3sx coordinates (red dots) are most likely due to the changes of the source structures (jet anomalies) in time as seen by the X band radio signals as observations. The median formal errors of the daily right ascension and declination coordinate estimates are found within 10 to 50 µas. The WRMS repeatabilities of the daily source coordinates estimated in the analysis of the VLBI daily sessions do not vary significantly (<100 µas) for most of the sources w.r.t. the change of the mapping function and elevation cut-off angle. However, as can also be seen from Figure 6.23 the WRMS repeatabilities of the daily source coordinates at the northern celestial hemisphere are smaller than those of sources of the southern hemisphere. Besides, the repeatabilities at the sources near the celestial poles are larger about 1000 µas than those of equatorial sources. These results suggest when the elevation cut-off angles are increased, not large differences occurred in the total number of observations per source. Comparing to those of northern hemisphere stations, fewer stations are located in the southern hemisphere. This causes the total number of observations and their geometry becomes less and inhomogeneous in the southern hemisphere and worsens the repeatabilities of the sources at the southern hemisphere and the poles (see Figure 6.23.) The WM of the daily declinations w.r.t. ICRF3sx catalog coordinates become larger with the increase in elevation cut-off angles. But this is not seen as for the right ascensions. The WM of the daily coordinates (weighted mean biases) w.r.t. ICRF3sx catalog does not even vary with the change of mapping functions. Unlike WRMS repeatabilities, not any systematic declination dependency of the WM biases of the source coordinates is detected in this study (see Figure 6.24.). Strictly stating that the mean biases between the ICRF3sx catalog coordinates and the estimated daily source coordinates are not worse than those at the southern celestial hemisphere and the poles.

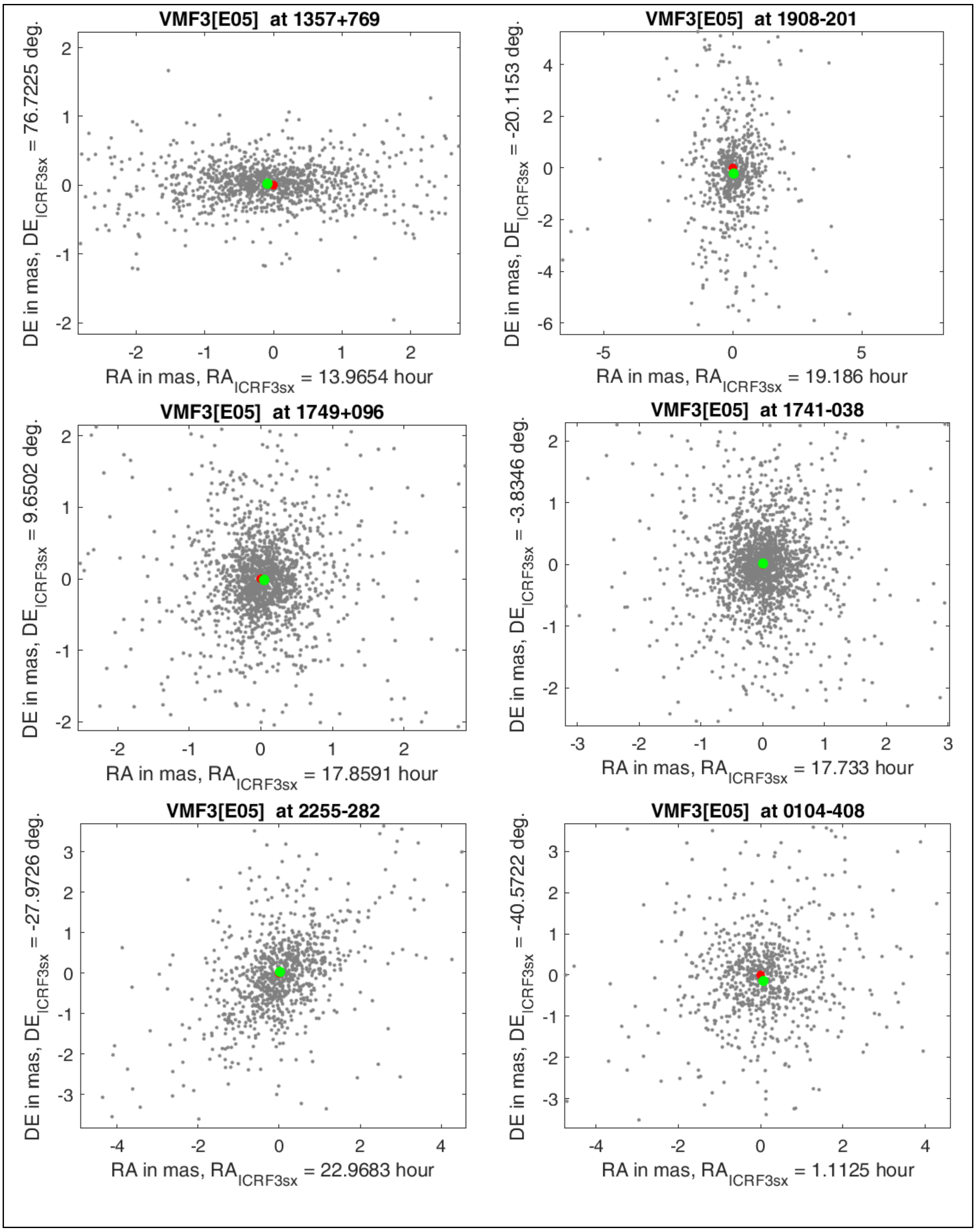

Figure 6.22. Daily source coordinates w.r.t. ICRF3sx catalog, when VMF3 mapping function and 5 degrees elevation cut-off angle is used in the analysis of the VLBI daily sessions, are depicted as grey points. The red dots denote the ICRF3sx catalog positions of the sources which correspond to 0 by 0 coordinates in the plots. The green dots illustrate the WM of the estimated daily source coordinates.

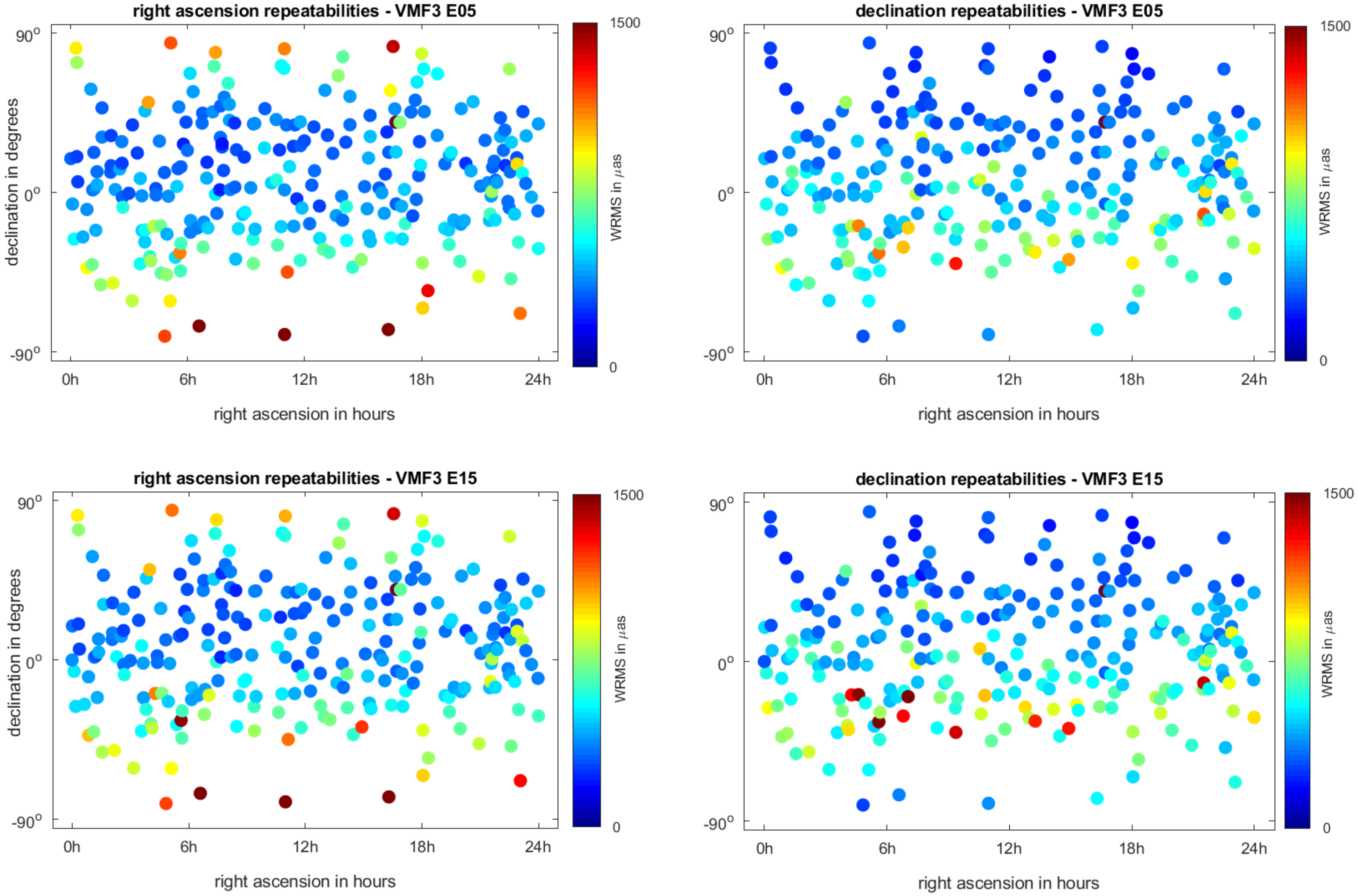

Figure 6.23. The WRMS repeatabilities of the daily source coordinates estimated in the analysis of the VLBI daily sessions when elevation cut-off angles 5 and 15 degrees as well as troposphere mapping function, VMF3 are used.

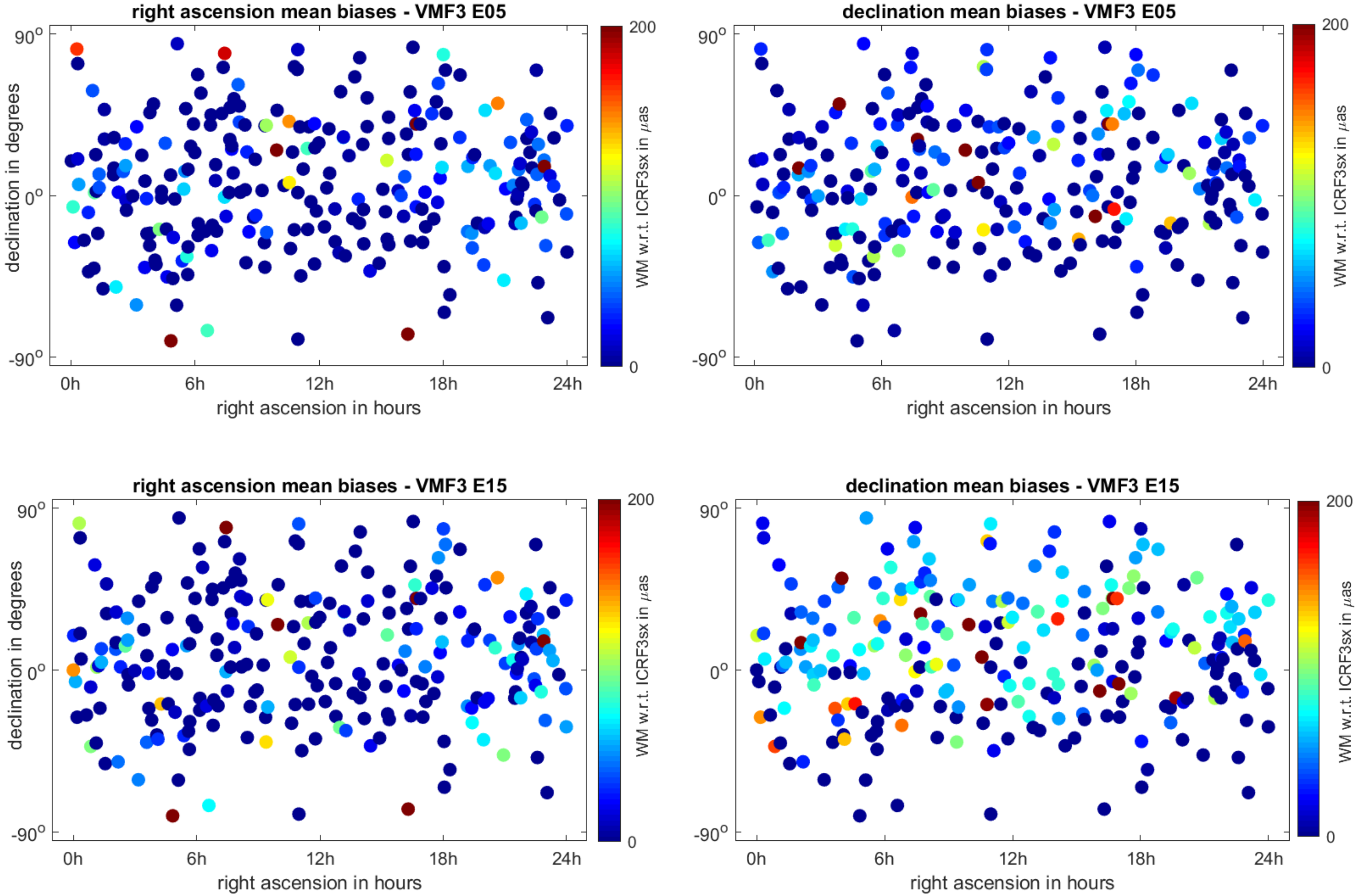

Figure 6.24. The WM of the daily source coordinates (weighted mean biases) w.r.t. ICRF3sx catalog, estimated in the analysis of the VLBI daily sessions when elevation cut-off angles 5 and 15 degrees as well as troposphere mapping function, VMF3 are used.

7. CONCLUSION

Although several effects contaminate the radio signals recorded in the S and X band during the VLBI sessions, the troposphere is currently the biggest source of error that cannot be properly reduced from the observations. As a result of the studies carried out within the scope of this thesis, the effects of the troposphere delay errors on the estimated parameters i.e. zenith total delays (ZTD), coordinates of the stations and the radio sources as well as Earth orientation parameters were assessed in terms of using different mapping functions and elevation cut-off angles in the analysis of the daily sessions. The mapping functions: VMF1, VMF3, GMF3, and the elevation cut-off angles: 5, 7, 10, and 15 degrees are used in each of the analyses. As an objective and unbiased criteria, the weighted root-mean-square (WRMS) repeatabilities and the WRMS differences were calculated for and between each set of the estimated parameters (i.e. the troposphere ZTD, station positions, source positions, and EOP), respectively.

The WRMS of the estimated parameters as the repeatabilities were used for the assessments. Based on the results of using different troposphere mapping functions (VMF1, VMF3, GMF3) and elevation cut-off angles (5, 7, 10, 15 degrees) on the estimates of the ZTD, EOP, and the coordinates of the radio sources and the stations following conclusions are drawn: The seasonal variations of the atmospheric pressure as well as the humidity are superior at the several sites like Tsukuba (Japan). GMF3 mapping function ZTD results exhibit high correlations with VMF1 and VMF3 mapping functions. This is expected since GMF is a global spherical harmonic seasonal approximation of VMF. ZTD agreement between VMF1-VMF3 is found to be 2 to 3 times better than GMF3-VMF1 and GMF3-VMF3 agreements in terms of the WRMS differences. Not a significant difference between mapping functions above e.g. 15 or 20 degrees elevation cut-off angle were found when the ZTD and station coordinates are compared. This result indicates that the benefit of using VMF3 is started after reducing the elevation cut-off angle to about 5-10 degrees. When different elevation cut-off angles are used, the biases between ZTD estimates do not reduce. As an inference from these results, changing elevation cut-off angle does not considerably affect the ZTD biases between mapping functions. The larger WRMS of ZTD differences at southern hemisphere sites should be resulted from not just less number but also inhomogeneous geometry of the observations.

The WM of the stations' daily positions are not sensitive to the change of mapping functions. The differences in the station position repeatabilities between the mapping functions decrease when the elevation cut-off angles increase. The choice of mapping function in the analysis of VLBI observations has utmost importance for the estimation of accurate parameters especially the station positions.

The repeatabilities of EOP are much more sensitive to the number and the geometry of the observations i.e. the elevation cut-off angle. When overall EOP repeatabilities are considered, it can be inferred that 5 degrees elevation cut-off angle should be used regardless of which mapping function is introduced in the analysis. It is worth to note that this conclusion can only be drawn for the daily EOP estimation in the analysis of the daily sessions.

The total number of observations and their geometry become less and inhomogeneous in the southern hemisphere. This worsens the WRMS repeatabilities of the source daily coordinates at the southern hemisphere and the poles. Unlike WRMS repeatabilities, not any systematic declination dependency of the WM biases of the source coordinates is detected in this study.

REFERENCES

Alizadeh, M.M., Wijaya, D.D., Hobiger, T., Weber, R. and Schuh, H., Ionospheric Effects on Microwave Signals. Atmospheric Effects in Space Geodesy, Böhm, J. and Schuh, H. (Eds.), Springer Atmospheric Sciences, Springer-Verlag Berlin Heidelberg, 35-72, **2013**.

Altamimi, Z., Sillard, P. and Boucher, C., ITRF2000: A new release of the international terrestrial reference frame for earth science applications, Journal of Geophysical Research, 107(B10) (**2002**) 2214.

Altamimi, Z., Collilieux, X., Legrand, J., Garayt, B. and Boucher, C., ITRF2005: a New Release of The International Terrestrial Reference Frame Based on Time Series of Station Positions and Earth Orientation Parameters, Journal of Geophysical Research, 112 (**2007**) B09401.

Altamimi, Z., Collilieux, X., Métivier, L., Analysis and Results of ITRF2008 International Earth Rotation Service Tech. Note 37, Verlag des Bundesamts für Kartographie und Geodäsie, Frankfurt am Main, 2012, https://www.iers.org/IERS/EN/Publications/TechnicalNotes/tn37.html (Date of Access: **07.07.2020**).

Altamimi, Z., Rebischung, P., Métivier, L. and Collilieux, X., ITRF2014: A new release of the International Terrestrial Reference Frame modeling nonlinear station motions, Journal of Geophysical Research: Solid Earth, Vol. 121 (**2016**) 8 6109-6131, doi:10.1002/2016jb013098.

Altamimi, Z., Rebischung, P., Métivier, L., Collilieux, X., Analysis and Results of ITRF2014 International Earth Rotation Service Tech. Note 38, Verlag des Bundesamts für Kartographie und Geodäsie, Frankfurt am Main, 2017, https://www.iers.org/IERS/EN/Publications/TechnicalNotes/tn38.html (Date of Access: **07.07.2020**).

Angermann, D., Drewes, H., Krügel, M., Meisel, B., Gerstl, M., Kelm, R., Müller, H., Seemüller, W. and Tesmer, V., ITRS Combination Center at DGFI: A Terrestrial Reference Frame Realization 2003, Deutsche Geodätische Kommission, Reihe B, Heft Nr. 313, München, **2004**.

Angermann, D., Drewes, H., Krügel, M. and Meisel, B. in International Association of Geodesy Symposia, Vol. 130, Dynamic Planet: Monitoring and Understanding a Dynamic Planet with Geodetic and Oceanographic Tools. Tregoning, P. and Rizos, C. (Eds.), IAG Symposium Cairns, Australia, 22-26 August 2005, Springer, Berlin, Heidelberg, **2007**, p. 595-602

Angermann, D., Drewes, H., Gerstl, M., Krügel, M. and Meisel, B. in International Association of Geodesy Symposia, Vol. 134, Geodetic Reference Frames, Drewes, H. (Ed.), IAG Symposium Munich, Germany, 9-14 October 2006, Springer, Berlin, Heidelberg, **2009**, p. 11–16.

Angermann, D., Seitz, M. and Drewes, H., Global Terrestral Reference Systems and Their Realizations. Sciences of Geodesy II, Innovations and Future Developments, Xu, G. (Ed.), Springer Verlag, 97-129, **2013**.

Aoki, S., Guinot, B., Kaplan, G.H., Kinoshita, H., McCarthy, D.D. and Seidelmann, P.K., The new definition of universal time, Astronomy And Astrophysics, 105 (**1982**) 359-361.

Arias, E.F., Feissel, M. and Lestrade, J.F., An Extragalactic Celestial Reference Frame Consistent with The BIH Terrestrial System (**1987**), BIH Annual Report, 1988.

Arias, E.F., Charlot, P., Feissel, M. and Lestrade, J.F., Astronomy And Astrophysics, 303 (**1995**) 604-608.

Argus, D.F. and Gordon, R.G., No-net-rotation model of current plate velocities incorporating plate motion model NUVEL-1, Geophysical Research Letters 18 (**1991**) 2039–2042.

Argus, D.F., Geophysical Research Letters 23 (**1996**) 973

Behrend, D., Cucurull, L., Vila, J. and Haas, R., An inter-comparision study to estimate zenith wet delays using VLBI, GPS, and NWP models. Earth, Planets and Space, 52 (**2000**) 691-694.

Behrend, D., Haas, R., Pino, D., Gradinarsky, L., Keihm, S., Schwarz, W., Cucurull, L. and Rius, A. MM5 derived ZWDs compared to observational results from VLBI, GPS and WVR. Physics and Chemistry of the Earth, 27 (**2002**) 3301-3308.

Berg, H., Allgemeine Meteorologie, Dümmlers Verlag, Bonn, **1948**.

Bizouard, C., Lambert, S., Gattano, C., Becker, O., Richard, J.Y., The IERS EOP 14 C04 solution for Earth orientation parameters consistent with ITRF 2014, Journal of Geodesy, (**2018**), doi:10.1007/s00190-018-1186-3.

Boucher, C. and Altamimi, Z., Towards An Improved Realization of The BIH Terrestrial Reference Frame, Mueller, I.I. (Ed.), The MERIT/COTES Report on Earth Rotation and Reference Frames, Vol. 2, OSU/DGS, Columbus, Ohio, **1985**.

Boucher, C., Altamimi, Z., Feissel, M. and Sillard, P., Results and Analysis of The ITRF94, IERS Technical Note No. 20, Observatoire de Paris, Paris, 1996, https://www.iers.org/IERS/EN/Publications/TechnicalNotes/tn20.html (Date of Access: **07.07.2020**)

Boucher, C., Altamimi, Z. and Sillard, P., Results and Analysis of The ITRF96, IERS Technical Note No. 24, Observatoire de Paris, Paris, 1998, https://www.iers.org/IERS/EN/Publications/TechnicalNotes/tn24.html (Date of Access: **07.07.2020**)

Boucher, C., Altamimi, Z. and Sillard, P., the International Terrestrial Reference Frame (ITRF97), IERS Technical Note No. 27, Observatoire de Paris, Paris, 1999, https://www.iers.org/IERS/EN/Publications/TechnicalNotes/tn27.html (Date of Access: **07.07.2020**)

Boucher, C., Altamimi, Z., Sillard, P. and Feissel-Vernier, M., The ITRF2000, IERS Technical Note 31, Verlag des Bundesamts für Kartographie und Geodäsie, Frankfurt am Main, 2004, https://www.iers.org/IERS/EN/Publications/TechnicalNotes/tn27.html (Date of Access: **07.07.2020**)

Böhm, J., Troposphärische Laufzeitverzögerungen in der VLBI, PhD Dissertation, Technische Universität Wien, **2004**.

Böhm, J., Atmospheric Effects in Geodesy (Lecture Notes ed.), Vienna, Austria, Institute of Geodesy and Geophysics, Vienna Universtiy of Technology, **2009**.

Böhm, J. and Schuh, H., Vienna mapping functions in VLBI analyses, Geophysical Research Letters, 31 (**2004**) L01603.

Böhm, J., Niell, A., Tregoning, P. and Schuh, H., Global mapping function (GMF): A new empirical mapping function based on numerical weather model data, Geophysical Research Letters, 33 (**2006**) L07304.

Böhm, J., Werl, B. and Schuh, H., Troposphere mapping functions for GPS and very long baseline interferometry from european centre for medium-range weather forecasts operational analysis data, Journal of Geophysical Research, 111 (**2006**) B2.

Böhm, J. and Schuh, H., Troposphere gradients from the ECMWF in VLBI analysis, Journal of Geodesy 81 (**2007**) 403-408.

Böhm, J., Heinkelmann, R. and Schuh, H. in International Association of Geodesy Symposia, Vol.134, Geodetic Reference Frames, Drewes, H. (Ed.), IAG Symposium Munich, Germany, 9-14 October 2006, Springer, Berlin, Heidelberg, **2009**, p. 317-321.

Böhm, J., Kouba, J. and Schuh, H., Forecast Vienna mapping functions 1 for real-time analysis of space geodetic observations, Journal of Geodesy, 83(5) (**2009**) 397-401.

Böhm, J., Böhm, S., Nilsson, T., Pany, A., Plank, L., Spicakova, H., Teke, K. and Schuh, H., The new Vienna VLBI Software VieVs, IAG Symposia Series, Buenos Aires, **2010**.

Böhm, J., Spicakova, H., Urquhart, L., Steigenberger, P. and Schuh, H., Impact of A Priori Gradients on VLBI-Derived Terrestrial Reference Frames. Proceedings of the 20th Meeting of the European VLBI Group for Geodesy and Astronomy., Alef, W., Bernhart, S. and Nothnagel, A. (Eds.), Institut für Geodäsie und Geoinformation, Universität Bonn, Germany, **2011**, 128-132.

Böhm, J., Böhm, S., Boisitis, J., Girdiuk, A., Gruber, J., Hellerschmied, A., Krásna, H., Landskron, D., Madzak, M., Mayer, D., McCallum, J., McCallum, L., Scharter, M and Teke, K., Vienna VLBI and Satellite Software (VieVS) for Geodesy and Astrometry, Publications of the Astronomical Society of the Pacific, 130 (**2018**) 1-6.

Brosche, P. in Polar Motion: Historical and Scientific Problems, Dick, S., McCarthy, D.D. and Luzum, B. (Eds.), IAU Colloquium 178, ASP Conference Series Vol. 208, Cagliari, Italy, 27-30 September 1999, San Francisco, **2000**, p.101-108.

Brzeziński, A., Bizouard, C. and Petrov, S.D., Influence of the atmosphere on Earth rotation: what new can be learned from the recent atmospheric angular momentum estimates?, Surveys in Geophysics 23 (**2002**) 33-69.

Brzeziński, A., Dobslaw, H. and Dill, R. in International Association of Geodesy Symposia, Vol. 136, Geodesy for Planet Earth: Proceedings of the 2009 IAG Symposium, Buenos Aires, 31 August - 4 September 2009. Kenyon, S.C., Pacino, M.C. and Marti U.J (Eds.), Springer, Berlin, Heidelberg, **2012**, p. 499-505.

Campbell, J., Die Radiointerferometrie auf langen Basen als geodätisches Messprinzip hoher Genauigkeit, Number Heft 314 in Reihe C. München: DGK, **1979**.

Campbell, J., From Quasar to benchmarks: VLBI links heaven and Earth. International VLBI Service for Geodesy and Astrometry, Vandenberg, N. and Baver, K. (Eds.) Volume NASA/CP-2000 of General Meeting Proceedings, 21-24 February 2000, Kötzting, Germany, **2000**, p.19-35.

Capitaine, N., Guinot, B. and Souchay, J., A Non-rotating Origin on the Instantaneous Equator: Definition, Properties and Use, Celestial Mechanics and Dynamical Astronomy, 39 (**1986**) 283-307.

Capitaine, N. in Towards Models and Constants for Sub-Microarcsecond Astrometry, Johnston, K.J., McCarthy, D.D., Luzum, B.J. and Kaplan, G.H. (Eds.), IAU Colloquium 180, Washington, DC, USA, 27-30 March 2000, U.S. Naval Observatory, Washington, DC, USA, 2000, p. 153-163.

Capitaine, N., Guinot, B. and McCarthy, D.D.,Definition of the Celestial Ephemeris origin and of UT1 in International Celestial Reference Frame, Astronomy and Astrophysics, 335(1) (**2000**) 398-405.

Capitaine, N., Gambis, D., McCarthy, D.D., Petit, G., Ray, J., Richter, B., Rothacher, M., Standish, M. and Vondrák, J., Proceedings of the IERS Workshop on the Implementation of the New IAU Resolutions, IERS Technical Note No. 29, Verlag des Bundesamts für Kartographie und Geodäsie, Frankfurt am Main, 2002, https://www.iers.org/IERS/EN/Publications/TechnicalNotes/tn29.html (Date of Access: **07.07.2020**)

Carter, M. and Carter, W. in ASP Conference Series Vol. 208 Polar Motion: Historical and Scientific Problems, Dick, S., McCarthy, D.D. and Luzum, B. (Eds.), IAU Colloquium 178, Cagliari, Italy, 27-30 September 1999, San Francisco, **2000**, p. 109-118.

Carter, W.E. and Robertson, D.S., Studying the earth by very long baseline interferometry, Scientific American, 255(No.5) (**1986**) 46-54.

Chandler, S.C., On the variation of latitude, I., Astronomical Journal, 11 (**1891a**) 59-61.

Chandler, S. C., On the variation of latitude, II., Astronomical Journal, 11 (**1891b**) 65-70.

Chandler, S. C., On the variation of latitude, VII., Astronomical Journal, 12 (**1892**) 97-101.

Chao, C.C., The troposphere calibration model for mariner mars 1971, Tracking System Analytic Calibration Activities for the Mariner Mars 1971 Mission, Technical Report 32-1587, NASA JPL, Pasadena, CA, 61-76, **1974**.

Chao, B.F., Ray, R.D., Gipson, J.M, Egbert, G.D. and Ma, C., Diurnal/semidiurnal polar motion excited by oceanic tidal angular momentum, Journal of Geophysical Research, 101(B9) (**1996**) 20151.

Chapront, J., Chapront-Touzé, M. and Francou, G., A new determination of lunar orbital parameters, precession constant and tidal acceleration from LLR measurements, Astronomy and Astrophysics, 387 (**2002**) 700-709.

Charlot et al., The Third Realization of the International Celestial Reference Frame, Astronomy & Astrophysics, (**2018**).

Chen, G., Herring T., Effects of atmospheric azimuthal asymmetry on the analysis from space geodetic data, Journal of Geophysical Research, 102(B9) (**1997**) 20489-20502.

Collioud, A. and Charlot, P., in The Bordeaux VLBI image database. Bourda, G., Charlot, P. and Collioud, A. (Eds.), Proceedings of the 19th European VLBI for Geodesy and Astrometry Working Meeting, Bordeaux, 24–25 Mar 2009, **2009**, p. 19-22.

Cucurull, L., Navascues, B., Ruffini, G., Elosegui, P., Rius, A. and Vila, J., The use of GPS to validate NWP systems: the HIRLAM model, Journal of Atmospheric and Oceanic Technology, 17(6) (**2000**) 773-787.

Davis, J. L., Herring, T.A., Shapiro, I.I., Rogers, A.E.E. and Elgered, G., Geodesy by radio interferometry: Effects of atmospheric modeling errors on estimates of baseline length, Radio Science, 20 (**1985**) 1593-1607.

Davis, J.L., Elgered, G., Niell, A.E. and Kuehn, C.E., Ground-based measurement of gradients in the “wet” radio refractivity of air, Radio Science, 28 (**1993**) 1003-1018.

DeMets, C., Gordon, R.G., Argus, D.F. and Stein, S., Effect of recent revisions to the geomagnetic time scale on estimates of current plate motions, Geophysical Research Letters, 21 (**1994**) 2191-2194.

De Viron, O. and Dehant, V., Earth’s rotation and high frequency equatorial angular momentum budget of the atmosphere, Surveys in Geophysics, 20 (**1999**) 441-462.

Dick, S.J. in Polar Motion: Historical and Scientific Problems, Dick, S., McCarthy, D.D. and Luzum, B. (Eds.), IAU Colloquium 178, ASP Conference Series, Vol. 208, Cagliari, Italy, 27-30 September 1999, San Francisco, **2000**, p. 1-24

Drewes, H. in Observing our Changing Earth, Sideris, M.G. (Ed.), International Association of Geodesy Symposia, Vol. 133, Proceedings of the 2007 IAG General Assembly, Perugia, Italy, 2-13 July 2007, Springer, Heidelberg, **2009**, p 3-10.

Einstein, A., On the Influence of gravitation on the propagation of light, Annalen derPhysik, 35 (**1911**) 898-908.

Einstein, A., The foundation of the General Theory of Relativitiy, Annalen der Physik, 49 (**1916**) 769-822.

Elgered, G., Davis, J.L., Herring, T.A. and Shapiro, I.I., Journal of Geophysical Research, 96 (**1991**) 6541.

Emardson, T., Elgered, G. and Johansson, J., Three months of continuous monitoring of atmospheric water vapor with a network of Global Positioning System receivers, Journal of Geophysical Research, 103(D2) (**1998**) 1807-1820.

Eubanks, T. (Ed.), Proceedings of the U. S. Naval Observatory Workshop on Relativistic Models for Use in Space Geodesy, U. S. Naval Observatory, Washington, D.C., **1991**.

Eubanks, T.M., Variations in the Orientation of the Earth. Contributions of Space Geodesy to Geodynamics: Earth Dynamics Geodynamics Series, Smith, D.E. and Turcotte, D.L. (Eds.), Vol. 24, American Geophysical Union, Washington, D.C., p. 1-54, **1993**.

Fallon, F.W. and Dillinger, W.H., Journal of Geophysical Research, 97 (**1992**) 2179.

Fey, A.L., Gordon, D. and Jacobs, C., The Second Realization of the International Celestial Reference Frame by Very Long Baseline Interferometry, IERS Technical Note No. 35, Frankfurt am Main: Verlag des Bundesamts für Kartographie und Geodäsie, 2009, https://www.iers.org/IERS/EN/Publications/TechnicalNotes/tn35.html (Date of Access: **07.07.2020**)

Fey, A.L., Gordon, D., Jacobs, C.S., Ma, C. and Gaume, R.A., Arias, E. F., Bianco, G., Boboltz, D. A., Böckmann, S. and Bolotin, S., The second realization of the international celestial reference frame by very long baseline interferometry, The Astronomical Journal, 150 (**2015**) 58.

Fey, A.L., Clegg, A.W. and Fomalont, E.B., Astrophysical Journal Supplement Series, 105 (**1996**) 299.

Fienga, A., Laskar, J., Morley, T., Manche, H., Kuchynka, P., Le Poncin-Lafitte, C., Budnik, F., Gastineau, M. and Somenzi, L., INPOP08, a 4-D planetary ephemeris: from asteroid and time-scale computations to ESA Mars Express and Venus Express contributions, Astronomy and Astrophysics, 507 (**2009**) 1675-1686.

Fleagle, R.G., and Businger, J.A., Atmospheric Physics, 2nd Edition, Academic Press, New York, **1980**.

Fricke, W., Determination of the equinox and equator of the FK5, Astronomy and Astrophysics, 107 (**1982**) L13-L16.

Fricke, W., Schwan, H. and Lederle, T., Fifth Fundamental Catalogue, Part I. Veröffentlichungen des Astronomischen Rechen-Instituts, Heidelberg, **1988**.

Folkner, W.M., Charlot, P., Finger, M.H., Williams, J.G., Sovers, O.J., Newhall, X.X. and Standish, E.M., Determination of the extragalactic-planetary frame tie from joint analysisof radio interferometric and lunar laser ranging measurements, Astronomy and Astrophysics, 287 (**1994**) 279-289.

Folkner, W.M., Williams, J.G. and Boggs, D.H., The Planetary and Lunar Ephemeris DE 421, IPN Progress Report 42-178, August 15 2009, California Institute of Technology, California, 2009, https://ipnpr.jpl.nasa.gov/progress_report/42-178/178C.pdf (Date of Access: **07.07.2020**)

Gradinarsky, L.P, Haas, R., Elgered, G. and Johansson, J.M., Wet path delay and delay gradients inferred from microwave radiometer, GPS and VLBI observations, Earth Planets Space, 52 (10) (**2000**) 695-698.

Gross, R.S., The excitation of the Chandler wobble, Geophysical Research Letters, 27 (2000) 2329-2332.

Gross, R.S., Fukumori, I. and Menemenlis, D., Atmospheric and oceanic excitation of the Earth's wobbles during 1980–2000, Journal of Geophysical Research, 108(B8) (**2003**) 2370.

Gross, R.S., Fukumori, I., Menemenlis, D. and Gegout, P., Atmospheric and oceanic excitation of length-of-day variations during 1980–2000, Journal of Geophysical Research, 109(B01) (**2004**) 1-15.

Gross, R.S., Earth Rotation Period - Long Period, Herring, T.A. (Ed.), Treatise on Geophysics, Elsevier, Massachusetts Institute of Technology, Cambridge, USA, , Volume 3, **2007**.

Hazard, C., Sutton, J., Argue, A.N., Kenworthy, C.N., Morrison, L.V. and Murray, C.A., Accurate radio and optical positions of 3C273B, Nature Physical Science, 233 (**1971**) 89-91.

Heinkelmann, R., VLBI Geodesy: Observations, Analysis and Results. Geodetic Sciences: Observations, Modeling and Applications, Jin, S. (Ed.), IntechOpen, 129-156, **2013**.

Henstock, D.R., Browne, I.W.A., Wilkinson, P.N., Taylor, G.B., Vermeulen, R.C., Pearson, T.J. and Readhead, A.C.S., 1994, Astrophysical Journal Supplement Series, 100 (**1994**) 1.

Herring, T.A., Gwinn, C.R. and Shapiro, I.I., Geodesy by radio interferometry: Studies of the forced nutations of the Earth: 1. Data Analysis, Journal of Geophysical Research, 91 (**1986**) 4745-4754.

Herring, T., Davis, J. and Shapiro, I., Geodesy by Radio Interferometry: The Application of Kalman Filtering to the Analysis of Very Long Baseline Interferometry Data, Journal of Geophysical Research, 95(B8) (**1990**) 12561-12581.

Herring, T.A., in Modeling atmospheric delays in the analysis of space geodetic data. De Munk, J.C. and Spoelstra, T.A. (Eds.), Symposium on Refraction of Transatmospheric Signals in Geodesy, Netherlands Geodetic Commission, Delft, (**1992**) 157-164.

Hofmann-Wellenhof, B., Lichtenegger, H. and Collins, J., Global Positioning System: Theory and Practice, 5rd Edition, Wien, Springer-Verlag, **1994**.

Holman, K., Distribution of an Ultrastable Frequency Reference Using Optical Frequency Combs, PhD dissertation, University of Colorado, Department of Physics, **2005**.

Hopfield, H.S, Two-quartic tropospheric refractivity profile for correcting satellite data, Journal of Geophysical Research, 74 (**1969**) 4487-4499.

Hopfield, H.S., Troposheric effect on electromagnetically measured range: Prediction from surface weather data, Radio Science, 6 (**1971**) 357-367.

Höpfner, J. in Polar Motion: Historical and Scientific Problems, Dick, S., McCarthy, D.D. and Luzum, B. (Eds.), IAU Colloquium 178, ASP Conference Series, Vol. 208, Cagliari, Italy, 27-30 September 1999, San Francisco, **2000**, p. 139-146.

IAU Resolutions, 2000. http://www.iau.org/static/resolutions/IAU2000_French.pdf (Date of Access: **07.07.2020**)

IAU Resolutions, 2006. http://www.iau.org/static/resolutions/IAU2006_French.pdf (Date of Access: **07.07.2020**)

International Union of Geodesy and Geophysics (IUGG) Resolution Number 2, IUGG General Assembly, 2-13 July 2007, Perugia, 2007.

Iskenderian, H. and Salstein, D.A. Regional sources of mountain torque variability and high frequency fluctuations in atmospheric angular momentum, Monthly Weather Review, 126 (**1998**) 1681-1694.

IVS, International VLBI Service for Geodesy and Astrometry, https://ivscc.gsfc.nasa.gov/about/org/components/ns-list.html (Date of Access: **07.07.2020**).

Janes, H.W., Langley, R.B. and Newby, S.P., A comparisan of several models for the prediction of tropospheric propagation delay. Proceedinds of the Fifth International Geodetic Symposium on Satellite Positioning, March 13-17, vol.1, Las Cruces, New Mexico, 28-52, **1989**.

Kaplan, G.H., United States Naval Observatory Circular, U.S. Naval Observatory, Washington, DC., 163 (**1981**) 1.

Kaplan, G.H., Josties, F.J., Angerhofer, P.E., Johnston, K.J. and Spencer, J.H., Precise radio source positions from interferometric observations, Astronomical Journal, 87 (**1982**) 570-576.

Kaplan, G.H., The IAU Resolutions on Astronomical Reference Systems, Time Scales, and Earth Rotation Models, U.S. Naval Observatory Circular No. 179, U.S. Naval Observatory, Washington, D.C., **2005**.

Kellermann, K.I. and Pauliny-Toth, I.I.K., 1981, Compact radio sources, Annual Review of Astronomy and Astrophysics, 19 (**1981**) 373-410.

Kertz, W., Einführung in die Geophysik. II. Obere Atmasphäre und Magnetosphäre, Hochschultaschenbücher, vol. 535, Bibliographisches Institut, Mannheim, Germany, **1971**.

Klioner, S.A., General relativistic model of VLBI observables, Proceedings of the AGU Chapman Conference on Geodetic VLBI: Monitoring Global Change, Carter, W.E. (Ed.), NOAA Technical Report NOS 137 NGS 49, American Geophysical Union, Washington D.C., **1991**, 188-202.

Kopeikin, S., Theory of relativity in observational radio astronomy, Soviet Astronomy, 34(1) (**1990**) 5-10.

Kopeikin, S.M. and Schäfer, G., Lorentz covariant theory of light propagation in gravitational fields of arbitrary-moving bodies, Physical Review D, 60 (**1999**) 124002.

Kouba, J., Testing of global pressure/temperature (GPT) model and global mapping function (GMF) in GPS analyses, Journal of Geodesy, 83 (**2009**) 199-208.

Krásná, H., Böhm, J., Plank, L., Nilsson, T. and Schuh, H., Atmospheric Effects on VLBI-Derived Terrestrial and Celestial Reference Frames, Earth on the Edge Science for a Sustainable Planet. Rizos, C. and Willis, P. (Eds.), International Association of Geodesy General Assembly, Melbourne, Australia, 28 June-2 July 2011, International Association of Geodesy Symposia, Vol. 139. Springer, Berlin, Heidelberg, **2014**, p. 203-208.

Krügel, M. and Angermann, D. in International Association of Geodesy Symposia, Vol. 130, Dynamic Planet: Monitoring and Understanding a Dynamic Planet with Geodetic and Oceanographic Tools, Tregoning, P. and Rizos, C. (Eds.), IAG Symposium Cairns, Australia, 22-26 August 2005, Springer, Berlin, Heidelberg, **2007**, p. 158-165.

Küstner, F., Neue Methode zur Bestimmung der Aberrations-Constante nebst Untersuchungen über die Veränderlichkeit der Polhöhe. Beobachtungs-ergebnisse der Königlichen Sternwarte zu Berlin, 3 (**1888**) 1-59.

Küstner, F., Über Polhöhen-Aenderungen beobachtet 1884 bis 1885 zu Berlin und Pulkowa, Astronomische Nachrichten, 125 (**1890**) 273-278.

Lambeck, K., The Earth's Variable Rotation, Geophysical Causes and Consequences,: Cambridge University Press, Cambridge, **1980**.

Lambert, S. and Bizouard, C., Positioning the Terrestrial Ephemeris Origin in the International Terrestrial Reference Frame, Astronomy and Astrophysics, 394 (**2002**) 317-321.

Landskron, D., and Böhm, J., VMF3/GPT3: refined discrete and empirical troposphere mapping functions, Journal of Geodesy, 92(4) (**2018**) 349-360.

Le Mouël, J.-L., Smylie, D.E. and Herring, T., Dynamics of Earth's Deep Interior and Earth Rotation, Geophysical Monograph 72, IUGG Volume 12, IUGG/AGU, Washington, DC, **1993**.

Lestrade, J.-F., Jones, D.L., Preston, R.A., Phillips, R.B., Titus, M.A., Kovalevsky, J., Lindegren, L., Hering, R., Froeschle, M., Falin, J.-L., Mignard, F., Jacobs, C.S., Sovers, O.J., Eubanks, M. and Gabuzda, D., Preliminary link of the HIPPARCOS and VLBI reference frames, Astronomy and Astrophysics, 304 (**1995**) 182.

Lindegren, L., Röser, S., Schrijver, H., Lattanzi, M.G., van Leeuwen, F., Perryman, M.A.C., Bernacca, P.L., Falin, J.L., Froeschlé, M., Kovalevsky, J., Lenhardt, H. and Mignard, F., A comparison of ground-based stellar positions and proper motions with provisional Hipparcos results, Astronomy and Astrophysics, 304 (**1995**) 44-51.

Lieske, J.H., Lederle, T., Fricke, W. and Morando, B., Expressions for the precession quantities based upon the IAU (1976) System of Astronomical Constants, Astronomy and Astrophysics, 58 (**1977**) 1-16.

Ma, C., Ryan, J.W. and Caprette, D.S., Crustal Dynamics Project data analysis—1991: VLBI geodetic results 1979-1990, NASA Tech. Memo., TM-104552, **1992**.

Ma, C. and Feissel, M., Definition and Realization of the International Celestial Reference System by VLBI Astrometry of Extragalactic Objects, IERS Technical Note No. 23, Observatoire de Paris, Paris, 1997, https://www.iers.org/IERS/EN/Publications/TechnicalNotes/tn23.html (Date of Access: **07.07.2020**)

Ma, C., Arias, E.F., Eubanks, T.M., Fey, A.L., Gontier, A.M., Jacobs, C.S., Sovers, O.J., Archinal, B.A. and Charlot, P., The international celestial reference frame as realized by very long baseline interferometry, The Astronomical Journal, 116 (**1998**) 516–546.

MacMillan, D. and Ma, C., Evaluation of very long baseline interferometry atmospheric modeling improvements, Journal of Geophysical Research, 99(B1) (**1994**) 637-651.

MacMillan, D.S., Atmospheric gradients from very long baseline interferometry observations, Geophysical Research Letters, 22 (**1995**) 1041-1044.

MacMillan, D.S. and Ma, C., Atmospheric gradients and the VLBI terrestrial and celestial reference frames, Geophysical Research Letters, 24 (**1997**) 453-456.

Madden, R. and Julian, P. Detection of a 40–50 day oscillation in the zonal wind in the tropical Pacific, Journal of Atmospheric Science, 28 (**1971**) 702-708.

Marini, J.W., Correction of satellite tracking data for an arbitrary tropospheric profile, Radio Science, 7 (**1972**) 223-231.

Marini, J.W. and Murray, C.W., Correction of Laser Range Tracking Data for Atmospheric Refraction at Elevation Angles above 10 Degrees, Technical Report X-591-73-351, NASA, **1973**.

Mathews, P.M., Herring, T.A. and Buffett, B.A., Modeling of nutation and precession: new nutation series for nonrigid Earth, and insights into the Earth's Interior, Journal of Geophysical Research, 107(B4) (**2002**) ETG 4-1 – ETG 4-12.

McCarthy, D.D. and Petit, G., IERS Conventions 2003, IERS Technical Note No. 32, Frankfurt am Main, Germany: Verlag des Bundesamts für Kartographie und Geodäsie, 2004, https://www.iers.org/IERS/EN/Publications/TechnicalNotes/tn32.html (Date of Access: **07.07.2020**)

McCarthy, D.D. and Seidelmann, K.P., Time – From Earth Rotation to Atomic Physics, WILEY-VCH Verlag GmbH & Co. KGaA, Weinheim, **2009**.

Mekik, Ç., GPS'e Atmosferin Etkileri, Harita ve Kadastro Mühendisleri Odası Dergisi, 86 (**1999**) 14-20.

Mendes, V.B., Modeling of the Neutral-Atmosphere Propagation Delay in Radiometric Space Techniques, PhD Dissertation, Department of Geodesy and Geomatics Engineering Technical Report No.199, University of New Brunswick, Fredericton, New Brunswick, Canada, **1999**.

Mignard, F. and Froeschlé, M., Global and local bias in the FK5 from the Hipparcos data, Astronomy and Astrophysics, 354 (**2000**) 732-739.

Moran, J.M., in Astrophysics: Radio Observations, Methods of Experimental Physics, Vol. 12, Part C, Meeks M.L. (Eds.), Academic Press, New York, p. 174-228, **1976**.

Moritz, H., and Mueller, I.I., Earth Rotation: Theory and Observation, New York: Ungar, **1987**.

Munk, W.H. and MacDonald, G.J.F., The Rotation of the Earth: A Geophysical Discussion, Cambridge University Press, Cambridge, **1960**.

Newhall, X.X., Preston, R.A. and Esposito, P.B., in International Astronomical Union Symposium, No:109, Astrometric Techniques, Eichhorn, H.K. and Leacock, R.J. (Eds.), Gainesville, Florida, U.S.A., 9-12 January 1984, Springer, Dordrecht, **1986**.

Niell, A., Global mapping functions for the atmosphere delay at radio wavelengths, Journal of Geophysical Research, 101(B2) (**1996**) 3227-3246.

Niell, A.E., Improved atmospheric mapping functions for VLBI and GPS, Earth Planets Space, 52 (**2000**) 699-702.

Niell, A., Coster, A., Solheim, F., Mendes, V., Toor, P., Langley, R. and Upham, C., Comparision of measurements of atmospheric wet delay by radiosonde, water vapor radiometer, GPS, and VLBI, Journal of Atmospheric Oceanic Technology, 18, (**2001**) 830-850.

Niell, A.E., Interaction of atmosphere modeling and vlbi analysis strategy, International VLBI Service for Geodesy and Astrometry 2006 General Meeting Proceedings. Behrend, D. and Baver, K. (Eds.), number NASA/CP-2006-214140, 252-256, **2006**.

Nilsson, T., Böhm, J., Dudy, D.W., Tresch, A., Nafisi, V. and Schuh, H., Path Delays in the Neutral Atmosphere. Atmospheric Effects in Space Geodesy, Böhm, J. and Schuh, H. (Eds.), Springer Atmospheric Sciences, Springer-Verlag Berlin Heidelberg, 73-136, **2013**.

Perryman, M.A.C., Lindegren, L., Kovalevsky, J., Hog, E., Bastian, U., Bernacca, P.L., Creze, M., Donati, F., Grenon, M., Grewing, M., van Leeuwen, F., van der Marel, H., Mignard, F., Murray, C.A., Le Poole, R.S., Schrijver, H., Turon, C., Arenou, F., Froeschle, M. and Petersen, C.S., The hipparcos catalogue, Astronomy and Astrophysics, 323 (**1997**) L49-52.

Petit, G. and Luzum, B., IERS Conventions (2010), IERS Technical Note No. 36, Verlag des Bundesamts für Kartographie und Geodäsie, Frankfurt am Main, **2010**, https://www.iers.org/IERS/EN/Publications/TechnicalNotes/tn36.html

Pitjeva, E.V., Ephemerides EPM2008: The updated model, constants, data. Proceedings of the “Journées 2008 Systèmes de référence spatio-temporels” and “X. Lohrmann-Kolloquium”, Soffel, M. and Capitaine, N. (Eds.), Lohrmann-Observatorium and Observatoire de Paris, 57-60, **2009**.

Petrov, L. and Boy, J.P.,Study of the atmospheric pressure loading signal in Very Long Baseline Interferometry observations, Journal of Geophysical Research, 109(B3) (**2004**) B03405. doi:10.1029/2003JB002500

Plag, H-P. and Pearlman, M. (Eds.), The Global Geodetic Observing System: Meeting the Requirements of a Global Society on a Changing Planet in 2020, Springer, Berlin, **2009**.

Polatidis, A.G., Wilkinson. P.N., Xu, W., Readhead, A.C.S., Pearson, T.J., Taylor, G.B. and Vermeulen, R.C., Astrophysical Journal Supplement Series, 98 (**1995**) 1.

Ray, R.D., Steinberg, D.J., Chao, B.F. and Cartwright, D.E., Diurnal and semidiurnal variations in the Earth’s rotation rate induced by oceanic tides, Science, 264 (**1994**) 830.

Ray, R.D. and Ponte, R.M., Barometric tides from ECMWF operational analyses, Annals of Geophysics, 21 (**2003**) 1897–1910

Rogers, A.E.E., Receiver Phase and Group Delay Calibrator for Use in Very Long Baseline Interferometry, Haystack Observatory Technical Note, Haystack Observatory, Westford, MA, **1975**.

Rothacher, M. in International Association of Geodesy Symposia, Vol. 120, Towards an Integrated Global Geodetic Observing System (IGGOS), Rummel, R., Drewes, H., Bosch, W. and Hornik, H. (Eds.), Springer, New York, **2000**, p. 41-52.

Saastamoinen, J., Atmospheric correction for the troposphere and stratosphere in radio ranging of satellite. The Use of Artificial Satellites for Geodesy, Henriksen, S.W., Mancini, A. and Chovitz, B.H. (Eds.), Vol. 15, American Geophysical Union, Washington, D.C., p. 247-278, **1972**.

Salstein, D., Mean properties of the atmosphere, Van Nostrand Reinhold, New York, NY, USA, 19-49, **1995**.

Sasao, T. and Wahr, J.M., An excitation mechanism for the free ‘core nutation’, Geophysical Journal of the Royal Astronomical Society, 64 (**1981**) 729-746.

Schindelegger, M., Böhm, S., Böhm, J. and Schuh, H., Atmospheric Effects on Earth Rotation, Atmospheric Effects in Space Geodesy, Böhm, J. and Schuh, H. (Eds.), Springer Atmospheric Sciences, Springer-Verlag Berlin Heidelberg, 181-233, **2013**.

Schlüter, W. and Behrend, D., The International VLBI Service for Geodesy and Astrometry (IVS): current capabilities and future prospects, Journal of Geodesy 81 (6-8) (**2007**) 379-387.

Schubert, S.D., Pjaendtner, J. and Rood, R., An assimilated data set for earth science applications, Bulletin of the American Meteorological Society, 74 (**1993**) 2331-2342.

Schuh, H., Die Radiointerferometrie auf langen Basen zur Bestimmung von Punktverschiebungen und Erdrotationsparametern, Number Heft 328 in Reihe C. Verlag der Bayerischen Akademie der Wissenchaften, DGK, **1987**.

Schuh, H., in International VLBI Service for Geodesy and Astrometry, Vandenberg, N. and Baver, K. (Eds.) Volume NASA/CP-2000 of General Meeting Proceedings, 21-24 February 2000, Kötzting, Germany, **2000**, p. 219-229.

Schuh, H., Nagel, S. and Seitz, T., Linear drift and periodic variations observed in long time series of polar motion, Journal of Geodesy, 74 (**2001**) 701-710.

Schuh, H. and Böhm, J., Status Report of the IVS pilot project-tropospheric parameters, International VLBI Service for Geodesy and Astrometry 2002 Annual Report, Vandenberg, N. and Baver, K. (Eds.), NASA/TP-2003-211619. Goddard Space Flight Center, Maryland: Goddard Space Flight Center, Maryland, 13-21, **2003**.

Schuh, H. and Behrend, D., International VLBI Service for Geodesy and Astrometry (IVS), in H. Drewes, H. Hornik (Eds.), Report of the International Association of Geodesy 2007-2011, Travaux de l’Association Internationale de Géodésie, **2011**, Vol. 37, pp. 423-432.

Schuh, H. and Böhm. S., Earth rotation, Encyclopedia of Solid Earth Geophysics, Gupta, H.K. (Ed.), Springer, Dordrecht, The Netherlands, 123-129, **2011**.

Schuh, H. and Böhm, J., in Sciences of Geodesy II, Innovations and Future Developments, Xu, G. (Ed.), Springer-Verlag, Berlin, Heidelberg, Chapter 7, **2013**.

Schwan, H., Precession and galactic rotation in the system of the FK5, Astronomy and Astrophysics, 198 (**1988**) 116-124.

Seidelmann, P.K., 1980 IAU theory of nutation: The final report of the IAU Working Group on Nutation, Celestial Mechanics and Dynamical Astronomy, 27 (**1982**) 79-106.

Seidelmann, P.K., Guinot, B. and Doggett, L.E., in Explanatory Supplement to the Astronomical Almanac, Seidelmann, P.K. (Ed.), University Science Books, Mill Valley, CA, 39, **1992**.

Seitz, M., Angermann, D., Bloßfeld, M., Drewes, H. and Gerstl, M., The 2008 DGFI Realization of the ITRS: DTRF2008, Journal of Geodesy, 86 (**2012**) 1097-1123.

Shapiro, I.I., Fourth test of general relativity, Physical Review Letters, 13 (**1964**) 789-791.

Shapiro, I.I., New method for the detection of light deflection by solar gravity, Science 157 (**1967**) 806-808.

Smith, E.K. and Weintraub, S., The constants in the equation for atmospheric refractive index at radio frequencies. Proceedings of I.R.E., 41 (**1953**) 1035-1037.

Soffel, M., Müller, J., Wu, X. and Xu, C., Consistent relativistic VLBI theory with picosecond accuracy, Astronomical Journal, 101(6) (**1991**) 2306-2310.

Sovers, O. and Jacobs, C., Observation model and parameter partials for the JPL VLBI parameter estimation software ”MODEST” - 1994, Volume 83-39 of Rev. 5: Jet Propulsion Laboratory, Pasedana, California, **1994**.

Sovers, O., Fanselow, J. and Jacobs, C., Astrometry and geodesy with radio interferometry: experiments, models, results, Reviews of Modern Physics 70(4) (**1998**) 1393-1453.

Standish, E.M., Newhall, X.X., Williams, J.G. and Folkner, W.M., JPL Planetary and Lunar Ephemerides, Willmann-Bell Inc., Richmond, VA., **1997**.

Taylor, G.B., Vermeulen, R.C., Pearson, T.J., Readhead, A.C.S., Henstock, D.R., Browne, I.W.A. and Wilkinson, P.N., in Compact Extragalactic Radio Sources, Proceedings of a workshop at Socorro, NM, Zensus, J.A. and Kellermann, K.I. (Eds.), 11-12 February 1994, **1994**.

Teitelbaum, L.P., Linfield, R.P., Resch, G.M., Keihm, S.J. and Mahoney, M.J., Geophysical Research Letters, 23 (**1996**) 3719.

Teke, K., Sub-daily parameter estimation in VLBI data analysis, Geowissenschaftliche Mitteilungen, Heft Nr. 87, Vienna University of Technology, Vienna, Austria, **2011**.

Teke, K., Kayıkçı, E.T., Böhm, J. and Schuh, H., Modeling Very Long Baseline Interferometry (VLBI) observations, Journal of Geodesy and Geoinformation, Vol. 1, No. 1 (**2012**) 17-26.

Thakkar, D.D., Xu, W., Readhead, A.C.S., Pearson, T.J., Taylor, G.B., Vermulen, R.C., Polaitidis, A.G. and Wilkinson, P.N., Astrophysical Journal Supplement Series, 98 (**1995**) 33.

Thomas, J. B., Jet Propulsion Laboratory Publications, Pasadena, CA, (**1980**) 80-84.

Thomas, J. B., Jet Propulsion Laboratory Publications, Pasadena, CA, (**1981**) 81-49.

Thomas, J. B., Jet Propulsion Laboratory Publications, Pasadena, CA, (**1987**) 87-29.

Titov, O., Tesmer, V. and Böhm, J. in OCCAM v.6.0 Software for VLBI Data Analysis, Vandenberg, N. and Baver, K. (Eds.), International VLBI Service for Geodesy and Astrometry 2004 General Meeting Proceedings, NASA/CP-2004-212255, **2004**.

Treuhaft, R. and Thomas, J., Incorporating atmospheric delay into the relativistic VLBI time delay, IOM 335 6-91-016, JPL Technical Memorandum, **1991**.

Verdun, A. and Beutler, G. in Polar Motion: Historical and Scientific Problems, Dick, S., McCarthy, D.D. and Luzum, B. (Eds.), IAU Colloquium 178, ASP Conference Series, Vol. 208, Cagliari, Italy, 27-30 September 1999, San Francisco, **2000**, p. 67-82.

Vigue, Y., Lichten, S.M., Blewitt, G., Heflin, M.B. and Malla, R.P., Geophysical Research Letters 19 (**1992**) 1487.

Wu, X., Ray, J. and van Dam, T., Geocenter motion and its geodetic and geophysical implications, Journal of Geodesy, 58 (**2012**) 44-61.

Zensus, J.A. and Pearson, T.J. in International Astronomical Union Syposium, No. 129, The Impact of VLBI on Astrophysics and Geophysics: International Astronomical Union, Cambridge, Massachusetts, 10-15 May 1987, Reid, M.J. and Moran, J.M. (Eds.), Klıuwer Academic Publishers, Dordrecht, **1988**, p. 7-16.